Doctoral Dissertation

Two critical behaviors in Einstein-scalar field theory with double-well potential

重力と相互作用する二重井戸型ポテンシャルを持つスカラー場の二種類の臨界現象の研究

Taishi Ikeda

Department of Physics,
Graduate School of Science,
Nagoya University

Supervisor: Professor
Yasusada Nambu,
Chul-Moon Yoo

Abstract

Nature is often described by non-linear equations with complicated dynamics. Therefore, in order to understand the system, it is instructive to focus on their universal properties. "Critical behavior" is one of the universal properties which often appears in non-linear equations. It is often observed around boundaries between two different phases in phase space of the dynamical system. The critical behavior in gravitational collapse, which is called "critical collapse", is a typical example of the critical behavior in dynamical systems with gravity. Let us prepare a one-parameter family of initial data sets which is parametrized by p and has a threshold p_* of black hole formation. Time evolution of the initial data around the threshold has universal behavior which does not depend on the parametrization of details of the initial data. In particular, the black hole mass obeys the scaling law for the initial parameter, and the index does not change even if other families of the initial data sets are used. These universal behaviors in gravitational collapse are the critical collapse.

The purpose of this study is to reveal the non-trivial phase space structure in the Einstein-scalar field theory with double-well potential by using critical behaviors. Since the scalar field with double-well potential might exist in the early universe, many researchers have been studied the effect of the scalar field on cosmology, from various viewpoints. Therefore, to understand fundamental dynamical properties of the scalar field is important. The scalar field with the double well potential without gravity has longevity localized solutions, which are called "oscillon". The oscillons have many different phases in which its typical behaviors are qualitatively different. It is known that the critical behavior appears around the boundary of the phases. It is expected that the oscillons and its critical behavior appear in the Einstein-scalar field theory with double-well potential. Therefore, the system also is interesting as a research of the critical behavior.

Firstly, we examine the critical behavior in gravitational collapse of a spherically symmetric domain wall, which is a boundary between the two different vacuum regions, and discuss the effect of the potential on the behavior. As a result, we find that the critical behavior appears in the domain wall collapse, and the behavior is similar to that in the gravitational collapse in a massless scalar field, in our parameter region. The index of the mass scaling also takes a similar value to the index of the critical behavior in a massless scalar field.

Secondly, we analyze the critical behavior in oscillons. The oscillons are longevity, localized, and time-dependent solution of the scalar field with double-well potential. Since it is possible that the oscillons were produced during the reheating after the inflation, it is meaningful to understand the fundamental properties of oscillons. It is known that there are many phases of the oscillons in the phase space. The lifetime of the oscillons diverges logarithmically around the boundary between the phases, and the time scale of the divergent behavior does not depend on the details of the initial data. In this study, we construct the oscillons in relatively

weak gravity cases, and examine the properties and the effect of the self-gravity on the critical behavior. As a result, we show that modulations appear in the lifetime of the oscillon around the boundary between the phases due to self-gravity, and a new type of the critical behavior appears.

Acknowledgments

I am particularly grateful for the assistance given by Chul-Moon Yoo. Furthermore, Vitor Cardoso also gave me many useful comments and discussions. I am also indebted to Yasusada Nambu, Akira Matsumura, Kazuhisa Okamoto, Tomohiro Harada, Hirotada Okawa, Rong-Gen Cai, and Matt Choptuik who provided technical help and sincere encouragement. Finally, I would also like to express my gratitude to my family.

Contents

Notation

- metric of spacetime: $g(=(-,+,+,+))$.
- 3-metric : γ
- covariant derivative of the metric g : ∇
  In this thesis, we use a covariant derivative associated with Levi-Civita connection, which has the following properties.

  1. linearity :
  $$\nabla_\mu(\alpha v^{\nu\cdots}{}_{\cdots} + \beta u^{\nu\cdots}{}_{\cdots}) = \alpha\nabla_\mu v^{\nu\cdots}{}_{\cdots} + \beta\nabla_\mu u^{\nu\cdots}{}_{\cdots}. \tag{1}$$
  2. Leibnitz rule :
  $$\nabla_\mu(v^{\nu\cdots}{}_{\cdots}u^{\rho\cdots}{}_{\cdots}) = (\nabla_\mu v^{\nu\cdots}{}_{\cdots})u^{\rho\cdots}{}_{\cdots} + v^{\nu\cdots}{}_{\cdots}\nabla_\mu u^{\rho\cdots}{}_{\cdots}. \tag{2}$$
  3. action for scalar quantity:
  $$\nabla_\mu f = \partial_\mu f, \tag{3}$$
  where f is a scalar function.
  4. torsion free :
  $$\nabla_\mu\nabla_\nu f = \nabla_\nu\nabla_\mu f. \tag{4}$$
  5. metric condition:
  $$\nabla_\mu g_{\alpha\beta} = 0. \tag{5}$$

  From above conditions, we have
  $$\begin{aligned} \nabla_\mu v^\nu &= \partial_\mu v^\nu + \Gamma^\nu{}_{\mu\rho}v^\rho, & (6)\\ \nabla_\mu v_\nu &= \partial_\mu v_\nu - \Gamma^\rho{}_{\mu\nu}v_\rho, & (7) \end{aligned}$$
  where $\Gamma^\nu{}_{\mu\rho}$ is a Levi-Civita connection, which is given as
  $$\Gamma^\lambda{}_{\mu\nu} = \frac{1}{2}g^{\lambda\rho}(\partial_\mu g_{\nu\rho} + \partial_\nu g_{\mu\rho} - \partial_\rho g_{\mu\nu}). \tag{8}$$

- covariant derivative of the 3-metric γ : D
  D also satisfies above five conditions.

- Riemann tensor associated with g

$$R^{\gamma}{}_{\nu\alpha\beta} = \partial_\alpha \Gamma^{\gamma}{}_{\beta\nu} - \partial_\beta \Gamma^{\gamma}{}_{\alpha\nu} + \Gamma^{\gamma}{}_{\mu\alpha}\Gamma^{\mu}{}_{\beta\nu} - \Gamma^{\gamma}{}_{\mu\beta}\Gamma^{\mu}{}_{\alpha\nu} \tag{9}$$

- Ricci tensor

$$R_{\alpha\beta} = R^{\mu}{}_{\alpha\mu\beta} \tag{10}$$

- Ricci scalar

$$R = R_{\mu\nu} g^{\mu\nu} \tag{11}$$

- We denote the Riemann tensor, Ricci tensor and Ricci scalar in 3-dim hypersurface as ${}^3R^{i}{}_{jkl}$, ${}^3R_{ij}$, and ${}^3R$.

- Einstein tensor : $G_{\mu\nu}$

$$G_{\mu\nu} := R_{\mu\nu} - \frac{1}{2} g_{\mu\nu} R, \tag{12}$$

- Energy momentum tensor

$$T_{\mu\nu} = -\frac{2}{\sqrt{-g}} \frac{\delta S_m}{\delta g^{\mu\nu}} \tag{13}$$

- Einstein equations

$$G_{\mu\nu} = 8\pi T_{\mu\nu}, \tag{14}$$

- Greek indices $\alpha,\ \beta\ \cdots$ run over $0, 1, 2, 3$, and the Latin indices $i,\ j\ \cdots$ run over $1, 2, 3$.

Chapter 1

Introduction

Many important equations describing gravity and elementary particles are non-linear. The non-linearity often plays an important role in non-trivial solutions of the non-linear equations. In general, the solutions are complicated, and analyses of them are difficult. Their universal properties give us many vital clues to understanding the non-linear equations. Some of non-linear equations have many phases in their phase space, which are classified by typical time evolution of the equations. "Critical behavior" is one of the universal properties which often is observed around the boundary between two different phases. Critical behavior in gravitational collapse, which is called "critical collapse" is a typical example of the critical behavior.

Gravitational collapse is one of the most important phenomena predicted in general relativity (GR). Gravity affects all objects and is an attractive force which is proportional to the mass of the object. Gravitational collapse is the process in which a large mass object implodes due to the self-gravity. If a repulsive force which is stronger than the self-gravity does not effectively work during the gravitational collapse, a black hole is formed. A black hole is a strong gravity region from which nothing can escape, and it is a distinctive object in GR. Physics of black hole gives us many guides to understand the properties of GR, test the theory, and so on. Therefore, to study a black hole is important. Gravitational collapse is one of the black hole formation processes. The time evolution is described by non-linear equations, and the analysis is complicated. Since critical collapse is universal feature of the non-linear equations, it gives us useful insights into the dynamics.

Critical collapse often is observed in several systems with gravity. In general, evolution equations describing gravitational collapse has two typical phases in the phase space. One is a black hole formation phase, and another is a no black hole formation phase. The critical collapse observed around the boundary between the two phases. It was firstly discovered in gravitational collapse of a massless scalar field by Choptuik [3]. Let us consider a one-parameter family of initial data sets which is parametrized by p. We assume that the parameter p characterizes the initial energy of the scalar field, and there is a threshold p_* of a black hole formation. That is, if p is larger than p_*, the final state of the gravitational collapse is a black hole. On the other hand, if p is less than p_*, after the gravitational

collapse, the black hole is not formed, and the scalar field dissipates. Under this setup, Choptuik examined the behavior of the gravitational collapse around the threshold and found the following remarkable properties: (1)The intermediate state of the gravitational collapse around the threshold p_* does not change, even if other one-parameter families of initial data sets with the threshold are used. This universal intermediate state is called a "critical solution". (2)In the massless scalar field case, the critical solution has a discrete self-similarity. The definition of a discrete self-similarity is given in Sec.2. (3)Around the threshold p_*, the black hole mass M obeys the scaling law;

$$M \propto |p - p_*|^{\nu}, \tag{1.1}$$

where ν is about 0.374 and this value is independent of choice of the one-parameter family of the initial data sets. After the Choptuik's discovery, similar behaviors were found in many gravitational systems. It is shown that the critical behavior of the gravitational collapse is associated with the existence of a co-dimension one attractor in the phase space of the system, and there are a few types of the critical collapse.

If a system has a co-dimension one attractor in the phase space, the critical behavior appears in the system even without gravity. The typical example is the critical behavior of an oscillon. Oscillons are localized, longevity, and time-dependent solutions of a scalar field with some non-linear potential. A typical example of the potential is a double-well potential. Oscillons of the scalar field with the double-well potential can be formed from the initial data which has a large energy of the scalar field. Here, let us prepare a family of the initial data set which is parametrized by p. When the initial parameter p is tuned around the critical value p_*, the critical behavior of the oscillon appears, and the lifetime τ of the oscillon obeys the following scaling law;

$$\tau \simeq -\gamma \ln |p - p_*| + C, \tag{1.2}$$

where γ and C are constants. p_* corresponds to the boundary at which the typical dynamical behavior changes, that is, it is a boundary between two phases in the phase space. Since the critical behavior appears in not only the gravitational collapse but also the system without gravity, the classification of the type of the critical behavior and understanding which system shows the critical behavior gives us much insight into the non-linear equations.

The purpose of this study is to reveal the non-trivial phase space structure in the Einstein-scalar field theory with double-well potential by using critical behaviors. The scalar field with the double-well potential might exist in the early universe, and many researchers have been studied the effect of the scalar field on the universe, from various viewpoints. To discuss the effect of the scalar field, we must understand fundamental dynamical properties of the scalar field. Furthermore, since it is expected that the theory has a complicated phase space structure, and the system is instructive to understand the critical behavior. It is expected that at least two critical behaviors appear in the system. The first critical behavior is that in the gravitational collapse. The second critical behavior is that of the oscillon under the weak gravity case. In this thesis, we focus on the following points

in each critical behavior. For the critical behavior of the gravitational collapse, we focus on the influence of the double well potential on the critical collapse. For the critical behavior of the oscillon, we focus on the effect of self-gravity of the oscillon on the critical behavior of the oscillon.

Firstly, we examine the critical behavior in the gravitational collapse. We use spherically symmetric domain wall solutions as a family of an initial data set. The domain wall is an object which appears on a boundary of two spatial regions in which the scalar field stays different vacua of the potential. The spherically symmetric domain wall which radius is large has large energy. On the other hand, one which radius is small has small energy. If the initial radius of the domain wall is very large, after the collapse, a black hole is formed. If the initial radius of the domain wall is small, after the collapse, the black hole is not formed, and the scalar field dissipates. Therefore, there is a threshold of the black hole formation for the radius of the domain wall, and it is expected that the critical collapse appears around the threshold. In this study, we examine the gravitational collapse of the spherically symmetric domain wall around the threshold of the black hole formation and show that the critical collapse appears. Furthermore, it is shown that the critical collapse of the spherically symmetric domain wall is similar to the one of the Einstein-massless scalar field theory. The result means that the structure of phase space which is related to the critical collapse is similar to the one in the case of the Einstein-massless scalar filed theory, at least in our parameter region.

Secondly, we focus on critical behavior in an oscillon of the Einstein-scalar field theory with the double-well potential. As is mentioned above, the oscillon solution exists in the scalar field theory with the double-well potential in the Minkowski background, and when the initial parameter is fine-tuned to critical value, the critical behavior in the lifetime of the oscillon appears. Therefore, it is expected that in the weak gravity case of the Einstein-scalar field theory with the double well potential, the oscillon solutions exist, and the critical behavior appears. In this study, we examine the oscillon in the Einstein-scalar field theory with the double-well potential, and the critical behavior, and show that the oscillon naturally appears in the theory. Furthermore, it is shown that a new type of the critical behavior may appear. The result means that the gravity changes the structure of the phase space which is associated with the critical behavior of the oscillon.

This thesis is organized as follows: In chap.2, we review the fundamental properties of the critical behavior, the standard picture by using the phase space, and other developments. Chap.3 is devoted to the critical behavior in the domain wall collapse. and chap.4 is devoted to the critical behavior of the oscillon.

Chapter 2

Fundamental properties of critical behavior

In this chapter, we review fundamental properties of the critical behavior in non-linear dynamical systems [1, 2].

2.1 Critical behavior in gravitational collapse

Critical behavior in gravitational collapse, which is often called "critical collapse", is firstly discovered with sophisticated numerical simulations of the Einstein-massless scalar field theory in a spherically symmetric spacetime by M.Choptuik in 1993 [3]. After the Choptuik's discovery, many researchers observed similar behavior. Let us introduce the Choptuik's original work.

He considered a spherically symmetric gravitational collapse in the Einstein-massless scalar field theory and used the areal radius as a radial coordinate (the polar-radius coordinates). Then, the line element is

$$ds^2 = -\alpha^2(t,r)dt^2 + a^2(t,r)dr^2 + r^2 d^2\Omega, \tag{2.1}$$

where α is the lapse function. α and a are functions of t and r. The Einstein equations are expressed as

$$(\Phi')^{\cdot} = \left(\frac{\alpha}{a}\Pi\right)', \tag{2.2}$$

$$\dot{\Pi} = \frac{1}{r^2}\left(r^2\frac{\alpha}{a}\Phi'\right)', \tag{2.3}$$

$$\frac{\alpha'}{\alpha} = \frac{a'}{a} - \frac{1-a^2}{r}, \tag{2.4}$$

$$\frac{a'}{a} = -\frac{a^2-1}{2r} + 2\pi r(\Pi^2 + \Phi'^2), \tag{2.5}$$

where the dot and the prime denote the t-derivative and the r-derivative, respectively. Π is defined as $\Pi \equiv a\dot{\Phi}/\alpha$, where Φ is the scalar field. His numerical method consists of two steps : (1) The scalar field Φ is evolved forward in time by using Eqs.(2.2-2.3). (2) The lapse function α and a in next time step are determined

by solving Eqs.(2.4-2.5) along the radial direction from the center. When Eq.(2.5) is solved, the regularity condition $a(r = 0, t) = 1$ is imposed. The scheme, in which the constraint equations are solved in each time step is so called a "fully constrained" scheme. As will be discussed in App.A.2.1, the origin in spherically symmetric spacetime often becomes a source of numerical instability, and we must pay the attention to numerical schemes for stability in the origin. He overcame the numerical instability by using the above fully constrained scheme.

Let us prepare a one-parameter family of initial data sets which has a parameter p characterizing the strength of the initial energy of the scalar field, and suppose that p has a threshold p_* of a black hole formation, that is, a black hole finally is formed for $p > p_*$ (supercritical region) and the black hole is not formed and the scalar field dissipates for $p < p_*$ (subcritical region). Under this setup, he examined the gravitational collapse of the family of initial data set and discovered the following interesting phenomena: (1) Near the threshold, the intermediate state of the time evolution does not change, even if other one-parameter family of initial data sets with the threshold is used. This intermediate state is a so called "critical solution". The profile of the scalar field of the critical solution is denoted by Φ_*. (2)The critical solution has a discrete self-similar symmetry, that is, the profile of the scalar field $\Phi_*(t, r)$ satisfies

$$\Phi_*(t, r) = \Phi_*(e^{\Delta}t, e^{\Delta}r), \tag{2.6}$$

where $\Delta \simeq 3.44$. (3)In the supercritical region, the black hole mass $M_{\rm BH}$ obeys the scaling law

$$M_{\rm BH} \propto |p - p_*|^{\nu}, \tag{2.7}$$

where $\nu \simeq 0.374$, and this value does not also change, even if other one-parameter family of initial data sets with the threshold is used. Above three properties were founded by Choptuik, and are called "critical collapse".

After the Choptuik's discovery, many researchers have analyzed the critical collapse, and there are a lot of progress. Here, we explain three developments of them. The first development is that the critical behavior was found in gravitational collapse of many other matter coupled to gravity. Abraham et al. [4] observed the critical behavior of a vacuum axisymmetric gravitational collapse. Recently, E.Sorkin [5] also studied the critical collapse in the system, in more detail. Evans et al. [6] discovered the critical behavior in gravitational collapse of a radiation fluid. According to their studies, the index of the mass scaling is about 0.37, which is close to the observed value in the massless scalar case. On the other hand, the property of the critical solution is different. Although the critical solution of the critical behavior in the massless scalar collapse has a discrete self-similarity, the critical solution in a radiation fluid has a continuous self-similarity. Furthermore, Maison [7] showed that in the perfect fluid collapse case, the index of the mass scaling depends on the parameter of the equation of state. In addition, Garfinkle et al. [8] and Sorkin [9] showed that the index of mass scaling depends on the spacetime dimension, in the massless scalar case.

The second development is that a fine structure of mass scaling for the critical collapse of the massless scalar theory was found. C.Gundlach predicted the fine

structure from the discrete self-similarity of the critical solution [10] and Hod at al [11] checked it numerically. The mass behavior which was predicted by them is

$$\ln M_{\rm BH} = \nu \ln |p - p_*| + f(\ln |p - p_*|) + C, \tag{2.8}$$

where $f(x)$ is a periodic function satisfying $f(x + \varpi) = f(x)$, and C is a constant. The period ϖ is about 4.6, and this value also does not change, even if other one-parameter family of initial data sets with the threshold is used. The third development is to clarify the reason why the behavior does not change even if the one-parameter family of initial data sets changes. We will explain it in the next section.

2.2 Renormalization group approach

Koike et al. [12] showed that the universality of the critical collapse is related to a structure of the phase space in the case of a radiation fluid. In this section, we summarize their statement.

Let us consider spherically symmetric gravitational collapse of a radiation fluid. Firstly, we prepare a one-parameter family of initial data sets which is labeled by p, and focus on the critical solution which appears as the intermediate state of the gravitational collapse around the threshold of black hole formation p_*. Since the critical solution of this system has a continuous self-similar solution, there is a homothetic vector field ξ, which satisfies $\mathcal{L}_\xi g_{\mu\nu} = -2g_{\mu\nu}$ (see App.C). There is a coordinate (τ, x, θ, ϕ) adopted to the homothety. In the coordinate, the τ dependence of the metric is determined as $g_{\mu\nu}(\tau, x, \theta, \phi) = l^2 e^{-2\tau} \bar{g}_{\mu\nu}(x, \theta, \phi)$, where l is the constant which has a length scale, and the homothetic vector is given as $\xi \equiv \frac{\partial}{\partial \tau}$. Let us introduce another coordinate (t, r, θ, ϕ), which is defined as

$$t \equiv -le^{-\tau}, \tag{2.9}$$

$$r \equiv -tx. \tag{2.10}$$

From the definition of t, the region which is spanned by the coordinate (τ, x, θ, ϕ) corresponds to the region of $t < 0$. The line element can be expressed as

$$ds^2 = l^2 e^{-2\tau}(Ad\tau^2 + 2Bd\tau dx + Cdx^2 + F^2 d\Omega^2), \tag{2.11}$$

$$= (A + 2xB + x^2 C)dt^2 + 2(B + xC)dtdr + Cdr^2 + t^2 F^2 d\Omega^2, \tag{2.12}$$

where A, B, C, F are functions of x. Furthermore, we can take the areal-polar gauge after an appropriate coordinate transformation of (t, r). In the areal-polar gauge, we can get the final state of the spacetime. On the other hand, since the region which is spanned by the coordinate (τ, x, θ, ϕ) corresponds to the region of $t < 0$, the coordinate does not cover the final state, in general. If we can set $p = p_*$ exactly, the spacetime approaches the critical solution as $\tau \to \infty$ which is $t = 0$. On the other hand, the spacetime around the threshold p_* approaches the critical solution, and after that, the spacetime starts to go away from the critical solution.

Here, we denote the dynamical variables as $Z(t, r) = \{$"metric function", "matter"$\}$ or $Z(\tau, x)$, and consider a perturbation around the critical solution which is spanned

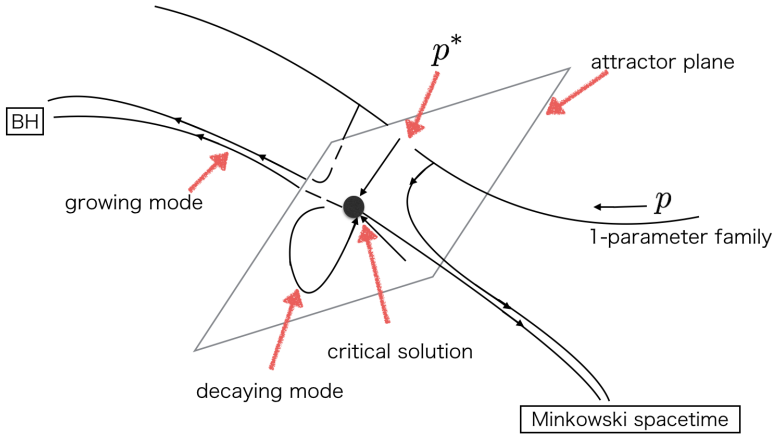

Figure 2.1: The phase space structure.

by the coordinate (τ, x, θ, ϕ). The spherically symmetric gravitational collapse of the radiation fluid has following important properties.

- The equations of motion do not have a typical scale.
- The linear perturbations around the critical solution has a unique growing mode, and other modes are decaying modes. That is, when the perturbation modes which are determined from the linear homogeneous differential equations under the appropriate boundary conditions is denoted as $\delta Z_{(i)} = e^{\kappa_{(i)}\tau} Z_{p(i)}(x)$, $\mathrm{Re}(\kappa_1) > 0$, and $\mathrm{Re}(\kappa_i) < 0$ for $i > 1$. $\mathrm{Re}(\kappa_1)$ is called "Lyapunov exponent". This means that the critical solution is a co-dimension one attractor in the phase space. The attractor plane of the critical solution is called "critical surface" or "stable manifold".

Focusing on these properties, we consider the time evolution of the initial data around the threshold. Since the intermediate state approaches the critical solution, the state in this stage can be approximated as a sum of the critical solution and the perturbation around it;

$$Z(\tau, x) \simeq Z_{\mathrm{CS}}(x) + \sum_i C_i(p) e^{\kappa_{(i)}\tau} Z_{p(i)}(x), \tag{2.13}$$

where $Z_{\mathrm{CS}}(x)$ denotes the critical solution, and $C_i(p)$ is a coefficient of each perturbation mode which depends on the initial parameter. From the second property, $i = 1$ mode grows and dominates later, that is, total variable $Z(\tau, x)$ is given as follows:

$$Z(\tau, x) \simeq Z_{\mathrm{CS}}(x) + C_1(p) e^{\kappa_{(1)}\tau} Z_{p(1)}(x). \tag{2.14}$$

If the initial parameter p is exactly equal to p_*, the spacetime approaches the critical solution, and the perturbation mode $Z_{p(1)}(x)$ does not dominate. Therefore,

when $p = p_*$, the coefficient $C_i(p)$ must vanish, and we have

$$C_1(p) = \bar{C}_1(p - p_*) + \mathcal{O}((p - p_*)^2), \tag{2.15}$$

where $\bar{C}_1$ is a constant. By using this expression, we get

$$Z(\tau, x) \simeq Z_{\rm CS}(x) + \bar{C}_1(p - p_*)e^{\kappa_{(1)}\tau} Z_{p(1)}(x). \tag{2.16}$$

Let us define $\tau_{\rm p}$ as a typical time in which the second term dominates, that is;

$$|\bar{C}_1(p - p_*)|e^{{\rm Re}(\kappa_{(1)})\tau_{\rm p}} = \epsilon, \tag{2.17}$$

where ϵ is a fixed small constant. From this equation, τ_p is given as

$$\tau_{\rm p} = -{\rm Re}(\kappa_{(1)})^{-1} \ln|p - p_*| + {\rm const.} \tag{2.18}$$

The state at $\tau = \tau_p$ is of the form

$$Z(\tau_p, x) \simeq Z_{\rm CS}(x) \pm \epsilon Z_{p(1)}(x), \tag{2.19}$$

where the plus sign corresponds to the supercritical case, and the minus sign corresponds to the subcritical case. Going back to the coordinate (t, r), we have

$$Z(t(\tau_p), r) \quad \simeq \quad Z_{\rm CS}(\frac{r}{L_p}) \pm \epsilon Z_{p(1)}(\frac{r}{L_p}), \tag{2.20}$$

where L_p is defined as

$$L_p \quad \equiv \quad l e^{-\tau_p}. \tag{2.21}$$

The important point of Eq.(2.20) is that the profile depends on only r/L_p. From the first property, the equation of motion does not have the typical length scale and the time evolution after this stage can be described as

$$Z(t, r) = f_{\pm}(\frac{t}{L_p}, \frac{r}{L_p}), \tag{2.22}$$

where the subscript $\pm$ denotes a supercritical $(+)$ and a subcritical $(-)$. In the supercritical region, a black hole appears after the intermediate state. Because the black hole mass M has a length scale, it is proportional to $L_{\rm p}$, that is

$$M \propto L_{\rm p} \propto |p - p_*|^{{\rm Re}(\kappa_{(1)})^{-1}}. \tag{2.23}$$

This is just a scaling law, and we have

$$\nu = \frac{1}{{\rm Re}(\kappa_{(1)})}. \tag{2.24}$$

Therefore, the index of the mass scaling law is related to the Lyapunov exponent of the system, and this is the origin of the universality of the index of the mass scaling.

In [12], in order to check that the above picture is correct, they constructed the critical solution in the gravitational collapse of radiation fluid and calculated the Lyapunov exponent, and finally, showed that the index which was given in [6] is related to the Lyapunov exponent in Eq.(2.24). In the case of the other system, the validity of above picture also has discussed (see App.D).

2.3 Further developments

In this subsection, the further developments are discussed.

2.3.1 Curvature scaling in subcritical region

The above picture of the critical behavior shows that the several quantities which have a length scale obey the scaling law. Therefore, it is expected that the scaling law of such quantities in a subcritical region also obeys the scaling law. In fact, in Ref. [13], Garfinkle et al. examined the critical collapse in massless scalar field, and showed that the maximal value of the curvature at the center $R_{\max}$ obeys the scaling law;

$$R_{\max}(p) = -2\nu \ln |p_* - p| + f(\ln |p - p_*|), \tag{2.25}$$

where ν is about 0.374 and the function $f(x)$ is a periodic function with the period about 4.6.

2.3.2 Type of critical behavior

In Sec.2.2, it was shown that the critical behavior deeply is related to the structure of the phase space in the system. In particular, Eq.(2.20) means that the symmetry of the critical solution is associated with the time evolution after the critical solution. In Einstein-massless scalar field theory, the critical solution has a discrete self-similarity and the behavior of the black hole mass obeys the scaling law with a wiggle. These points are different from the radiation fluid case and it implies that the discrete self-similarity is related to the wiggle around the mass scaling. In Ref. [10], Gundlach examined the critical collapse in a massless scalar field, and showed that the discrete self-similarity is associated with the wiggle around the mass scaling. Furthermore, he derived the following relation between the period of the wiggle ϖ and the period of the discrete self-similarity Δ;

$$\varpi = \frac{\Delta}{2\nu}. \tag{2.26}$$

In fact, this relation is satisfied in the case of critical collapse in massless scalar field. We discuss the detail of the relation in App.D.2.

Today, it is known that there are mainly two types of the critical collapse, and these are called "type I critical behavior" or "type II critical behavior" from the analogy of the phase transition. In the case of "type I critical behavior", the black hole mass does not converge to zero at the threshold, and the time τ until the black hole formation obeys the scaling law;

$$\tau = \nu \ln |p - p_*| + C, \tag{2.27}$$

where ν is a constant which is universal with respect to the parameterization of a family of the initial data set, and C is a constant (see App.D.1). The critical solution of type I critical behavior is a static solution, time-periodic solution, or long lifetime solution.

On the other hand, type II critical behavior can be divided into two cases. In the gravitational collapse of the perfect fluid, the black hole mass around the threshold obeys the scaling law;

$$M_{\rm BH} \propto |p - p_*|^{\nu}, \tag{2.28}$$

and, the critical solution has a continuous self-similarity. In this case, these behaviors are called type II critical behavior associated with the continuous self-similar solution. In the Einstein-massless scalar field theory, the black hole mass obeys scaling law with wiggle, that is

$$\ln M_{\rm BH} = \nu \ln |p - p_*| + f(\ln |p - p_*|), \tag{2.29}$$

where $f(x)$ is a periodic function satisfying $f(x+\varpi) = f(x)$. The critical solution is a discrete self-similar solution. This is called the type II critical behavior associated with the discrete self-similar solution.

2.3.3 Phase diagram

As is mentioned in the above subsection, it is known that there are type I and type II critical behaviors. In the case of type II critical behavior, it is important that the equation of motion does not contain the typical scale parameter. Therefore, it is expected that type II critical behavior does not appear in Einstein-massive scalar field theory. However, actually, in the Einstein-massive scalar field theory, the type of the critical collapse depends on the family of the initial data set, and we can get a nontrivial phase diagram for the critical behavior [15, 16]. Generally, even if a theory has a typical length scale, when the scale becomes the dynamically irrelevant, type II critical behavior can appear.

Here we summarize the result of [15, 16]. They considered the gravitational collapse in the Einstein-massive scalar field theory, and assumed that the initial data have two parameters w and A. w is a typical width of the profile of the scalar field, and A is an amplitude of it. Then, the type of the critical behavior for initial parameter A depends on the ratio of the Compton wavelength of the scalar field to w. When the Compton wavelength is larger than w, the type II critical behavior appears. On the other hand, when the Compton wavelength is shorter than w, type I critical behavior appears. Furthermore, it is known that the oscilaton in this system plays an important role in this phase diagram. The oscilaton is a solution which is a longevity and localized solution in the Einstein massive scalar field theory [17]. It is known that the critical collapse in a SU(2) Yang-Mills field also have such a non-trivial phase diagram [18].

2.3.4 Non-spherically symmetric spacetime

As was mentioned in Sec.2.2, an important point of the critical behavior is that the critical solution has only one growing perturbation mode. Therefore, even if the critical collapse appears in a spherically symmetric spacetime, the question whether the critical collapse appears in a non-spherically symmetric spacetime is a

non-trivial problem. In order to resolve the time evolution of the critical collapse, high-resolution numerical simulation is needed, and it is hard to calculate the time evolution of the critical collapse beyond the spherically symmetric spacetime.

J.M.Martin-Garcia et al. [19] constructed the critical solution of the critical collapse of a massless scalar field and examined non-spherical perturbations around the critical solution. As a result, they showed that all non-spherical perturbation modes around the critical solution are decaying modes. Therefore, the critical solution in the spherically symmetric spacetime is also the critical solution of the critical collapse in the non-spherically symmetric spacetime. After their analysis, the numerical simulation of the critical collapse in axisymmetric spacetime was performed by Choptuik, at al. [20]. Their numerical simulation predicted that an unstable non-spherical perturbation mode exits. The existence of such a mode is conflict with the result of [19]. Although they discuss whether the unstable non-spherical perturbation mode is a numerical artifact, they did not conclude it. Furthermore, the numerical simulation of the critical collapse in the axisymmetric spacetime with angular momentum was examined in Ref. [21]. The critical collapse beyond axisymmetric spacetime were also studied [22].

2.4 Critical behavior of the oscillon

In Sec.2.2, the origin of the critical collapse is the non-trivial structure of the phase space. Therefore, if the non-linear system without gravity has a similar phase structure, the system also has the critical behavior. In this section, as such an example, we introduce a critical behavior of a ocsillon in a scalar field with double well potential in the Minkowski background.

Oscillons are a localized, time-dependent and longevity solutions of a scalar field with a non-linear potential on the Minkowski background [48, 49]. Although the lifetime of these solutions is long, it is finite. The simple form of the potential of the scalar field is a double-well potential[1]:

$$V(\Phi) = \frac{1}{4}(\Phi^2 - 1)^2. \tag{2.34}$$

[1]In general, the double-well potential of a scalar field $\tilde{\Phi}$ is given as

$$V(\tilde{\Phi}) = \frac{\lambda}{4}(\tilde{\Phi}^2 - \sigma^2)^2, \tag{2.30}$$

where λ and σ are constants. Here, the dimensionful polar coordinate of Minkowski spacetime is denoted as $(\tilde{t}, \tilde{r}, \theta, \phi)$. We have Eq.(2.34) and Eq.(2.35) by the following redefinition:

$$t = m\tilde{t}, \tag{2.31}$$
$$r = m\tilde{r}, \tag{2.32}$$
$$\Phi = \tilde{\Phi}/\sigma, \tag{2.33}$$

where m is defined as $m = \sqrt{\lambda\sigma^2}$. In this section, we use the dimensionless quantities t, r, Φ. Each dimensionful quantities are given by using Eqs.(2.31)-(2.33).

The equation of motion of the scalar field is given as

$$\frac{\partial^2}{\partial t^2}\Phi = \left(\frac{\partial^2}{\partial r^2} + \frac{2}{r}\frac{\partial}{\partial r}\right)\Phi - V'(\Phi), \tag{2.35}$$

where $V'(\Phi)$ is the Φ derivative of the potential. The lifetime of oscillons of this potential has about $10^3 - 10^4$. When the scalar field inside and outside of the closed region are different vacuum, the boundary of the region is called a bubble. Oscillons generally can be formed by the bubble collapse. Therefore, after the inflation, the fluctuation of the inflaton field might lead to form the oscillons.

Here, to explain the fundamental properties of the oscillon, let us consider the time evolution of the oscillon. The initial data on which we focus here is a Gaussian bubble, as follows:

$$\Phi(t = 0, r) = -1 + 2e^{-r^2/r_0^2}, \tag{2.36}$$

where r_0 is a radius of the Gaussian bubble. For the purpose of comparison of the oscillon with a solution of a massive scalar field, we solve the time evolution of the Gaussian bubble in the massive scalar field. In this case, we can solve the equation, analytically, and have an envelope of the scalar field at the origin decay as $t^{-3/2}$. Therefore, in the massive scalar field, the amplitude of the scalar field decreases monotonically.

On the other hand, we numerically examine the evolution of the Gaussian bubble of the scalar field with the double-well potential. In order to understand the typical evolution, let us focus on the time evolution of the energy of the scalar field inside the sphere which has the large radius and of the scalar field at the origin (see Fig.2.2). From the left panel of Fig.2.2, the amplitude of the scalar

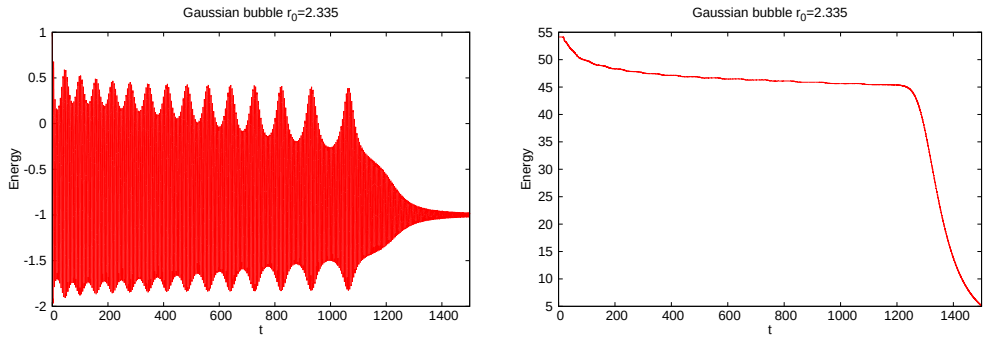

Figure 2.2: The evolution of the scalar field the origin, and the energy inside the sphere.

field does not decrease monotonically but modulates. This behavior is one of the features of the oscillons. From the right panel of Fig.2.2, there are three phases in the time evolution. In the first phase, the energy of the scalar field in the sphere decrease. After the energy is reduced, the second phase appears. Here, this phase is called an "oscillon phase". In the second phase, the energy is almost conserved, and is about 44. This value is the oscillon's energy, and it does not depend on r_0.

After the oscillon phase, the scalar field dissipates, soon. Even if the initial data is the Gaussian bubble, there are the cases in which the oscillon does not appear (see Fig.2.3). The necessary condition for oscillon formation is that the initial energy

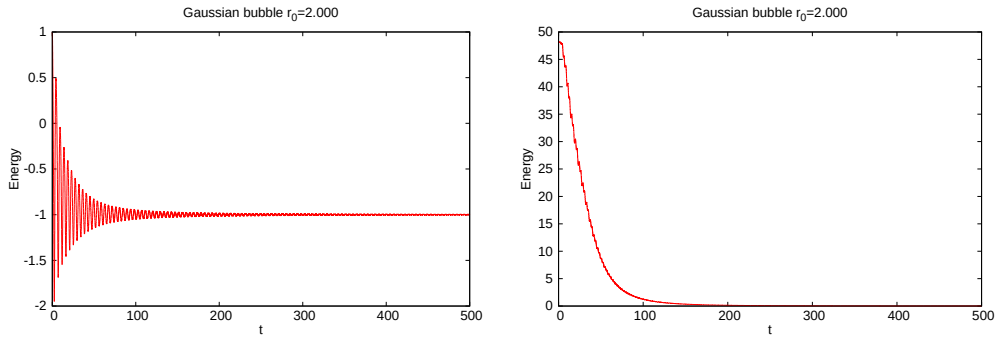

Figure 2.3: The evolution of the scalar field the origin, and the energy inside the sphere.

of the scalar field is larger than the oscillon energy.

Next, let us explain the critical behavior of the oscillon. The critical behavior of the oscillon was found in Ref. [50, 51]. They examined the relation between the oscillon's lifetime and the initial bubble radius, in detail. As a result, they found the resonant behavior in the relation. That is, when r_0 is tuned to some value r_{0*}, the lifetime τ of the oscillon obeys the scaling law:

$$\tau \simeq -\gamma \ln |r_0 - r_{0*}|. \tag{2.37}$$

Around the r_{0*}, the number of the modulation of the scalar field changes. That is, if the number of modulation is n in $r_0 < r_{0*}$, it is $n+1$ or $n-1$ in $r_0 > r_{0*}$. The critical solution corresponds to $r_0 = r_{0*}$. It is known that the fine structure appears repeatedly. Since the powers of the scaling are different in each resonant behavior, the critical solutions are different.

2.5 Einstein-scalar field theory with double-well potential

In this study, we consider the Einstein-scalar field theory with a double-well potential, which action is given as:

$$S = \int d^4x\sqrt{-g}\left\{\frac{R}{16\pi} - \frac{1}{2}\nabla_\mu\Phi\nabla^\mu\Phi - V(\Phi)\right\}, \tag{2.38}$$

where Φ is a scalar field, and $g_{\mu\nu}$ is the metric of the spacetime. R is the scalar curvature with respect to $g_{\mu\nu}$. $V(\Phi)$ is the double-well potential, which is given as follows:

$$V(\Phi) = \frac{\lambda}{24}(\Phi^2 - \sigma^2)^2, \tag{2.39}$$

where λ and σ are constants. In this system, there are two remarkable solutions. The first solution is a domain wall solution. The domain wall is one of the topological defects which may play an important role in the early universe. The fundamental properties of the domain wall are summarized in Sec.2.5.1. The second solution is the oscillon which is a longevity time-dependent localized solution. As was mentioned in Sec.2.4, the scalar field with the double-well potential in Minkowski background allows an oscillon profile. Therefore, at least, in the weak gravity limit, it is expected that the oscillon can appear after the bubble collapse.

The Einstein-scalar field theory with the double-well potential is similar to the Einstein massive scalar field theory in following two points. The first similar point is that there is a typical length scale in the action, which is $1/\sigma\sqrt{\lambda}$. The second similar point is an existence of a longevity localized solution. In the case of the scalar field with double-well potential, the solution is the oscillon, and in the case of the massive scalar field, the solution is an oscillaton [17]. As was mentioned in Sec.2.3.3, the oscillaton and the typical length scale of the system play an important role in the nontrivial phase diagram for the critical collapse in the massive scalar field. Therefore, in the Einstein-scalar field theory with the double-well potential, the nontrivial phase diagram also may appear in the critical behavior of the gravitational collapse.

The goal of this study is to clarify the characteristic structure of the phase space of this system through the critical behavior of the gravitational collapse and the oscillons. As a first step, we examine the critical collapse of this system in Chap.3. Secondly, we analyze the properties of the oscillons in weak gravity case and its critical behavior in Chap.4.

In the following, we summarize the fundamental behavior of the domain wall in flat spacetime.

2.5.1 Domain wall in flat spacetime

A domain wall is one of topological defects. Other examples of topological defects are a cosmic string, monopole, and texture. Topological defects are solutions of the scalar field which has a nontrivial vacuum structure. The homotopy of the vacuum manifold of the potential determines which topological defect appears. Such a scalar field is often suggested in the field theory beyond the standard model of the particle physics. Therefore, the topological defect may exist in the early universe, and in order to understand the role of the domain wall in the universe, it is important to understand the dynamical properties of topological defects coupled with gravity.

Here, we summarize the fundamental properties of the domain wall. When the potential of the scalar field has two disconnected vacua, the domain wall profile may exist. A typical example of the potential is a double-well potential:

$$V(\Phi) = \frac{\lambda}{24}(\Phi^2 - \sigma^2)^2, \tag{2.40}$$

where λ and σ are the parameters. $\pm\sigma$ correspond to the vacua of the potential. When the scalar field stays different vacuum in two spatial regions, the boundary

of the regions become the domain wall. Ignoring the effect of the gravity for simplicity, we have the field equation as follows:

$$\left(-\frac{\partial^2}{\partial t^2}+\nabla^2\right)\Phi = V'(\Phi). \tag{2.41}$$

Let us focus on the domain wall which is static and spread along x and y-direction. Then, the scalar field satisfies

$$\frac{\partial^2}{\partial z^2}\Phi = V'(\Phi). \tag{2.42}$$

The solution of this equation is

$$\Phi(x,y,z,t) = \sigma \tanh\left(\frac{z-z_0}{l}\right), \tag{2.43}$$

where l is the width of the domain wall, which is given by

$$l = \frac{2}{\sigma}\sqrt{\frac{3}{\lambda}}. \tag{2.44}$$

This profile expresses the static planar domain wall which spreads along x and y-axis. The energy-momentum tensor of the scalar field is given as

$$T_{\mu\nu} = -\left(\frac{\sigma}{l}\right)^2 \mathrm{diag}(-1,1,1,0). \tag{2.45}$$

In the above discussion, the effect of the self-gravity is neglected. However, when the energy of the domain wall is large, the self-gravity of the domain wall cannot be neglected. Then, we must analyze the time evolution of the Einstein-scalar field theory with the double-well potential.

Chapter 3

Critical behavior of domain wall collapse

In this chapter, we consider the critical collapse of the domain wall in the Einstein-scalar field theory with the double well potential, and examine the influence of the double well potential on the critical collapse.

3.1 Numerical scheme

In this section, we explain the formulation and the numerical scheme which are used in the study.

3.1.1 Formulation

We consider the Einstein-scalar field theory with double-well potential. The Lagrangian of this system is given as Eq.(2.38). From the Lagrangian, we have the equation of motion;

$$G_{\mu\nu} = 8\pi G\left(-\frac{1}{2}g_{\mu\nu}(\nabla\Phi)^2 + \nabla_\mu\Phi\nabla_\nu\Phi - g_{\mu\nu}V(\Phi)\right), \tag{3.1}$$

$$\nabla^2\Phi = V'(\Phi), \tag{3.2}$$

where $V(\Phi)$ is the double-well potential Eq.(2.39).

The line element of the spherically symmetric spacetime based on the ADM formalism can be rewritten as:

$$ds^2 = -\alpha^2 dt^2 + \gamma_{rr}(dr + \beta^r dt)(dr + \beta^r dt) + \gamma_{\theta\theta}d^2\Omega, \tag{3.3}$$

where α, β^r, γ_{rr} and $\gamma_{\theta\theta}$ are the lapse function, the radial component of the shift vector, the (r, r) component of the spatial metic, and (θ, θ) component of the spatial metric, respectively. These variables are the function of t and r. The solid angle element $d\Omega^2$ is defined as

$$d\Omega^2 = d\theta^2 + \sin^2\theta d\phi^2. \tag{3.4}$$

In this study, we do not use the variable α, β^r, γ_{rr} and $\gamma_{\theta\theta}$ as the numerical variable, but we decompose these variables referring to BSSN formulation. By using the conformal decomposition, ψ is defined as

$$\psi(t,r) = \left(\frac{\det(\gamma_{ij})}{\det(\bar{\gamma}_{ij})}\right)^{\frac{1}{12}}, \tag{3.5}$$

where $\bar{\gamma}_{ij}$ is defined as:

$$\bar{\gamma}_{ij} = \mathrm{diag}(1, r^2, r^2\sin^2\theta). \tag{3.6}$$

By using ψ, the conformal metric is defined as:

$$\tilde{\gamma}_{ij} = \psi^{-4}\gamma_{ij}. \tag{3.7}$$

From Eqs.(3.6)(3.7), the determinant of $\tilde{\gamma}_{ij}$ becomes;

$$\det(\tilde{\gamma}_{ij}) = r^4\sin^2\theta. \tag{3.8}$$

Therefore, the component of $\tilde{\gamma}_{ij}$ can be parameterized as follows:

$$\tilde{\gamma}_{ij} = \mathrm{diag}(\gamma^{-2}, \gamma r^2, \gamma r^2\sin^2\theta), \tag{3.9}$$

where γ is a function of t and r. Therefore, the line element of the spacetime can be expressed as

$$ds^2 = -\alpha^2(t,r)dt^2 + \psi^4(t,r)\left\{\gamma(t,r)^{-2}(dr + r\beta(t,r)dt)^2 + \gamma(t,r)r^2d\Omega^2\right\}, \tag{3.10}$$

where β is defined as $\beta \equiv \beta^r/r$. The extrinsic curvature K_{ij} of the spherically symmetric spacetime has two independent components, that is K_{rr} and $K_{\theta\theta}$. I use the following variables as the numerical variables:

$$K \equiv \gamma^{ij}K_{ij}, \tag{3.11}$$

$$A \equiv \frac{K_{\theta\theta} - \frac{1}{3}K\gamma_{\theta\theta}}{\psi^4 r^2}, \tag{3.12}$$

From Einstein equations, we get the following evolution equations:

$$(\partial_t - r\beta\partial_r)\psi = \frac{1}{6}\psi(3\beta + r\beta' - \alpha K), \tag{3.13}$$

$$\begin{aligned}(\partial_t - r\beta\partial_r)K &= \alpha\left\{\frac{1}{3}K^2 + 6\frac{A^2}{\gamma^2} + 8\pi\Pi^2 - 8\pi V(\Phi)\right\} \\ &\quad -\psi^{-4}\gamma^2\left\{\Delta\alpha + 2\alpha'(\frac{\psi'}{\psi} + \frac{\gamma'}{\gamma})\right\},\end{aligned} \tag{3.14}$$

$$(\partial_t - r\beta\partial_r)\gamma = -2\alpha A - \frac{2}{3}r\gamma\beta', \tag{3.15}$$

$$(\partial_t - r\beta\partial_r)A = \alpha KA - 2\alpha\frac{A^2}{\gamma} - \frac{2}{3}rA\beta' + \psi^{-4}\left\{-\frac{1}{6}\gamma^3(\Delta\alpha - 3\alpha'') - \frac{1}{3}\alpha\gamma^3(\frac{\Delta\psi}{\psi} - 3\frac{\psi''}{\psi})\right.$$

$$-\frac{1}{6}\alpha(1+\gamma)\Delta\gamma+\frac{1}{6}\alpha(1+\gamma+\gamma^2)\gamma''-\frac{1}{3}\alpha(1+\gamma+\gamma^2)(-\frac{\gamma-1}{r^2}+\frac{\gamma'}{r})$$
$$+\frac{1}{6}\alpha'\gamma^2\gamma'-\frac{4}{3}\alpha'\gamma^3\frac{\psi'}{\psi}+\frac{1}{3}\alpha\gamma^2\gamma'\frac{\psi'}{\psi}-2\alpha\gamma^3\frac{\psi'^2}{\psi^2}+\frac{8}{3}\pi\alpha\gamma^3\Phi'^2\Big\}, \qquad (3.16)$$

where a prime denotes the derivative with respect to r. From the equation of motion of the scalar field, we have

$$(\partial_t - r\beta\partial_r)\Phi = -\alpha\Pi, \qquad (3.17)$$
$$(\partial_t - r\beta\partial_r)\Pi = \alpha\Pi K - \psi^{-4}\alpha\gamma^2\left\{\Delta\Phi + 2\Phi'(\frac{\gamma'}{\gamma}+\frac{\psi'}{\psi}+\frac{\alpha'}{2\alpha})\right\} + \alpha V'(\Phi), \qquad (3.18)$$

where Π is the conjugate momentum of Φ. The Hamiltonian constraint and the momentum constraint are written as

$$\frac{\Delta\psi}{\psi}+\frac{1}{8}(5\frac{\Delta\gamma}{\gamma}-3\frac{\gamma''}{\gamma})+\pi\Phi'^2+2\pi\gamma^{-2}\psi^4V(\Phi)$$
$$+\frac{(\gamma^2+\gamma+1)(\gamma-1)}{4\gamma^3r^2}+\frac{\gamma'}{\gamma}(2\frac{\psi'}{\psi}+\frac{3}{16}\frac{\gamma'}{\gamma})+\frac{\psi^4}{\gamma^2}(\frac{3A^2}{4\gamma^2}+\pi\Pi^2-\frac{1}{12}K^2) = 0, \qquad (3.19)$$
$$A'+\frac{\gamma}{3}K'+4\pi\gamma\Pi\Phi'+\frac{3A}{r}+\frac{A\gamma'}{2\gamma}+6A\frac{\psi'}{\psi} = 0. \qquad (3.20)$$

As is discussed in App.A.2.1, we must pay attention to the boundary condition at the origin. The $1/r$ and $1/r^2$ terms in the evolution equations and constraint equations are regularized by the boundary condition. However, even if the boundary conditions are imposed, these terms may become the origin of the numerical instabilities at the center. In this study, in order to avoid the numerical instability, we evaluate the Hamiltonian constraint Eq.(3.19) by using the following auxiliary field;

$$\Gamma \equiv \gamma' + \frac{3}{r}(\gamma-1). \qquad (3.21)$$

By using Γ, the Hamiltonian constraint becomes

$$\frac{\Delta\psi}{\psi}+\frac{1}{8}(5\frac{\Delta\gamma}{\gamma}-3\frac{\gamma''}{\gamma})+\pi\Phi'^2+2\pi\gamma^{-2}\psi^4V(\Phi)+\frac{\gamma^2+\gamma+1}{8\gamma^3}(\Delta\gamma-\frac{1}{3}\gamma''-\frac{2}{3}\Gamma')$$
$$+\frac{\gamma'}{\gamma}(2\frac{\psi'}{\psi}+\frac{3}{16}\frac{\gamma'}{\gamma})+\frac{\psi^4}{\gamma^2}(\frac{3A^2}{4\gamma^2}+\pi\Pi^2-\frac{1}{12}K^2) = 0. \qquad (3.22)$$

Furthermore, the evolution equation for Γ is

$$(\partial_t - r\beta\partial_r)\Gamma = \alpha\frac{\gamma'}{\gamma}A+8\pi\alpha\gamma\Pi\Phi'+12\alpha A\frac{\psi'}{\psi}+\frac{2}{3}\alpha\gamma K'-2\alpha'A-\frac{8}{3}\gamma\beta'$$
$$+\frac{1}{3}r\gamma'\beta'-\frac{2}{3}r\gamma\beta''+\beta\Gamma. \qquad (3.23)$$

We monitor the violation of Hamiltonian constraint (3.19) and (3.21) during the time evolution. Furthermore, we do not solve the Eq.(3.16), but solve the Momentum constraint Eq.(3.20) for A at each time step.

3.1.2 Boundary condition

To calculate the time evolution, the boundary condition must be imposed. The boundary conditions of the spherically symmetric spacetime are discussed in Sec.A.2.1. In this study, the boundary condition at the outer region is asymptotically Minkowski spacetime. As was mentioned in Sec.A.2.1, we must pay attention to the boundary condition at the origin. At first, in order that the fields are smooth at the origin, the Neumann boundary conditions are imposed on several variables:

$$\psi'|_{r=0} = K'|_{r=0} = \gamma'|_{r=0} = A'|_{r=0} = \Phi'|_{r=0} = \Pi'|_{r=0} = 0. \tag{3.24}$$

Furthermore, in order that the metric is conformally flat around the center, we have

$$\gamma(t, r = 0) = 1, \ A(t, r = 0) = 0. \tag{3.25}$$

The right-hand side of the evolution equations and constraint equations are regularized by the local flatness conditions Eq.(3.25). Therefore, these conditions make $1/r$, $1/r^2$ terms finite value. If these conditions are imposed on the initial data, and evolution equations can be exactly solved, the local flatness condition is kept for every time step. However, when the evolution equations are solved, numerically, these conditions can be violated due to the numerical error. Then, the $1/r$, $1/r^2$ terms may become the origin of numerical instability. As was discussed in the previous subsection, in order to avoid this instability, we define Γ and use the momentum constraint instead of the evolution equation of A.

3.1.3 Gauge conditions

In order to calculate the time evolution, we must impose the gauge conditions for the lapse function and the shift vector. In this subsection, we impose them.

For the shift vector, we use the normal coordinate:

$$\beta(t, r) = 0. \tag{3.26}$$

For the lapse function, we choose the Maximal slice condition. The maximal slice condition implies that the extrinsic curvature vanishes at all time;

$$K(t, r) = 0. \tag{3.27}$$

Imposing this equation on the evolution equation of K, we have the condition for the lapse function:

$$\Delta\alpha + 2\alpha'(\frac{\psi'}{\psi} + \frac{\gamma'}{\gamma}) = \alpha\psi^4\gamma^{-2}\left\{6\frac{A^2}{\gamma^2} + 8\pi\Pi^2 - 8\pi V(\Phi)\right\}. \tag{3.28}$$

This equation is solved with the boundary condition $\alpha'|_{r=0} = 0$ at each time step. Since this equation is invariant under the transformation: $\alpha \to k\alpha$, we can normalize α so that α is unity at the outer region.

3.1.4 Numerical scheme

As was mentioned in above subsection, we use the maximal slice condition and normal coordinate condition. Therefore, from Eq.(3.13), ψ does not evolve. In our numerical code, evolution equations Eqs.(3.15)(3.16)(3.17)(3.18)(3.23) are solved by using the iterative Crank-Nicolson scheme. Furthermore, in order to overcome the numerical instability, the spatial derivatives in $r < 0.01/\mu$ are evaluated by using the 2nd order central difference, and the spatial derivatives in $r < 0.01/\mu$ are evaluated by using the 4th order central difference. Since the Laplacian is singular around the center, following method is used:

$$\begin{aligned}\nabla^2 u &= \frac{u(x+\Delta h,y,z)-2u(x,y,z)+u(x-\Delta h,y,z)}{\Delta h^2} \\ &\quad +\frac{4}{\Delta h^2}(\tilde{u}(\sqrt{x^2+\Delta h^2},y,z)-u(x,y,z)),\end{aligned} \tag{3.29}$$

for 2nd order accuracy, and

$$\begin{aligned}\nabla^2 u &= \frac{-u(r+2\Delta)+16u(r+\Delta)-30u(r)+16u(r-\Delta)-u(r-2\Delta)}{12\Delta^2} \\ &\quad +\frac{-\tilde{u}(\sqrt{r^2+4\Delta^2})+16\tilde{u}(\sqrt{r^2+\Delta^2})-15u(r)}{3\Delta^2},\end{aligned} \tag{3.30}$$

for 4th order accuracy. The value $\tilde{u}$ is evaluated by using the Lagrange interpolation.

3.2 Initial data

In this section, we discuss the construction of the initial data.

In this study, we use the spherically symmetric, static domain wall as the initial data. Then, the profile of a scalar field is assumed to be the following form:

$$\Phi(r,t=0)=\sigma\tanh\left(\frac{r-r_0}{l}\right)+\sigma\left\{-1-\tanh\left(\frac{r-r_0}{l}\right)\right\}\exp\left\{-\left(\frac{r}{l}\right)^4\right\}, \tag{3.31}$$

where r_0 is the initial radius of the domain wall, and l is the width of the domain wall which is given as

$$l=\frac{2}{\sigma}\sqrt{\frac{3}{\lambda}}=\sqrt{\frac{2}{\mu^2}}. \tag{3.32}$$

Fig.3.1 shows the schematic picture of the profile of the scalar field. The first term in Eq.(3.31) corresponds to the domain wall profile. As r_0 becomes large, the first term approaches to the planar domain wall solution. The second term regularizes the scalar field at the origin: $\partial_r\Phi(t=0,r=0)=0$. The static condition of the initial data means that

$$K(t=0,r)=A(t=0,r)=\Pi(t=0,r)=0. \tag{3.33}$$

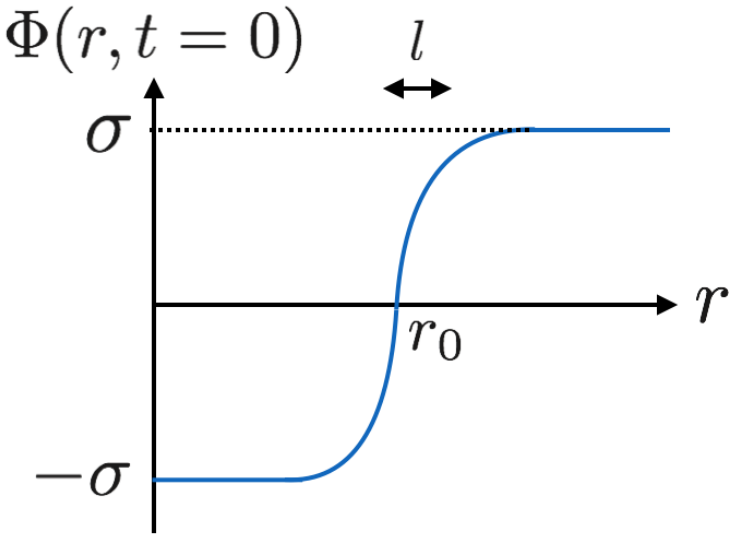

Figure 3.1: Initial profile of the scalar field.

The spatial components of the metric is assumed to be conformally flat, that is

$$dh^2 = \psi^4 \left(dr^2 + r^2 d\Omega^2 \right). \tag{3.34}$$

In other words, γ is unity on the initial data;

$$\gamma(t = 0, r) = 1. \tag{3.35}$$

Since the initial data is momentary static, the momentum constraint equation Eq.(3.20) is trivially satisfied. The profile of the conformal factor ψ is determined from the Hamiltonian constraint Eq.(3.19)

3.3 Inhomogeneous grid

It is expected that the critical collapse appears around the threshold of black hole formation. Since the curvature in the visible region becomes very large during the critical collapse, the high numerical resolution is needed. There are some methods for high-resolution numerical simulation. In this study, we use the inhomogeneous grid method. Inhomogeneous grid method is a coordinate transformation from original coordinate to new coordinate in which the region where high-resolution needed is zoomed up. We use the following coordinate transformation from original coordinate $\tilde{r}$ to new coordinate r:

$$r = \begin{cases} \tilde{r} & (0 < \tilde{r} < R), \\ \tilde{r} + \left(\frac{\tilde{r}-R}{w}\right)^{\rho} & (R < \tilde{r}), \end{cases} \tag{3.36}$$

where R, w and ρ are constant parameters (see Fig.3.2). The following parameters

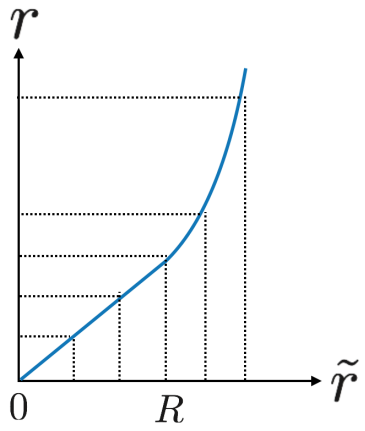

Figure 3.2: Inhomogeneous grid.

in the inhomogeneous grid are used:

$$\text{Param}-1 \quad : \quad R = 0.1/\mu,\ w = 0.05/\mu,\ \rho = 6,\ 0 < r\mu < 0.2, \tag{3.37}$$

$$\text{Param}-2 \quad : \quad R = 0.03/\mu,\ w = 0.01/\mu,\ \rho = 6,\ 0 < r\mu < 0.05, \tag{3.38}$$

In both cases, the maximum value of the areal radius is abount $60/\mu$.

3.4 Result

In this section, we summarize the convergence check of our numerical code and our numerical results.

3.4.1 Convergence

Let us discuss the convergence of our numerical code. Here, we focus on the convergence of the value of the scalar field at the origin. If it obeys the n-th order convergence, we have

$$\Phi_0(t, \Delta) = \Phi_{\rm t}(t) + \eta\Delta^n, \tag{3.39}$$

In our numerical code, time evolution is calculated by using the iterative Crank-Nicolson scheme and the spatial derivatives are determined by using 2nd or 4th order central difference. Therefore, our numerical code is totally 2nd order accuracy, and it is expected that at least n is greater than 2. The convergence of our numerical code is plotted in Fig.3.3 From Fig.3.3, we have $n \simeq 3.5$.

3.4.2 Threshold of black hole formation

As was mentioned above, the initial data is the static spherically symmetric domain wall. This initial data has one parameter which is a radius of the domain wall. Additionally, the double-well potential of this system has two parameters: λ, σ.

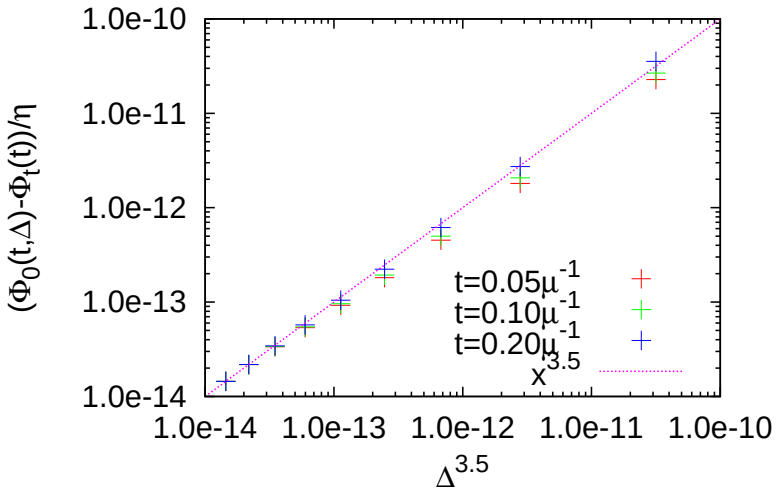

Figure 3.3: The convergence of $\Phi_0(t, \Delta)$ for each time step.

The width l of the domain wall is naturally given as $l = (2/\sigma)\sqrt{3/\lambda} = \sqrt{2/\mu^2}$, where $\mu \equiv \sqrt{2\lambda/3}\sigma$. In this study, all variables are expressed in the unit of μ. Therefore, the relevant parameter in the potential is λ.

We examine dynamics around the black hole formation threshold in the case of $\lambda = 1000\mu^2$ and $\lambda = 2000\mu^2$. As a result of the numerical simulation, the threshold r_* in each case are as follows:

$$r_* \simeq 1.4556243366/\mu \quad \text{for} \quad \lambda = 1000\mu^2, \tag{3.40}$$

$$r_* \simeq 2.199078357/\mu \quad \text{for} \quad \lambda = 2000\mu^2. \tag{3.41}$$

Table 3.1 shows the parameter setting for each simulation.

There is a parameter region in which the final state cannot be determined for $\lambda = 2000\mu^2$. In this region, the lapse function diverges at the origin during the time evolution. This behavior may be resolved by using the other slice condition. Since this region is not near the threshold, it is not important to investigate the critical behavior.

3.4.3 Mass scaling and the fine structure

In this study, the black hole mass $M_{\rm BH}$ is defined as the half of the apparent horizon at the moment of the apparent horizon formation. As a result of our numerical simulation, we have a relation between the initial domain wall radius and the black hole mass, which is shown in Fig.3.4. Fig,3.4 implies that the relation between obeys the scaling law, which index is close to one in the massless scalar case. This means that the critical collapse appears in the domain wall collapse, and the behavior is similar to one of the Einstein-massless scalar system.

$\lambda = 1000\mu^2$

Sub/Super critical	Initial domain wall radius $[\mu^{-1}]$	Grid interval $[\mu^{-1}]$	Param-1/2
Super	$2.500000000 \sim 1.455625000$	5.0×10^{-5}	Param-1
Super	$1.455624950 \sim 1.455624600$	2.5×10^{-5}	Param-1
Super	$1.455624500 \sim 1.455624350$	1.0×10^{-6}	Param-2
Sub	$1.455624200 \sim 1.455624000$	1.0×10^{-6}	Param-2
Sub	$1.455623500 \sim 1.440000000$	5.0×10^{-5}	Param-1

$\lambda = 2000\mu^2$

Sub/Super critical	Initial domain wall radius $[\mu^{-1}]$	Grid interval $[\mu^{-1}]$	Param-1/2
Super	$4.200000000 \sim 2.216000000$	5.0×10^{-5}	Param-1
Super	$2.206000000 \sim 2.199162000$	5.0×10^{-5}	Param-1
Terminated	$2.215000000 \sim 2.207000000$	Terminated	
Super	$2.199160000 \sim 2.199078380$	2.0×10^{-5}	Param-1
Super	$2.199078377 \sim 2.199078367$	5.0×10^{-6}	Param-2
Sub	$2.199078332 \sim 2.199077000$	5.0×10^{-6}	Param-2
Sub	$2.199076000 \sim 2.199010000$	2.5×10^{-5}	Param-1
Sub	$2.199000000 \sim 2.194000000$	5.0×10^{-5}	Param-1

Table 3.1: Table of the parameter region and the grid interval of our numerical simulation. The leftmost column shows whether the parameter is in the supercritical region or the subcritical region. The rightmost column represents the parameter of the inhomogeneous grid (see Eq.(3.37)).

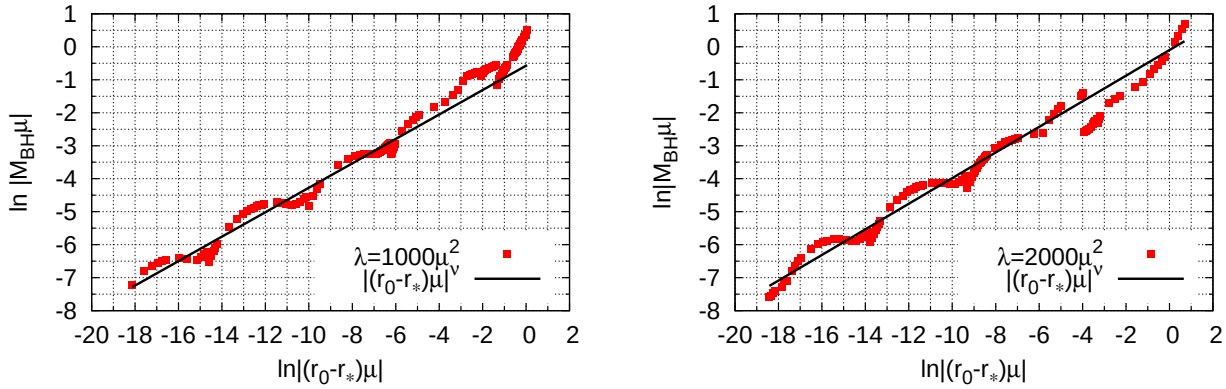

Figure 3.4: The relation between the black hole mass which is defined by using the apparent horizon and the initial domain wall radius. The horizontal line is the initial parameter around the threshold, and the vertical line is the black hole mass in log scale. The result of $\lambda = 1000\mu^2$ is plotted in the left panel, and the result of $\lambda = 2000\mu^2$ is plotted in the right panel. In both panels, the numerical data corresponds to red points. The black line corresponds to the scaling law $M_{\rm BH} = \zeta|(r_0 - r_*)\mu|^\nu$, which index ν is determined by using the least squares fitting in the region $\ln|(r_0 - r_*)\mu| < -5$. As a result, for $\lambda = 1000\mu^2$, $\zeta \simeq 0.564$, $\nu \simeq 0.370$ and for $\lambda = 2000\mu^2$, $\zeta \simeq 0.905$, $\nu \simeq 0.388$.

Furthermore, the fine structure around the scaling law is observed. In order to see the fine structure, the difference between the black hole mass and the scaling law is shown in Fig. 3.5. Fig.3.5 shows that $M_{\rm BH}$ oscillates around the scaling law. The period of the fine structure is about 4.5 in log scale, which is also close to the one of the massless scalar case.

3.4.4 Mass discontinuity

As is shown in Fig.3.5, the black hole mass discontinuously changes with respect to the initial domain wall radius. In order to understand this behavior, let us focus on the time evolution of the trapped region (see Fig.3.6). Fig.3.6 shows the time evolution of the trapped region for the initial data which initial parameter is close to the one of mass discontinuity point. Apparent horizon is an outermost boundary of the trapped region in each time. Fig.3.6 implies that there are two disconnected trapped regions at the moment of the apparent horizon formation. In this study, since black hole mass is defined from the areal radius of the apparent horizon at the moment of the apparent horizon formation, the black hole mass depends on which trapped region appears first. In the case of $r_0 = 2.1991670/\mu$ (upper panel in Fig.3.6), the apparent horizon at the moment of the formation is given from the upper shaded region. On the other hand, in the case of $r_0 = 2.1991700/\mu$ (lower panel in Fig.3.6), the apparent horizon at the moment of the formation is given from the lower shaded region. This dependence is the origin of the mass discontinuity. The mass discontinuity of the critical collapse is reported in massless

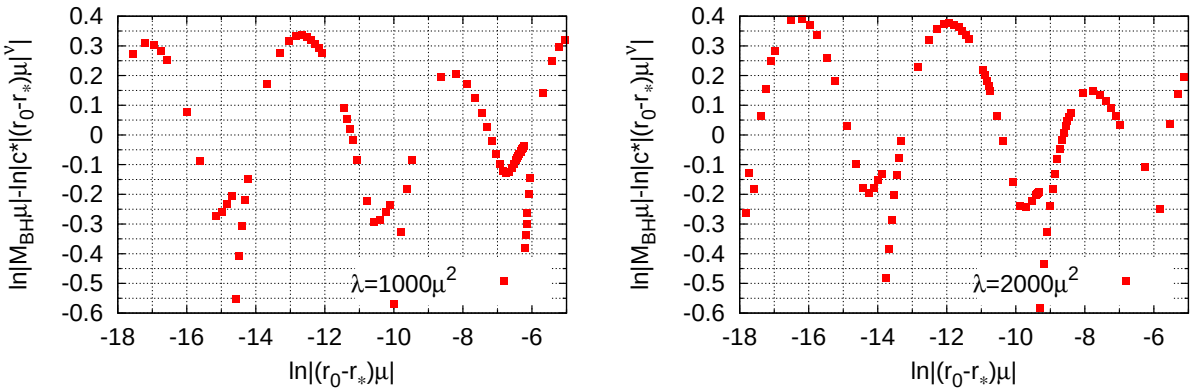

Figure 3.5: The difference between $M_{\rm BH}$ which is given from our numerical simulations and the scaling relation $\zeta|(r_0 - r_*)\mu|^\nu$. The left panel shows the case $\lambda = 1000\mu^2$, and the right panel shows the case $\lambda = 2000\mu^2$. We can observe the periodic behaviors in $\ln|(r_0 - r_*)\mu| \lesssim -9$. The periods are about 4.5 in the log scale.

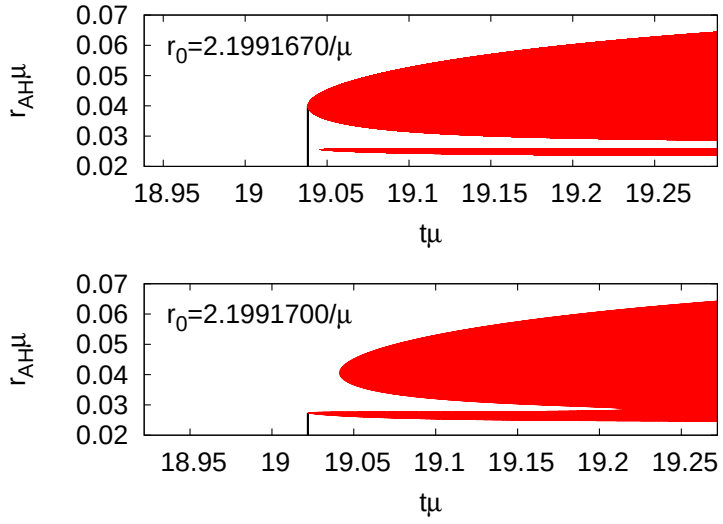

Figure 3.6: Time evolution of the trapped region in the case of $r_0 = 2.1991670/\mu$ (upper), and in the case of $r_0 = 2.1991700/\mu$ (lower). These two initial parameters correspond to the boundary of the discontinuity change. The vertical black line on the each graph corresponds to the moment of the apparent horizon formation. These graph shows that there are two disconnected trapped region (shaded region).

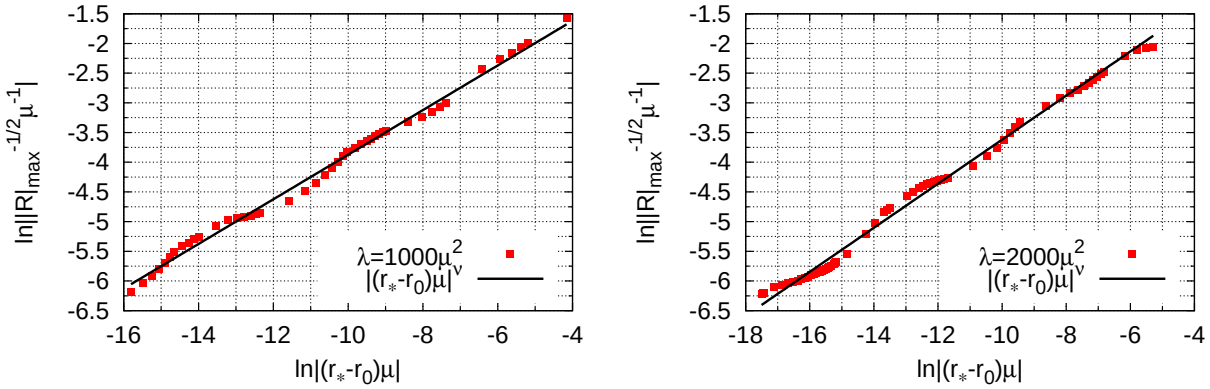

Figure 3.7: The relation between $|R|_{\max}$ and the initial radius of the domain wall. The horizontal line is the initial parameter around the threshold, and the vertical line is $|R|_{\max}^{-1/2}$ in log scale. The red points are the numerical data and the black line denotes the fitting function $\zeta|(r_* - r_0)\mu|^{\nu}$.

scalar case [31].

3.4.5 Scaling behavior in the subcritical region

We examine the scaling behavior in the subcritical region. As is reported in [13], it is expected that the maximal absolute value of scalar curvature $|R|_{\max}$ and $|R_{\mu\nu}R^{\mu\nu}|_{\max}$ also obeys the scaling law in subcritical region. Fig.3.7 shows the relation between $|R|_{\max}$ and the initial parameter. As is shown in Fig.3.7, $|R|_{\max}$ obeys the following scaling law:

$$\ln|R_{\max}(p)| = -2\nu \ln|p_* - p| + f(\ln|p - p_*|), \tag{3.42}$$

where ν is about 0.376 for $\lambda = 1000\mu^2$ and 0.371 for $\lambda = 2000\mu^2$. $f(\ln|p - p_*|)$ is a periodic function. The index of the scaling law in the subcritical region is close to one in the case of a massless scalar system.

So far, it has been shown that the mass scaling in the supercritical region and the curvature scaling in the subcritical region are close to them in the case of the gravitational collapse of a massless scalar field. In order to understand why these behaviors are close to them in the case of a massless scalar field, let us focus on the absolute maximal value of the conjugate momentum of the scalar field $|\Pi|_{\max}$ in the subcritical region. The relation between the initial parameter and $|\Pi|_{\max}$ is depicted in Fig.3.8. From Fig.3.8, $|\Pi|_{\max}$ obeys the following scaling law:

$$\ln|\Pi|_{\max}^{-1} = \nu \ln|p - p_*| + f(\ln|p - p_*|), \tag{3.43}$$

where $f(x)$ is a periodic function, and ν is about 0.37. It implies that $|\Pi|_{\max}$ is very large around the threshold. This means that the temporal derivative of a scalar field becomes large, and the kinetic term of the scalar field is larger than the potential term during the critical collapse. Since the kinetic term dominates

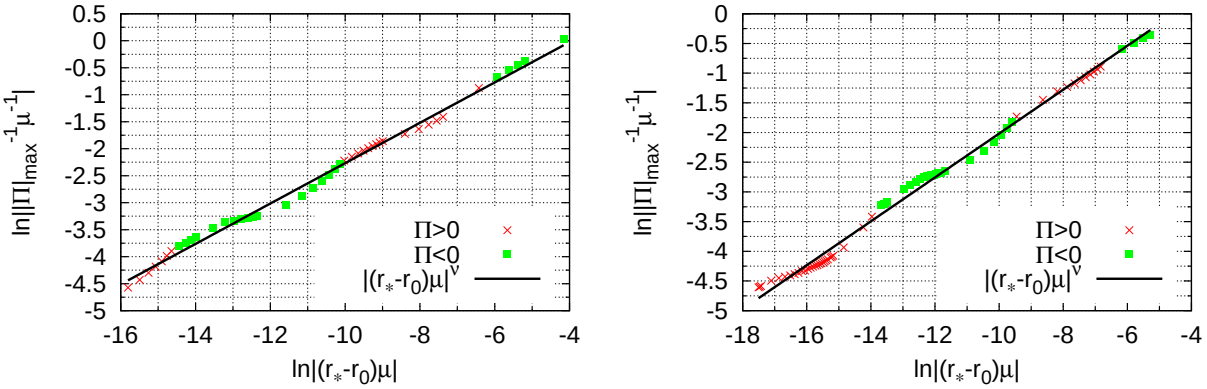

Figure 3.8: The relation between the absolute maximum value of the conjugate momentum of the scalar field and the initial radius of the domain wall. The case of $\lambda = 1000\mu^2$ is plotted in the left panel. The case of $\lambda = 2000\mu^2$ is plotted in the right panel. In both panel, the horizontal line is the initial parameter around the threshold, and the vertical line is $|\Pi|^{-1}_{\rm max}$ in log scale. Each red(green) point corresponds to a case in which the maximum absolute value is realized by a positive (negative) value of the conjugate momentum. $|\Pi|_{\rm max}$ can be fitted by the function $\zeta|(r_* - r_0)\mu|^{-\nu}$ (black line). By using the least squares fitting, ν is given by 0.374 for $\lambda = 1000\mu^2$, and 0.370 for $\lambda = 2000\mu^2$.

over the potential term during the critical collapse, the critical behavior is close to the massless scalar case.

3.5 Result

Here, we summarize the critical behavior of the domain wall collapse. In this study, we examined the gravitational collapse of the domain wall in the case of $\lambda = 1000$ and $\lambda = 2000$. As a result, in supercritical region, scaling law of the black mass and the fine structure around the scaling law were observed (see Fig.3.4, Fig.3.5, and Eq.(2.29)). Furthermore, in the subcritical region, we showed that the absolute maximum value of the scalar curvature obeys the scaling law with the wiggle (see Fig.3.7 and Eq.(3.42)). In these behaviors, the index of the scaling and the period of the fine structure are close to them in the gravitational collapse of the massless scalar field. In order to understand why these values are similar to them in the gravitational collapse of the massless scalar field, we focus on the absolute maximum value of the momentum conjugate of the scalar field at the origin, and show that this value also obeys the scaling law (see Fig.3.8 and Eq.(3.43)). As a result, during the critical collapse, the kinetic term of the scalar field becomes large, and the potential term can be neglected. Therefore, the critical behavior of domain wall collapse is similar to the critical behavior of the gravitational collapse of a massless scalar field.

Chapter 4

Critical behavior of self-gravitating oscillon

In this chapter, we examine the critical behavior of the oscillon in Einstein-scalar field theory with double-well potential in weak gravity case. In this thesis, we call the oscillon of this theory as self-gravitating oscillon.

4.1 Numerical scheme

4.1.1 Formulation

In this section, we explain the numerical scheme to calculate the time evolution of self-gravitating oscillon. In order to determine the lifetime of the oscillon, long time numerical simulation is needed. Thus, we use the G-BSSN (generalized Baumgarte-Shapiro-Shibata-Nakamura) formulation which is stable for free evolution numerical scheme. G-BSSN formulation is the generalization of BSSN formulation to the case of curvilinear coordinate, and it is known that this formulation is powerful method [32]. G-BSSN formulation in general curvilinear coordinate is summarized in App. E. In this section, G-BSSN formulation in spherically symmetric spacetime is discussed.

The metric of general spherically symmetric spacetime can be expressed as:

$$\gamma_{ij} = e^{4\phi}\tilde{\gamma}_{ij} = e^{4\phi}\mathrm{diag}(a, br^2, br^2\sin^2\theta), \tag{4.1}$$

where a and b depend on t and r. ϕ is defined with the evolution of $\tilde{\gamma}(=\det(\tilde{\gamma}_{ij}))$ and its initial condition. As is summarized in App.E, there are two standard choices of the evolution of it. The first choice is the Lagrangian type, and the second choice is the Eulerian type. Furthermore, we use the flat metric under the polar coordinate (t, r) as a reference metric. As will be mentioned below, we introduce the inhomogeneous grid. Since the reference metric is also transformed as a tensor, we assume the following general form:

$$\bar{\gamma}_{ij} = \mathrm{diag}(\bar{a}, \bar{b}r^2, \bar{b}r^2\sin^2\theta), \tag{4.2}$$

where $\bar{a}$ and $\bar{b}$ depend on r. Since the reference metric is flat metric, $\bar{a}$ and $\bar{b}$ are given from the spatial coordinate transformation;

$$\bar{a} = (\frac{\partial r}{\partial r_{\rm f}})^2, \tag{4.3}$$

$$\bar{b} = (\frac{r}{r_{\rm f}})^2, \tag{4.4}$$

where $r_{\rm f}$ is an areal radius of flat metric, that is, the spatial line element of the reference metric is given as

$$d\bar{l}^2 = \bar{a}dr^2 + \bar{b}r^2 d^2\Omega \tag{4.5}$$

$$= dr_{\rm f}^2 + r_{\rm f}^2 d^2\Omega. \tag{4.6}$$

In the G-BSSN formulation, the extrinsic curvature is decomposed into the trace part of it which is denoted as K, and the conformal traceless part of it which is denoted as $\tilde{A}_{ij}$. These quantities are defined as

$$K_{ij} = e^{4\phi}\tilde{A}_{ij} + \frac{1}{3}\gamma_{ij}K, \tag{4.7}$$

where K is defined as $K \equiv \gamma^{ij}K_{ij}$. From the spherical symmetry, the conformal traceless part of the extrinsic curvature can be expressed as:

$$\tilde{A}_{ij} = {\rm diag}(A, Br^2, Br^2\sin^2\theta), \tag{4.8}$$

where A and B are functions of t and r. Nontrivial component of the shift vector β^i and the auxiliary field $\tilde{\Lambda}^i$ is a radial component:

$$\beta^i = (\beta, 0, 0), \tag{4.9}$$

$$\tilde{\Lambda}^i = (\tilde{\Lambda}, 0, 0). \tag{4.10}$$

$\tilde{\Lambda}$ is defined as

$$\tilde{\Lambda} = \frac{a'}{2a^2} - \frac{1}{a}(\frac{b'}{b} + \frac{2}{r}) - \frac{\bar{a}'}{2a\bar{a}} + \frac{\bar{b}}{\bar{a}b}(\frac{\bar{b}'}{\bar{b}} + \frac{2}{r}). \tag{4.11}$$

The evolution equations of the G-BSSN formulation under this coordinate are expressed as:

$$\partial_t\phi = \beta\phi' - \frac{1}{6}\alpha K + \sigma\frac{1}{6}\mathcal{B}, \tag{4.12}$$

$$\partial_t a = \beta a' + 2a\beta' - 2\alpha A - \sigma\frac{2}{3}a\mathcal{B}, \tag{4.13}$$

$$\partial_t b = \beta b' + 2\beta\frac{b}{r} - 2\alpha B - \sigma\frac{2}{3}b\mathcal{B}, \tag{4.14}$$

$$\partial_t K = \beta K' - \mathcal{D} + \alpha\left(\frac{1}{3}K^2 + \frac{A^2}{a^2} + 2\frac{B^2}{b^2}\right) + 4\pi\alpha(E+S), \tag{4.15}$$

$$\partial_t A = \beta A' + 2A\beta' + e^{-4\phi}\left\{-\mathcal{D}_{rr}^{TF} + \alpha(R_{rr}^{TF} - 8\pi S_{rr}^{TF})\right\} + \alpha\left(KA - 2\frac{A^2}{a}\right) - \sigma\frac{2}{3}A\mathcal{B},$$

$$\partial_t B = \beta B' + \frac{e^{-4\phi}}{r^2}\left\{-\mathcal{D}^{TF}_{\theta\theta} + \alpha(R^{TF}_{\theta\theta} - 8\pi S^{TF}_{\theta\theta})\right\} + \alpha\left(KB - 2\frac{B^2}{b}\right) + 2\frac{\beta}{r}B - \sigma\frac{2}{3}B\mathcal{B}, \tag{4.16}$$

$$\begin{aligned}\partial_t\tilde{\Lambda} &= \beta\tilde{\Lambda}' - \tilde{\Lambda}\beta' + \frac{1}{a}\beta'' + \frac{1}{\bar{a}}\left(\frac{\bar{b}'}{b} + \frac{\bar{a}'}{2a}\right)\beta' + \left(\frac{\bar{a}''}{2a\bar{a}} - \frac{\bar{a}'^2}{2a\bar{a}^2} + \frac{\bar{a}'\bar{b}}{2\bar{a}^2 b}(\frac{\bar{b}'}{\bar{b}} + \frac{2}{r})\right)\beta \\ &\quad -\frac{\bar{b}'}{2\bar{a}b}\left(\frac{\bar{b}'}{\bar{b}} + \frac{4}{r}\right)\beta + \frac{2\bar{b}}{\bar{a}b}\frac{1}{r}\left(\beta' - \frac{\beta}{r}\right) - 2\frac{A}{a^2}\alpha' + \alpha\left((\frac{a'}{a} - \frac{\bar{a}'}{\bar{a}})\frac{A}{a^2} + 2(-\frac{b'}{a} + \frac{\bar{b}'}{\bar{a}})\frac{B}{b^2}\right. \\ &\quad \left. -4(\frac{b}{a} - \frac{\bar{b}}{\bar{a}})\frac{B}{b^2}\frac{1}{r}\right) + 2\alpha\left(6\frac{A}{a^2}\phi' - \frac{2}{3}\frac{K'}{a} - 8\pi\frac{1}{a}p\right) + \frac{\sigma}{3}\left(2\tilde{\Lambda}\mathcal{B} + \frac{1}{a}\mathcal{B}'\right),\end{aligned} \tag{4.17}$$

where R_{rr} and $R_{\theta\theta}$ are the (r,r) and (θ,θ) components of the spatial Ricci tensor, and $\mathcal{D}_{ij}$, $\mathcal{D}$ and $\mathcal{B}$ are defined by $\mathcal{D}_{ij} := D_iD_j\alpha$, $\mathcal{D} := \gamma^{ij}D_iD_j\alpha$ and $\mathcal{B} := \tilde{D}_k\beta^k$, respectively. A superscript TF is the trace-free part of a tensor with respect to γ_{ij}, therefore, for a tensor X_{ij}, we have

$$X^{TF}_{rr} = \frac{2}{3}(X_{rr} - \frac{a}{br^2}X_{\theta\theta}), \tag{4.19}$$

$$X^{TF}_{\theta\theta} = \frac{br^2}{2a}X^{TF}_{rr}. \tag{4.20}$$

$\mathcal{B}$, $\mathcal{D}_{rr}$, $\mathcal{D}_{\theta\theta}$, R_{rr} and $R_{\theta\theta}$ can be expressed as:

$$\mathcal{B} = \tilde{D}_k\beta^k = \beta' + \left(\frac{a'}{2a} + \frac{b'}{b} + \frac{2}{r}\right)\beta, \tag{4.21}$$

$$\mathcal{D}_{rr} = \alpha'' - \left(\frac{a'}{2a} + 2\phi'\right)\alpha', \tag{4.22}$$

$$\mathcal{D}_{\theta\theta} = r\alpha'\frac{b}{a} + \frac{r^2}{2}\alpha'\left(\frac{b'}{a} + 4\frac{b}{a}\phi'\right), \tag{4.23}$$

$$\begin{aligned}R_{rr} &= -4\phi'' + 2\phi'\left(\frac{a'}{a} - \frac{b'}{b}\right) - \frac{1}{2}\left(\frac{a''}{a} - \frac{\bar{a}''}{\bar{a}}\right) + \left(\frac{5}{4}\frac{\bar{a}'}{\bar{a}} - \frac{a}{2\bar{a}}\frac{\bar{b}'}{b}\right)\left(\frac{a'}{a} - \frac{\bar{a}'}{\bar{a}}\right) + \frac{1}{2}\left(\frac{a\bar{b}}{\bar{a}b} - 1\right)\frac{\bar{b}'^2}{\bar{b}^2} \\ &\quad +a\left(\tilde{\Lambda}' + \frac{a'}{2a}\tilde{\Lambda}\right) + \frac{3}{4}\left(\frac{a'}{a} - \frac{\bar{a}'}{\bar{a}}\right)^2 + \frac{\bar{b}}{b}\left(\frac{b'}{b} - \frac{\bar{b}'}{\bar{b}}\right)\left(-\frac{b'}{\bar{b}} + \frac{a\bar{b}'}{\bar{a}\bar{b}}\right) + \frac{1}{2}\left(\frac{b'}{b} - \frac{\bar{b}'}{\bar{b}}\right)^2 \\ &\quad +\frac{1}{r}\left(-4\phi' - \frac{a\bar{b}}{\bar{a}b}(\frac{a'}{a} - \frac{\bar{a}'}{\bar{a}}) - 2\frac{b'}{b}(1 - \frac{a\bar{b}}{\bar{a}b})\right) + \frac{2}{r^2}\left(\frac{a\bar{b}}{\bar{a}b} - 1\right),\end{aligned} \tag{4.24}$$

$$\begin{aligned}R_{\theta\theta} &= \left\{-\frac{2b}{a}\phi'' + \frac{a'b}{a^2}\phi' - 3\frac{b'\phi'}{a} - \frac{4b}{a}\phi'^2 - \frac{b''}{2a} + \frac{b\bar{b}''}{2a\bar{b}} + \frac{b}{2a}\left(\frac{\bar{b}'}{\bar{b}} + \frac{\bar{a}'}{2\bar{a}}\right)\left(\frac{b'}{b} - \frac{\bar{b}'}{\bar{b}}\right)\right. \\ &\quad +\frac{\bar{b}'b}{2a\bar{b}}\left(1 - \frac{a\bar{b}}{\bar{a}b}\right)\left(\frac{b'}{b} - \frac{\bar{b}'}{\bar{b}}\right) + \frac{1}{4\bar{a}}\frac{\bar{b}'^2}{\bar{b}}\left(1 - \frac{a\bar{b}}{\bar{a}b}\right) \\ &\quad \left.+\frac{3b}{4a}\left(\frac{b'}{b} - \frac{\bar{b}'}{\bar{b}}\right)^2 - \frac{1}{2}\left(\frac{b'}{a} - \frac{\bar{b}'}{\bar{a}}\right)\left(\frac{b'}{b} - \frac{\bar{b}'}{\bar{b}}\right) + \frac{a}{4b}\left(\frac{b'}{a} - \frac{\bar{b}'}{\bar{a}}\right)^2 + \frac{b'}{2}\tilde{\Lambda}\right\}r^2 \\ &\quad +\left\{-6\frac{b}{a}\phi' + \frac{\bar{b}'}{\bar{a}}\left(1 - \frac{a\bar{b}}{\bar{a}b}\right) + b\tilde{\Lambda} - \frac{b}{a}\left(\frac{b'}{b} - \frac{\bar{b}'}{\bar{b}}\right) - \frac{a}{b}\left(-\frac{b'}{a} + \frac{\bar{b}'}{\bar{a}}\right)\left(\frac{b}{a} - \frac{\bar{b}}{\bar{a}}\right)\right\}r - \frac{\bar{b}}{\bar{a}} + \frac{b}{a}.\end{aligned} \tag{4.25}$$

(4.25)

Furthermore, the constraint equations can be written as

$$\left\{\frac{\phi''}{a}+\frac{\phi'^2}{a}-\left(\frac{a'}{2a^2}-\frac{b'}{ab}-\frac{2}{ar}\right)\phi'\right\}e^{\phi}-\frac{e^{\phi}}{8}\tilde{R}+\frac{e^{5\phi}}{8}\left(\frac{A^2}{a^2}+2\frac{B^2}{b^2}\right)-\frac{e^{5\phi}}{12}K^2+2\pi e^{5\phi}E = 0, \tag{4.26}$$

$$6\phi'\frac{A}{a}+\frac{A'}{a}-\frac{a'A}{a^2}+\frac{b'}{b}\left(\frac{A}{a}-\frac{B}{b}\right)+\frac{2}{r}\left(\frac{A}{a}-\frac{B}{b}\right)-\frac{2}{3}K'-8\pi p = 0. \tag{4.27}$$

E, p and S_{ij} are energy density, momentum and stress tensor of the matter sector, respcetively. In our case, these quantities are expressed as:

$$E := T_{\mu\nu}n^\mu n^\nu = e^{-4\phi}\frac{\Pi^2+\Phi'^2}{2a}+V(\Phi), \tag{4.28}$$

$$p := T_{\nu\mu}\gamma_r^\nu n^\mu = -\frac{\Pi\Phi'}{e^{2\phi}\sqrt{a}}, \tag{4.29}$$

$$S_{rr} := T_{\mu\nu}\gamma_r^\mu\gamma_r^\nu = \frac{\Pi^2}{2}+\frac{\Phi'^2}{2}-e^{4\phi}aV(\Phi), \tag{4.30}$$

$$S_{\theta\theta} := T_{\mu\nu}\gamma_\theta^\mu\gamma_\theta^\nu = -\frac{br^2}{2a}(-\Pi^2+\Phi'^2)-e^{4\phi}br^2V(\Phi). \tag{4.31}$$

$\tilde{R}$ is the Ricci tensor with respect to $\tilde{\gamma}_{ij}$, and the expression of $\tilde{R}$ is given as

$$\tilde{R}=\frac{3a'^2}{4a^3}+\frac{b'^2}{2ab^2}+\tilde{\Lambda}'+\frac{a'}{2a}\tilde{\Lambda}-\frac{a''}{2a^2}-\frac{b''}{ab}+\frac{b'}{b}\tilde{\Lambda}+\frac{1}{r}\left(-\frac{a'+2b'}{ab}+2\tilde{\Lambda}\right). \tag{4.32}$$

The evolution equation of the scalar field Φ and the momentum conjugate of the scalar field Π can be given as:

$$\begin{aligned}\partial_t\Pi &= \beta\Pi'+\left(\frac{2}{3}\alpha K+2\alpha\frac{B}{b}+\beta'\right)\Pi \\ &\quad+\left(\frac{\alpha'}{e^{2\phi}\sqrt{a}}+\frac{2\alpha\phi'}{e^{2\phi}\sqrt{a}}-\frac{\alpha}{2e^{2\phi}\sqrt{a^3}}a'\right. \\ &\quad\left.+\frac{\alpha}{e^{2\phi}\sqrt{a}}\frac{b'}{b}+\frac{2\alpha}{re^{2\phi}\sqrt{a}}\right)\Phi'+\frac{\alpha}{e^{2\phi}\sqrt{a}}\Phi''-\alpha e^{2\phi}\sqrt{a}\frac{dV}{d\Phi}(\Phi),\end{aligned} \tag{4.33}$$

$$\partial_t\Phi = \beta\Phi'+\frac{\alpha}{e^{2\phi}\sqrt{a}}\Pi. \tag{4.34}$$

4.1.2 Gauge condition

In order to determine the time evolution, we must impose the gauge conditions for the lapse function α and the shift vector β. In this study, we impose the harmonic gauge condition for the lapse function:

$$\partial_t\alpha = \mathcal{L}_\beta\alpha-K\alpha^2. \tag{4.35}$$

For shift vector, we use the normal coordinate:

$$\beta = 0. \tag{4.36}$$

4.1.3 Boundary condition

In this subsection, we mention the boundary condition.

As was mentioned in Sec.A.2.1, it is necessary to pay attention to the boundary condition at the center of the spherically symmetric spacetime. Firstly, the condition for the smoothness of the field can be written as:

$$\alpha'|_{r=0} = \phi'|_{r=0} = K'|_{r=0} = \tilde{\Lambda}|_{r=0} = \Phi'|_{r=0} = \Pi'|_{r=0} = 0, \tag{4.37}$$

$$a'|_{r=0} = b'|_{r=0} = A'|_{r=0} = B'|_{r=0} = 0. \tag{4.38}$$

On the other hand, the following additional conditions for a, b, A and B are needed;

$$a|_{r=0} - 1 = b|_{r=0} - 1 = A|_{r=0} = B|_{r=0} = 0. \tag{4.39}$$

These conditions guarantee the regularity of left hand side in evolution equations for $A, B, \tilde{\Lambda}$. (see Eqs.(4.16)(4.17)(4.18)). As was discussed in Sec.A.2.1, if second conditions Eq.(4.39) are satisfied on the initial data, evolution equation guarantees this condition in arbitrary time. However, in the case that the evolution equation is numerically solved, even if the boundary condition is satisfied initially, numerical error violate this condition, and its violation may be origin of the numerical instability. In this study, in order to avoid the numerical instability, Eq.(4.37) and Eq.(4.39) are imposed. In order to explain the boundary condition for a,b, A and B at $r = 0$, let us focus on the even function of r at the origin $f(r)$. The boundary condition of this function is the Neumann boundary condition: $f'|_{r=0} = 0$ ($^\forall t$). Therefore, we have $\partial_t f'|_{r=0} = 0$. Using the forward finite differencing, we get the following formula:

$$f_1^{n+1} = \frac{1}{3}(4f_2^{n+1} - f_3^{n+1} - 3f_1^n + 4f_2^n - f_3^n), \tag{4.40}$$

where f_i^n denotes the value at the n's time step and i's grid number. The grid $i = 0$ corresponds to $r = 0$. Since the boundary conditions Eq.(4.38) for a,b, A and B are the Neumann boundary condition, the time evolution of these variables is determined from Eq.(4.40).

Since the spacetime is asymptotically flat, following outer boundary conditions are imposed:

$$\phi(t, r_{\max}) = \log\left(1 + \frac{M_{\rm ADM}}{2r_{\max}}\right), \tag{4.41}$$

$$\alpha(t, r_{\max}) = a(t, r_{\max}) = b(t, r_{\max}) = 1, \tag{4.42}$$

$$A(t, r_{\max}) = B(t, r_{\max}) = K(t, r_{\max}) = \tilde{\Lambda}(t, r_{\max}) = \Pi(t, r_{\max}) = 0, \tag{4.43}$$

$$\Phi(t, r_{\max}) = \sigma, \tag{4.44}$$

where $M_{\rm ADM}$ is an ADM mass, and $r_{\max}$ is the coordinate value at the outer boundary.

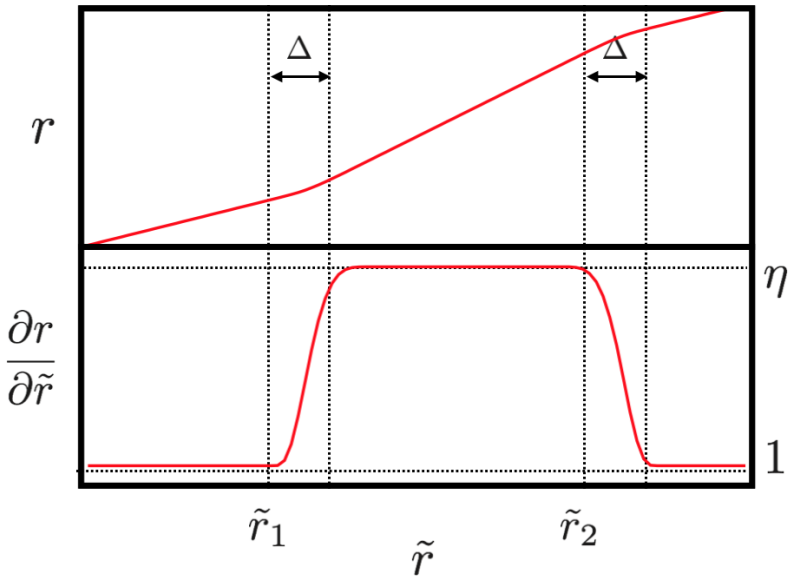

Figure 4.1: r and $\partial r/\partial\tilde{r}$ are schematically depicted as functions of $\tilde{r}$.

4.1.4 Inhomogeneous grid

Since the oscillon is a longevity dynamical profile, it is necessary to perform the long-time numerical simulation. In order that the outer numerical boundary does not affect the properties of the self-gravitating oscillon, we use the inhomogeneous grid, such that physical radius of the outer boundary is large. In this study, the following radial coordinate transformation is performed:

$$\frac{\partial r}{\partial \tilde{r}} = \begin{cases} 1 & (0 < \tilde{r} < \tilde{r}_1) \\ 1 + (-1+\eta)\left\{\Delta^4 - (\tilde{r}_1 + \Delta - \tilde{r})^4\right\}^4 \Delta^{-16} & (\tilde{r}_1 < \tilde{r} < \tilde{r}_1 + \Delta) \\ \eta & (\tilde{r}_1 + \Delta < \tilde{r} < \tilde{r}_2) \\ 1 + (-1+\eta)\left\{\Delta^4 - (\tilde{r}_2 - \tilde{r})^4\right\}^4 \Delta^{-16} & (\tilde{r}_2 < \tilde{r} < \tilde{r}_2 + \Delta) \\ 1 & (\tilde{r}_2 + \Delta < \tilde{r}), \end{cases} \tag{4.45}$$

where $\tilde{r}$ is the new radial coordinate, and Δ and η are parameters of the inhomogeneous grid spacing (See Fig. 4.1).

4.1.5 Definition of the Kodama mass and lifetime

In order to examine the relation between the oscillon's lifetime and the initial parameter, we define the oscillon's lifetime. In this study, the lifetime of the oscillon is defined by using the Kodama mass. Kodama mass is a conserved energy of the spherically symmetric spacetime. [52,53] In order to define the Kodama mass, let us introduce the Kodama vector. We focus on the two dimensional manifold charted by (t, r) whom angular coordinates in four-dimensional manifold are constant. G_{AB} is a two dimensional metric in the two dimensional manifold. This surface is a time like surface. The following vector K^A in this surface is introduced:

$$K^A = \epsilon^{AB}\partial_B R, \tag{4.46}$$

where the index A, B denote the coordinate t and r. R is the areal radius of the 2-sphere with constant t and r. ϵ_{AB} is defined by $\epsilon_{AB} = \sqrt{-G}\varepsilon_{AB}$ with the Levi-Civita tensor ε_{AB}, and G is a determinant of G_{AB}. The vector K^A can be naturally extended to K^μ in four dimensional manifold. K^μ is called Kodama vector. By using Kodama vector, we define S^μ as follows:

$$S^\mu = T^{\mu\nu}K_\nu, \tag{4.47}$$

where $T^{\mu\nu}$ is the energy momentum tensor of the matter sector. S^μ satisfies the following conservation law:

$$\partial_\mu(\sqrt{-g}S^\mu) = 0. \tag{4.48}$$

This conservation law means that the following quantity M is conserved energy of this system:

$$M(t, r_0) = \int_{\text{sphere}} S^t \alpha\sqrt{\gamma}dx^3, \tag{4.49}$$

where S^t is expressed as follows:

$$S^t = E\frac{1}{\alpha}\sqrt{\frac{b}{a}}r\left(2\phi' + \frac{b'}{2b} + \frac{1}{r}\right) - p\frac{1}{\alpha}\sqrt{\frac{b}{a}}r\left(\frac{1}{3}K + \frac{B}{b}\right). \tag{4.50}$$

$M(t, r_0)$ is called the Kodama mass inside the sphere which radius is r_0. Eq.(4.48) can be expressed as:

$$\frac{\partial}{\partial t}\left\{M(t, r_0) + P(t, t_0, r_0)\right\} = 0, \tag{4.51}$$

where $P(t, t_0, r_0)$ is the integrated energy flux though the sphere of the radius r_0, defined by

$$P(t_1, t_2; r_0) = \int_{t_1}^{t_2} dt 4\pi\alpha e^{6\phi}a^{1/2}br_0^2 S^r|_{r_0}. \tag{4.52}$$

S^r is given as follows:

$$\begin{aligned} S^r &= -E\frac{\beta}{\alpha}\sqrt{\frac{b}{a}}r\left(2\phi' + \frac{b'}{2b} + \frac{1}{r}\right) + E\frac{\beta^2}{\alpha^2}e^{4\phi}\sqrt{ab}r\left(\frac{1}{3}K + \frac{B}{b}\right) \\ &\quad + pe^{-4\phi}\frac{1}{a}\sqrt{\frac{b}{a}}r\left(2\phi' + \frac{b'}{2b} + \frac{1}{r}\right) \\ &\quad - p\frac{\beta}{\alpha}\sqrt{\frac{b}{a}}r\left(\frac{1}{3}K + \frac{B}{b}\right) - S_{rr}e^{-4\phi}\frac{1}{a}\sqrt{\frac{b}{a}}r\left(\frac{K}{3} + \frac{B}{b}\right) \end{aligned} \tag{4.53}$$

In this study, by using the Kodama mass which is defined above, we define the oscillon's lifetime. Since the oscillon is a localized profile of the scalar field, r_0 can be assumed to be a larger than the typical radius of the oscillon. The lifetime τ of the oscillon is defined as:

$$\frac{M(\tau; r_0)}{M(0; r_0)} = \epsilon \ll 1. \tag{4.54}$$

This means that before the lifetime τ, almost energy of the system is confined inside the sphere of the radius r_0, and the energy radiates away from the sphere by the lifetime τ. We set $r_0 = 10(\lambda\sigma^2)^{-1/2}$ and $\epsilon = 0.01$ and checked that our results do not depend on the specific value r_0 and ϵ.

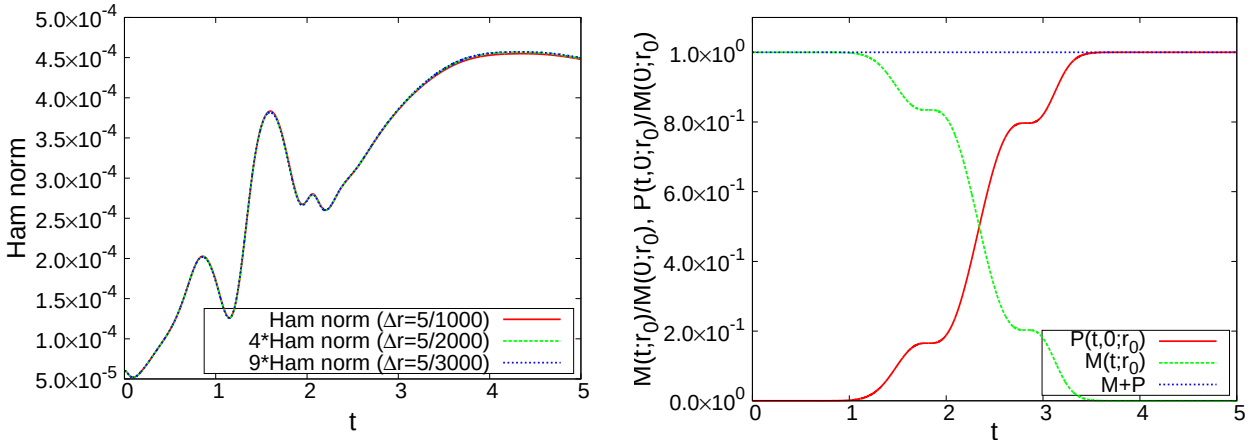

Figure 4.2: Convergence check of the L2 norm of Hamiltonian constraint violation (left panel) and the conservation of the Kodama mass.

4.1.6 Numerical scheme and convergence check

In order to solve the equations of G-BSSN formulation numerically, we develop the numerical code, which is written in C++. Our temporal integration scheme is iterative Crank-Nicolson scheme, which is 2nd order accuracy. The spatial derivative is evaluated by using the 2nd order finite difference.

We have performed a test simulation of our numerical code by using the massless scalar collapse. The initial data of the test simulation is as follows:

$$a(t=0,r) = b(t=0,r) = 1, \tag{4.55}$$
$$\Phi(t=0,r) = Ae^{-r^2/w^2}, \tag{4.56}$$

where $A = 0.2$ and $w = 0.5$. Fig.4.2 shows the convergence of L2 norm of Hamiltonian constraint and the conservation of the Kodama mass.

4.1.7 Initial data

In this study, we use the momentary static Gaussian bubble and spatially conformal flat initial data, which is given as:

$$\Phi(t=0,r) = -\sigma + 2\sigma e^{-r^2/R_0^2}, \tag{4.57}$$
$$a(t=0,r) = b(t=0,r) = 1, \tag{4.58}$$

where R_0 is a radius of the initial Gaussian bubble. Since the momentary static condition is imposed on the initial data, the momentum constraint is trivially satisfied. Solving the Hamiltonian constraint for ϕ numerically, we have the initial profile of ϕ.

4.2 Numerical result

Under the above ansatz, we have examined the self-gravitating oscillon formation and its dissipation.

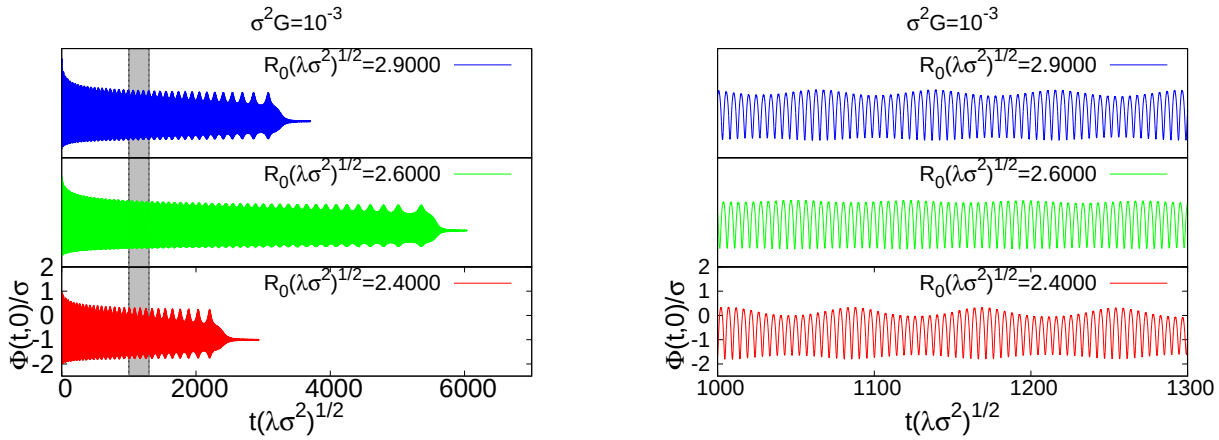

Figure 4.3: Time evolution of the scalar field $\Phi(t, r = 0)$ at the origin. The left panel shows the envelope of the time evolution of $\Phi(t, r = 0)$ in the case of $\sigma^2 G = 1.0 \times 10^{-3}$. The right panel shows the time evolution of $\Phi(t, r = 0)$ in the shaded region in the left panel.

This system has one independent parameter $\sigma^2 G$ which characterize the strength of the coupling between the gravity and scalar field. In this study, we have examined the critical behavior for the oscillon's lifetime in the case of $\sigma^2 G = 1.0 \times 10^{-4}$, 5.0×10^{-4}, 1.0×10^{-3} and 2.0×10^{-3}. These values of $\sigma^2 G$ correspond to relatively weak gravity case. Although it is expected that the behavior of the self-gravitating oscillon in the case of larger value $\sigma^2 G$ is different from one of the oscillon in Minkowski spacetime, as a first step, we have examined the weak gravity case.

In this section, we discuss the typical behavior of the self-gravitating osciillon and its critical behavior.

4.2.1 Typical behavior

We found that even if the self-gravity of the scalar field is considered, the oscillon can be formed, generally. In this subsection, the typical behaviors of the oscillon are discussed.

Although we show the result for $\sigma^2 G = 1.0 \times 10^{-3}$, the typical behavior discussed in this subsection is same as the other value of $\sigma^2 G$. The time evolution of the scalar field at the origin is depicted in Fig.4.3. Fig.4.3 implies that the scalar field oscillates with a high-frequency basic oscillating mode, and the envelop of the scalar field at the origin

In order to examine the time evolution of the high-frequency mode, we define the period T as the time interval between two neighboring times of $\Pi = 0$ and $\dot{\Pi} > 0$. Fig.4.4 implies that the period of the oscillation of the scalar field decreases, and when $T(\lambda\sigma^2)^{1/2}$ becomes about 4.6, the oscillon disappears and the scalar field dissipates.

Next, let us focus on the time evolution of the Kodama mass inside the sphere which radius is r_0. The time dependence of the Kodama mass is depicted in Fig.4.5. Fig.4.5 implies that there are mainly three stages. First, after the bubble starts to

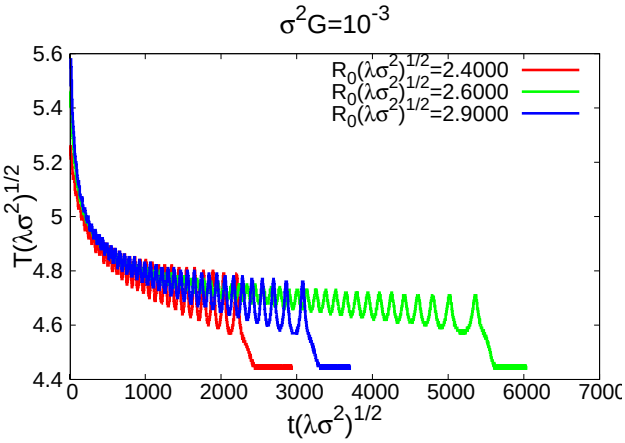

Figure 4.4: Time evolution of the period T of the scalar filed at the origin for $\sigma^2 G = 1.0 \times 10^{-3}$.

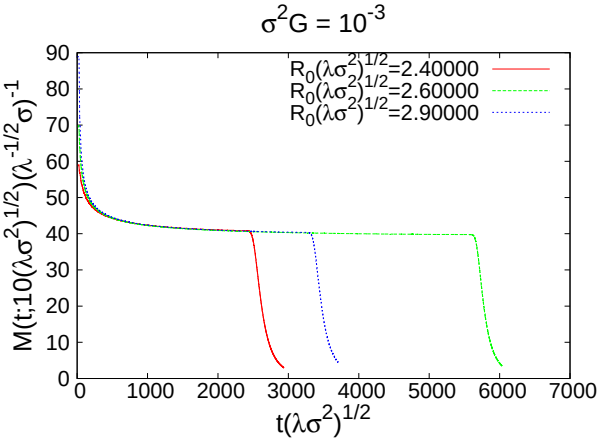

Figure 4.5: Time evolution of the energy inside the sphere with the radius $r_0(\lambda\sigma^2)^{-1/2} = 10$.

collapse, the Kodama mass rapidly decreases with the scalar field radiation. After this stage, oscillon forms, and the energy inside the sphere is almost constant $M_{\rm osiclon}$. In this stage, the scalar field is not radiated during this phase. Finally, the oscillon disappears and the scalar field dissipates.

The energy $M_{\rm osiclon}$ during the oscillon phase almost does not depends on the initial bubble radius, and depends on $\sigma^2 G$. The dependence is given in Table.4.1. Table.4.1 shows that $M_{\rm Oscillon}$ is smaller for the larger $\sigma^2 G$. The typical lifetime

Table 4.1: The dependence of $M_{\rm Oscillon}$ on $\sigma^2 G$.

$\sigma^2 G$	$M_{\rm Oscillon}(\lambda^{-1/2}\sigma)^{-1}$
1.0×10^{-4}	43
5.0×10^{-4}	41
1.0×10^{-3}	40
2.0×10^{-3}	38

of the oscillon is 10^3-$10^4(\lambda\sigma^2)^{-1}$. Furthermore, when the bubble radius is smaller than a certain value, the oscillon does not appear. The initial data which initial bubble radius is smaller than the value has the initial energy which is smaller than $M_{\rm Oscillon}$. These behavior of the time evolution of the energy and the lifetime are similar to the ones in the Minkowski background.

4.2.2 Fine structure of the lifetime

In [50], Honda et al. found the critical behavior of the oscillon on Minkowski background. Their statement is that when the initial bubble radius R_0 is fine-tuned to some value R_*, the lifetime of the oscillon becomes long and obeys the following scaling law:

$$\tau = -\gamma \ln |R - R_*| + C, \tag{4.59}$$

where C and γ are constants. The difference between $R_0 < R_*$ and $R_0 > R_*$ appears in the number of the modulation of the envelope. That is, when the number of the modulation in $R_0 < R_*$ is n, the number of the modulation in $R_0 > R_*$ is $n+1$ or $n-1$. Since the lifetime of the oscillon obeys the scaling law, this behavior is an analogy with type I critical behavior of gravitational collapse.

In this study, we examine the critical behavior of the oscillon in Einstein-scalar theory with double-well potential. Let us focus on the first three fine structures in each value of $\sigma^2 G$. The relation between the lifetime of the oscillon and the initial bubble radius is depicted in the left panel of Fig.4.6. The right panel of Fig.4.6 shows the behavior of the scalar field at the origin which initial parameter is around the third fine structure. These behavior is similar to the one of the Minkowski background. We also can found the scaling law (see Fig.4.7). The relation between the index of the each fine structure and $\sigma^2 G$ is depicted in Fig.4.8.

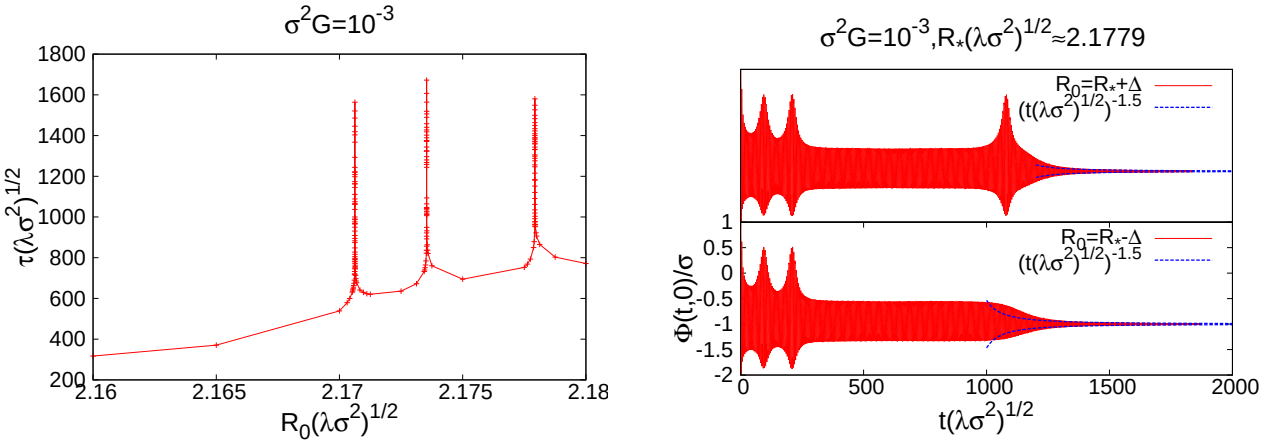

Figure 4.6: The left panel shows the relations between the initial radius of the bubble and the lifetime of the oscillons around the first three peaks for $\sigma^2 G = 1.0 \times 10^{-3}$. The right panel shows the envelope of the time evolution of the scalar field at the origin near the third peak for $\sigma^2 G = 1.0 \times 10^{-3}$. The dotted blue lines show power-law dissipation of $\propto t^{-3/2}$ which is the power in the massive scalar case.

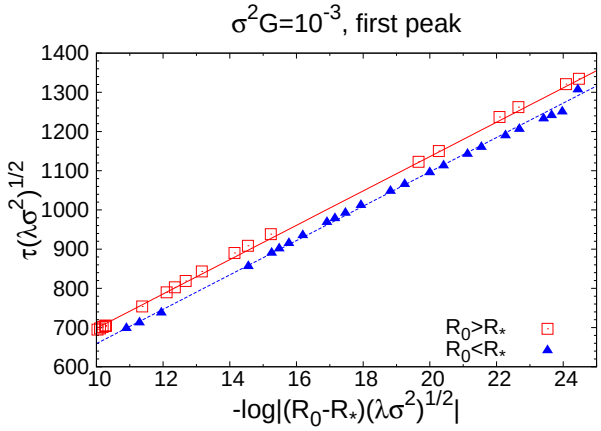

Figure 4.7: We can observe the scaling behavior near the first peak for $\sigma^2 G = 10^{-3}$.

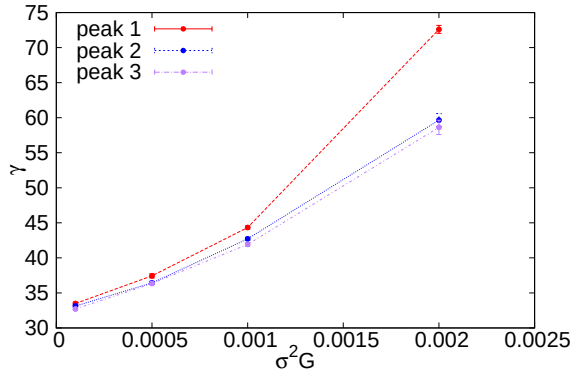

Figure 4.8: Relation between the exponent γ and $\sigma^2 G$.

4.2.3 Fine structure of the scaling law

In the previous subsection, we discuss the scaling law of the lifetime of the oscillon. Furthermore, we found the fine structure around the scaling law in the case of $\sigma^2 G = 2.0 \times 10^{-3}$. The relation between the lifetime τ and the initial bubble radius, and the deviation between the lifetime and the scaling law are depicted in Fig.4.9-4.11. These figures imply that the lifetime of the oscillon oscillates around the scaling law. The deviation of the lifetime from the scaling law can be fitted by the following function:

$$A\cos(-\frac{2\pi}{\tilde{T}}\log|(R_0-R_*)(\lambda\sigma^2)^{1/2}|+\varphi) \equiv \tau(R_0(\lambda\sigma^2)^{1/2})-(-\gamma\log|(R_0-R_*)(\lambda\sigma^2)^{1/2}|)-\delta, \tag{4.60}$$

where γ and δ are fixed with the fitting with the original scaling relation $\tau = \gamma \ln|R_0 - R_*| + C$, and A and φ are additional fitting parameters, which are fixed with the least square fitting with fixed γ and δ.

In relation to these oscillations of lifetime, we found a small modulation in the plateau of the envelope of the scalar field at the center. (see Fig.4.12 and Fig.4.13) The period $\mathcal{T}$ of the oscillation of the scalar field at the origin, the period $\tilde{T}$ of the fine structure of the scaling law and γ are given as follows;

$$\begin{array}{llll} \tilde{T} \simeq 5.2 & \mathcal{T} \simeq 380 & \gamma \simeq 73 & \text{(for the first peak)}, \\ \tilde{T} \simeq 5.2 & \mathcal{T} \simeq 340 & \gamma \simeq 59 & \text{(for the second and third peaks)}. \end{array}$$

These properties are not observed in the case of Minkowski background. Therefore, the origin of these behaviors is the gravitational effect. These behavior suggest that the oscillation of the lifetime and the envelop of the critical solution are associated with a new type of type I critical behavior.

4.2.4 Strong gravity case

In the case of $\sigma^2 G = 1.0 \times 10^{-4}, 5.0 \times 10^{-4}, 1.0 \times 10^{-3}$ and 2.0×10^{-3}, after the oscillon disappears, the scalar field energy does not return to the scalar field at

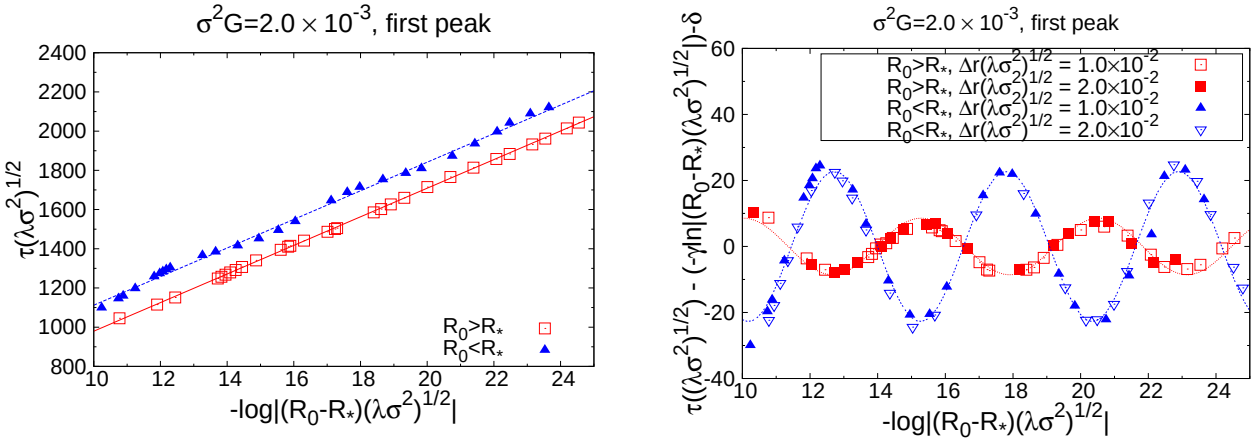

Figure 4.9: The left panel shows the relation between the lifetime τ and the initial bubble radius near the first peak for $\sigma^2 G = 2.0 \times 10^{-3}$. The right panel shows the deviation between the lifetime and the scaling law. In order to check the convergence of the oscillation behavior, we plot the two numerical results with different grid intervals Δr.

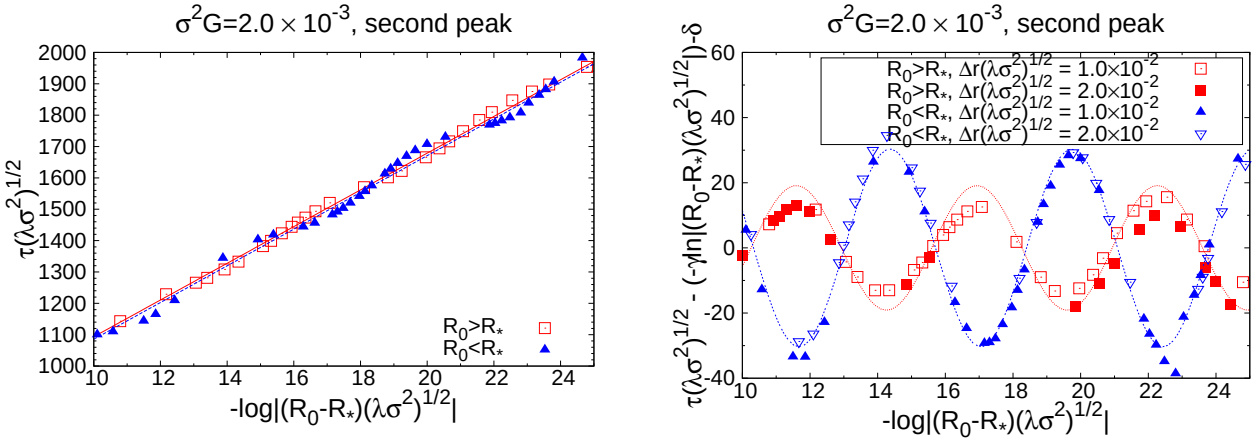

Figure 4.10: The left panel shows the relation between the lifetime τ and the initial bubble radius near the second peak for $\sigma^2 G = 2.0 \times 10^{-3}$. The right panel shows the deviation between the lifetime and the scaling law. In order to check the convergence of the oscillation behavior, we plot the two numerical results with different grid intervals Δr.

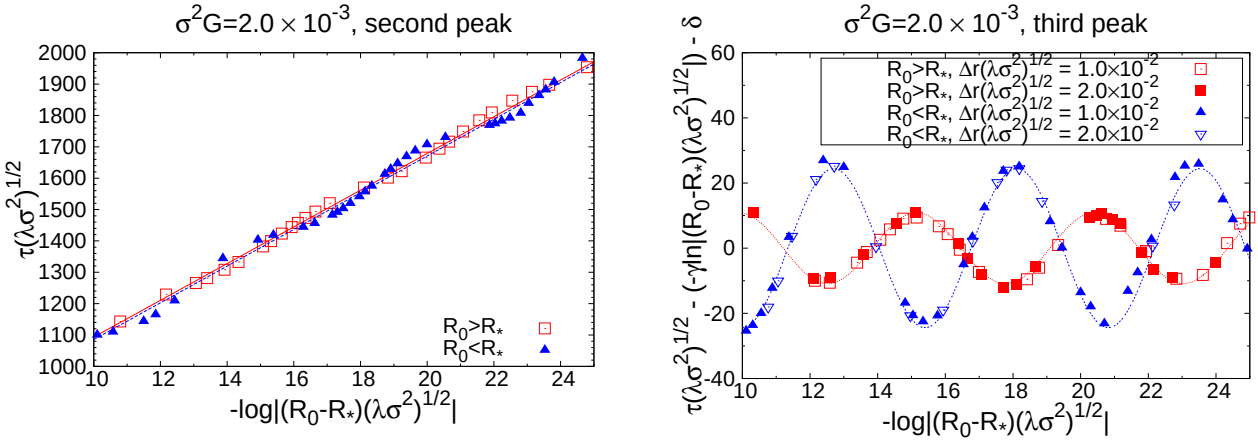

Figure 4.11: The left panel shows the relation between the lifetime τ and the initial bubble radius near the third peak for $\sigma^2 G = 2.0 \times 10^{-3}$. The right panel shows the deviation between the lifetime and the scaling law. In order to check the convergence of the oscillation behavior, we plot the two numerical results with different grid intervals Δr.

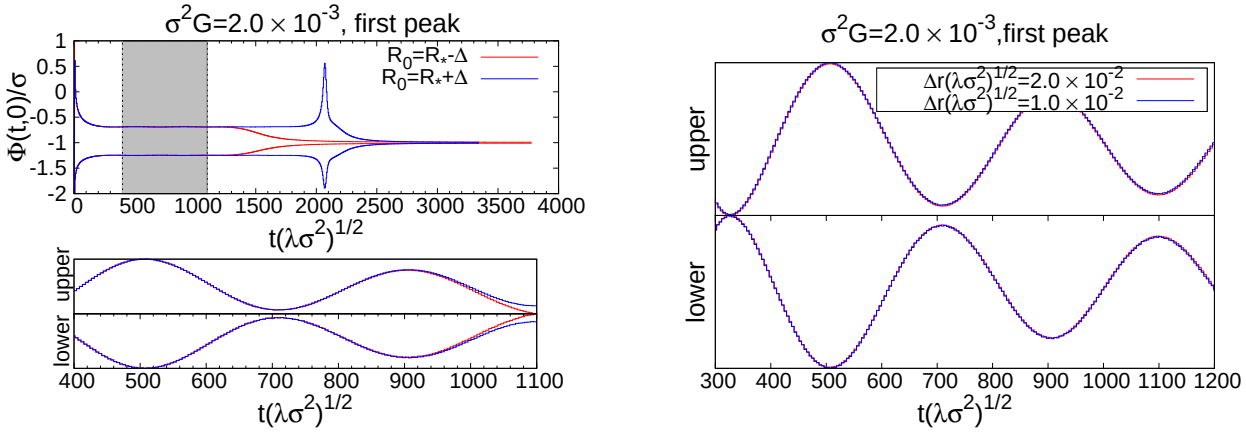

Figure 4.12: The left upper panel shows the time evolution of the envelop of the scalar field at the origin for the first peak for $\sigma^2 G = 2.0 \times 10^{-3}$. The left lower panel shows the oscillation of the envelope of the scalar filed at the origin in the shaded region of the upper panel. The right panel represents the convergence of the modulation in the plateau for different gird intervals Δr.

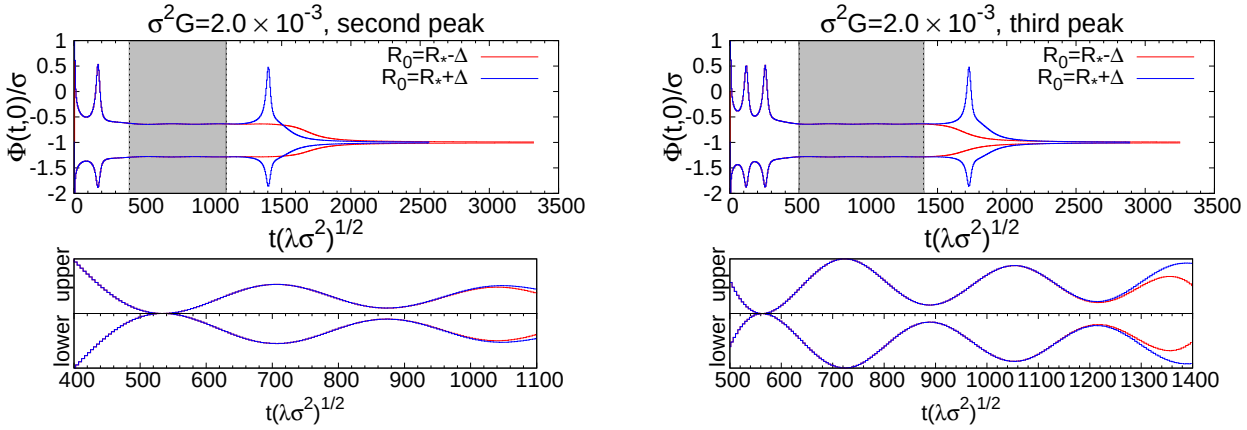

Figure 4.13: The left upper panel shows the time evolution of the envelop of the scalar field at the origin for the second peak for $\sigma^2 G = 2.0 \times 10^{-3}$. The left lower panel shows the oscillation of the envelop of the scalar filed at the origin in the shaded region of the upper panel. The right panel represents the convergence of the modulation in the plateau for different gird intervals Δr.

least until the time when the Kodama mass becomes 0.001 times smaller than the initial data. On the other hand, in the case of $\sigma^2 G > 0.002$, these are the cases in which the scalar field returns to center after the oscillon disappears. The example of the time evolution are depicted in Fig.4.14. Fig,4.14 shows that the energy of the scalar field return to the center after the oscillon disappear. Since the scalar field becomes once near the potential minimum after the oscillon disappears, the nonlinearity of the potential of the scalar field can be neglected. Therefore, the reason for the return of the energy is the gravitational attraction.

4.3 Result

Here, we summarize the properties of self-gravitating oscillon.

In this study, we considered the oscillon solution in the Einstein-scalar field theory with double well potential, in weak gravity case. Firstly, we showed that the self-gravitating oscillon generally can appear after the bubble collapse, and discussed the time evolution of the osciilon. These typical properties of the self-gravitating oscillon is similar to one of the oscillon in Minkowski background. Secondly, the critical behavior of the oscillon was discussed. As a result, we observed the type I critical behavior in the case of $\sigma^2 G = 1.0 \times 10^{-4}, 5.0 \times 10^{-4}, 1.0 \times 10^{-3}$. Furthermore, it was shown that the fine structure of the scaling law appears in the case of 2.0×10^{-3} (see Fig.4.9-4.11). This behavior may imply that there is a new type of the critical behavior.

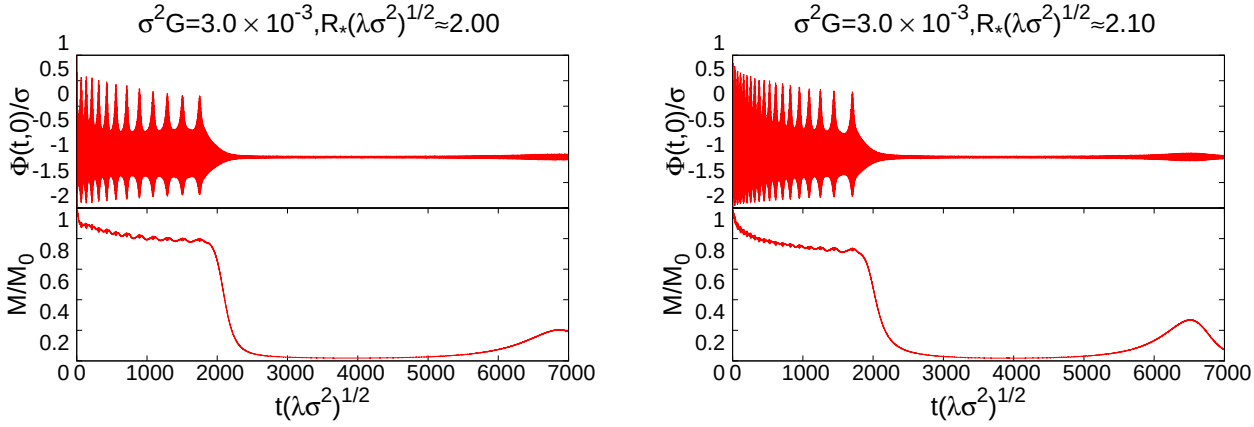

Figure 4.14: The time evolution of the envelope of the scalar filed for $\sigma^2 G = 3.0 \times 10^{-3}$. The upper panel shows the envelope the scalar field at the origin. The lower panel shows the time evolution of the Kodama mass in the sphere of the radius r_0.

Chapter 5

Summary

In this study, in oder to reveal the universal properties of time dependent solutions of the Einstein-scalar field theory with double well potential, we focus on two different types of the critical behavior in this theory. In Chap.2, we reviewed the fundamental properties of the critical behavior. Furthermore, we have seen that the critical collapse reflects to the non-trivial structure of the phase space, and it appears even in systems without gravity.

In Chap.3, and Chap.4, we have examined that the two critical behaviors in the Einstein-scalar field theory with double well potential. In Chap.3, gravitational collapse of a spherically symmetric domain wall was examined, and the critical collapse appears around the threshold of black hole formation. This critical behavior is similar to one of the gravitational collapse of a massless scalar field. That is, in the supercritical region, the black hole mass obeys the scaling law with wiggle around the threshold of the black hole formation. Furthermore, in the subcritical region, the maximal value of the curvature also obeys the scaling law with wiggle. The values of the index in the scaling law and the period of the wiggle are close to them of the massless scalar collapse, respectively.

In Chap.4, we discussed the critical behavior of the self-gravitating oscillons in relatively weak gravity case. The typical properties of oscillons in the system are similar to one in the Minkowski background. Furthermore, it was shown that it is possible that the new type of type I critical behavior appears.

There are two important future works in this study. The first is to investigate whether the behavior observed in Chap.4 is universal, or not. The critical behavior is universal behavior which does not depend on the details of the initial data. Therefore, we must check the universality of the behavior which is observed in Chap.4. Furthermore, constructing the critical solution, we must confirm that the solution is a co-dimension one attractor solution, and the critical exponent relates to the Lyapunov exponent.

The second point is the behavior of the oscillon in the strong gravity case. In Chap.4, we examined the behavior of the oscillon in relatively week gravity case. On the other hand, the behavior of the oscillon in strong gravity case may be interesting. This is because it is possible that the oscillon with the strong self-gravity may collapse to a black hole, just like the critical behavior of the Einstein-massive scalar field theory. In the Einstein-massive scalar field theory, the soliton

star [17] which is a longevity localized solution in the theory can collapse to black hole, which phase is called delayed collapse phase [16]. There also exits the prompt collapse phase, and the type I critical collapse appears on the boundary between the prompt collapse and the delayed collapse. Therefore, if the oscillon in the Einstein scalar field theory with double well potential can collapse to a black hole, it is expected that the type I critical collapse appears on the boundary between the phase in which the oscillon collapse to a black hole and scalar field promptly collapse to a black hole. The existence of these non-trivial phase may imply the existence of the non-trivial phase diagram.

These future works are interesting, we expect that they characterize the dynamical solution of the Einstein-scalar field theory with double well potential.

Appendix A

ADM decomposition and the spherically symmetric spacetime

ADM formulation is a important formulation for numerical simulation of general relativity. In this appendix, we summarize the ADM formalism.

A.1 ADM formalism

A.1.1 Definition of geometrical quantities

Einstein equations is written as covariant form. On the other hand, in order to calculate the time evolution, we impose the initial spatial profile at initial data, and examine the time evolution. Since the general relativity is a gauge theory, Einstein equations contains the time evolution parts and constraint parts. ADM formalism gives a method to decompose the Einstein equations into them. This procedure is called ADM decomposition. Schematic picture of ADM decomposition is given in Fig.A.1.

We denote $\mathcal{M}$ and g as the spacetime and the metric of $\mathcal{M}$, and assume that $\mathcal{M}$ is a globally hyperbolic spacetime. Then, $\mathcal{M}$ can be decomposed into a family of spacelike hypersurfaces Σ_t with is labeled by $t \in \mathbb{R}$. The constant t surface in the spacetime is a 3-dimensional spatial hypersurface. Σ_t denotes a 3-dimensional spatial hypersurface which corresponds to $t = \text{const}$. The initial data is a profile of physical quantities on Σ_{t_0}, and time evolution determine a profile on Σ_t. Since Σ_t is a 3 dimensional spatially hypersurface, it has a metric γ, and the all eigenvalue of the metric is positive, that is $\det(\gamma) > 0$. The normalized normal vector n of Σ_t is timelike vector, which is given as

$$n_\mu = -(\nabla_\mu t \nabla^\mu t)^{-1/2} \nabla_\mu t, \tag{A.1}$$

where ∇_μ is covariant derivative in $\mathcal{M}$.

The projection operator from the vector in $\mathcal{M}$ to the vector in Σ_t is

$$\gamma^\alpha{}_\beta = \delta^\alpha{}_\beta + n^\alpha n_\beta. \tag{A.2}$$

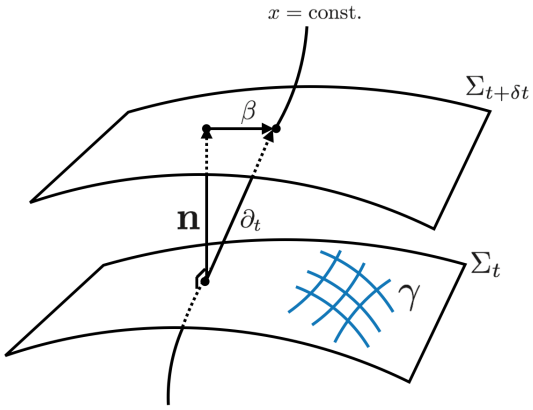

Figure A.1: ADM decomposition of spacetine

$\gamma^{\alpha}{}_{\beta}$ satisfies the following properties;

$$n_\alpha \gamma^{\alpha}{}_{\beta} = 0, \tag{A.3}$$
$$v_\alpha \gamma^{\alpha}{}_{\beta} = v_\beta, \tag{A.4}$$

where v is a vector on Σ_t, which is orthogonal to n. [1] These properties show that $\gamma^{\alpha}{}_{\beta}$ is a projection operator. The following properties show that $\gamma^{\alpha}{}_{\beta}$ is a projection operator. By using this operator, we can get a relation between 3-metric γ and 4-metric g, that is,

$$\gamma_{\alpha\beta} = \gamma^{\mu}{}_{\alpha}\gamma^{\nu}{}_{\beta} g_{\mu\nu} \tag{A.5}$$
$$= g_{\alpha\beta} + n_\alpha n_\beta. \tag{A.6}$$

The extrinsic curvature $K_{\alpha\beta}$ which is tensor on Σ_t and characterize how Σ_t is embedded in $\mathcal{M}$ is defined as follows;

$$K_{\alpha\beta} := -\gamma^{\mu}_{\alpha}\gamma^{\nu}_{\beta}\nabla_\mu n_\nu. \tag{A.7}$$

Above definition means that the extrinsic curvature is a derivative of the normal vector along Σ_t. From simple calculation, we have

$$K_{\alpha\beta} = -\nabla_\beta n_\alpha - a_\alpha n_\beta, \tag{A.8}$$

where a_μ is defined as

$$a_\mu := n^\nu \nabla_\nu n_\mu. \tag{A.9}$$

The relation between the covariant derivative ∇ associated with g and the covariant derivative D associated with γ is given as

$$D_\rho v^{\alpha\cdots}{}_{\beta\cdots} = \gamma^{\alpha}{}_{\mu}\gamma^{\nu}{}_{\beta}\gamma^{\sigma}{}_{\rho}\gamma \cdots \nabla_\sigma v^{\mu\cdots}{}_{\nu\cdots}, \tag{A.10}$$

[1] In order to define the inner product between v and n, v which is a 3-vector in Σ_t is extended to 4-vector in $\mathcal{M}$. We can do it, naturally.

where v is a tensor in Σ_t. The derivative D which is written as above definition satisfies six condition for covariant derivative associated with Levi-Civita connection; that is, linearity, Leibniz rule, commutativity with contraction, action for scalar, torsion free, and metric condition for γ. Conversely, we can show that the derivative which satisfies above condition is unique, and it is just a covariant derivative associated with Levi-Civita connection.

Original form of Einstein equations composes the curvature of spacetime $\mathcal{M}$. On the other hand, to calculate the time evolution, it is useful to write the equations in terms of the curvature of Σ_t and the extrinsic curvature. The relation between the curvature of $\mathcal{M}$ and the curvature of Σ_t is called Gauss relation and Codazzi relation. Gauss relation is

$$\begin{aligned}
\gamma^{\mu}{}_{\alpha}\gamma^{\nu}{}_{\beta}\gamma^{\gamma}{}_{\rho}\gamma^{\sigma}{}_{\delta}R^{\rho}{}_{\sigma\mu\nu} &= {}^3R^{\gamma}{}_{\delta\alpha\beta} + K^{\gamma}{}_{\alpha}K_{\delta\beta} - K^{\gamma}{}_{\beta}K_{\alpha\delta}, && \text{(A.11)}\\
\gamma^{\mu}{}_{\alpha}\gamma^{\nu}{}_{\beta}R_{\mu\nu} + \gamma_{\alpha\mu}n^{\nu}\gamma^{\rho}{}_{\beta}n^{\sigma}R^{\mu}{}_{\nu\rho\sigma} &= {}^3R_{\alpha\beta} + KK_{\alpha\beta} - K_{\alpha\mu}K^{\mu}_{\beta}, && \text{(A.12)}\\
R + 2R_{\mu\nu}n^{\mu}n^{\nu} &= {}^3R + K^2 - K_{ij}K^{ij}, && \text{(A.13)}
\end{aligned}$$

where K is a trace part of K_{ij}. Codazzi relation is

$$\begin{aligned}
\gamma^{\gamma}{}_{\rho}n^{\sigma}\gamma^{\mu}{}_{\alpha}\gamma^{\nu}{}_{\beta}R^{\rho}{}_{\sigma\mu\nu} &= D_{\beta}K^{\gamma}{}_{\alpha} - D_{\alpha}K^{\gamma}{}_{\beta}, && \text{(A.14)}\\
\gamma^{\mu}{}_{\alpha}n^{\nu}R_{\mu\nu} &= D_{\alpha}K - D_{\mu}K^{\mu}{}_{\alpha}. && \text{(A.15)}
\end{aligned}$$

A.1.2 ADM decomposition of Einstein equations

In this subsection, we decompose Einstein equations into the time evolution part and the constraint equation part. Since the spacetime $\mathcal{M}$ is assumed to be globally hyperbolic, $\mathcal{M}$ can be covered by $\{\Sigma_t\}_{t\in\mathbb{R}}$. Then, we assume that t is a time coordinate, and $\nabla_\mu t$ does not vanish at all point in spacetime. This assumption means that the different hypersurfaces Σ_t and $\Sigma_{t'}$ $(t \neq t')$ do not have intersection. The normalized normal vector n of Σ_t is

$$n_\mu = -\alpha\nabla_\mu t, \tag{A.16}$$

where α is defined as

$$\alpha := (-\nabla_\mu t\nabla^\mu t)^{-1/2}. \tag{A.17}$$

α is called the lapse function. By using the lapse function, we have

$$\begin{aligned}
a_\mu &:= n^\nu\nabla_\nu n_\mu = D_\mu \ln\alpha, && \text{(A.18)}\\
K_{\alpha\beta} &= -\nabla_\beta n_\alpha - D_\alpha \ln\alpha n_\beta. && \text{(A.19)}
\end{aligned}$$

Next, let us define the normal evolution vector m, which is defined as

$$m^\mu := -\alpha n^\mu. \tag{A.20}$$

This vector has a following properties;

$$\begin{aligned}
m^\mu\nabla_\mu t &= 1, && \text{(A.21)}\\
t(p + \delta t\ m) &= t(p) + \delta t && \text{(A.22)}
\end{aligned}$$

$$m^\mu \nabla_\mu t \;=\; t(p) + \delta t \;\; \text{for } p \in \mathbb{R}. \tag{A.23}$$

From above properties, m corresponds to the temporal development. We can rewrite the eq.A.19 as

$$\alpha K^\alpha_{\ \beta} = -\nabla_\beta m^\alpha - D^\alpha \alpha n_\beta + n^\alpha \nabla_\beta \alpha, \tag{A.24}$$

and we have

$$\mathcal{L}_m \gamma_{\alpha\beta} = -2\alpha K_{\alpha\beta}, \tag{A.25}$$

and

$$K_{\alpha\beta} = -\frac{1}{2}\mathcal{L}_n \gamma_{\alpha\beta}. \tag{A.26}$$

By using m, the components of Riemann tensor and Ricci tensor of $\mathcal{M}$ which are not contained in Gauss relation and Codazzi relation can be written in terms of the curvature in Σ_t. The relation is called Ricci equation, and it is of the form

$$\gamma_{\alpha\mu} n^\rho \gamma^\nu_{\ \beta} n^\sigma R^\mu_{\ \rho\nu\sigma} \;=\; \frac{1}{\alpha}\mathcal{L}_m K_{\alpha\beta} + \frac{1}{\alpha} D_\alpha D_\beta \alpha + K_{\alpha\mu} K^\mu_{\ \beta}, \tag{A.27}$$

$$\gamma^\mu_{\ \alpha} \gamma^\nu_{\ \beta} R_{\mu\nu} \;=\; -\frac{1}{\alpha}\mathcal{L}_m K_{\alpha\beta} - \frac{1}{\alpha} D_\alpha D_\beta \alpha + {}^3R_{\alpha\beta} + K K_{\alpha\beta} - 2K_{\alpha\mu} K^\mu_{\ \beta}. \tag{A.28}$$

Combing the Gauss-Codazzi equations with Ricci equation, we have

$$R + R_{\mu\nu} n^\mu n^\nu \;=\; {}^3R + K^2 - \frac{1}{\alpha}\mathcal{L}_m K - \frac{1}{\alpha} D^i D_i \alpha, \tag{A.29}$$

$$R \;=\; {}^3R + K^2 + K_{ij} K^{ij} - \frac{2}{\alpha}\mathcal{L}_m K - \frac{2}{\alpha} D^i D_i \alpha. \tag{A.30}$$

Before the decomposition of Einstein equations, we will decompose the energy momentum tensor $T_{\mu\nu}$ of matter fields. The energy momentum tensor contains the matter energy density, matter momentum density, and matter stress tensor, and these quantities are defined as follows;

$$E \;:=\; T_{\mu\nu} n^\mu n^\nu, \tag{A.31}$$

$$p_\alpha \;:=\; -T_{\mu\nu} n^\mu \gamma^\nu_{\ \alpha}, \tag{A.32}$$

$$S_{\alpha\beta} \;:=\; T_{\mu\nu} \gamma^\mu_{\ \alpha} \gamma^\nu_{\ \beta}. \tag{A.33}$$

By definition, p_α and $S_{\alpha\beta}$ are tangent to the hypersurface.

By using the above quantities, we can decompose the Einstein equations into the time evolution part and the constraint part. Firstly, both two indexes of Einstein equations are contracted with the projection tensor $\gamma_\alpha^{\ \beta}$, and using the Ricci equations, we have

$$\mathcal{L}_m K_{ij} = -D_i D_j \alpha + \alpha\{R_{ij} + K K_{ij} - 2K_{ik} K^k_{\ j} + 4\pi((S - E)\gamma_{ij} - 2S_{ij})\}, \tag{A.34}$$

where S is a trace part of S_{ij}. This equation is a evolution equation which determine the time evolution of the extrinsic curvature.

Next, one of two indexes of Einstein equations is contracted with the projection tensor, the other index is contracted with the normalized normal vector n, and Codazzi equation is used, we have

$$D_j K^j{}_i - D_i K = 8\pi p_i. \tag{A.35}$$

Since this equation does not have time derivative of variables, it is a constraint equation. It is called the Momentum constraint.

Furthermore, both two indexes of Einstein equations are contracted with n, and using the Gauss relation, we have

$$R + K^2 - K_{ij}K^{ij} = 16\pi E. \tag{A.36}$$

Since this equation also does not have the time derivative, it is a constraint equation. It is called the Hamiltonian constraint.

A.1.3 ADM decomposition of the metric and Einstein equations

In order to get the representation of the evolution equation which explicitly has a time derivative, let us introduce the basis ∂_t associated with t. The inner product between ∂_t and its dual $\nabla t (= dt)$ is unity:

$$\nabla_\mu t (\partial_t)^\mu = 1. \tag{A.37}$$

Because ∂_t is not m generally, the difference between them is denoted as β, which is called shift vector:

$$\begin{aligned} (\partial_t)^\mu &= m^\mu + \beta^\mu, & \text{(A.38)} \\ &= \alpha n^\mu + \beta^\mu. & \text{(A.39)} \end{aligned}$$

From eq.(A.21), the shift vector is tangent to Σ_t:

$$n^\mu \beta_\mu = 0. \tag{A.40}$$

Furthermore, we have

$$\partial_t \cdot \partial_t = -\alpha^2 + \beta \cdot \beta. \tag{A.41}$$

This means that if $\beta \cdot \beta < \alpha^2$, ∂_t is a time like vector, if $\beta \cdot \beta = \alpha^2$, ∂_t is a null vector, and if $\beta \cdot \beta > \alpha^2$, ∂_t is a space like vector. Additionally, the component of the normalized norm vector is as follows:

$$\begin{aligned} n^\alpha &= (\frac{1}{\alpha}, -\frac{\beta^i}{\alpha}), & \text{(A.42)} \\ n_\alpha &= (-\alpha, 0). & \text{(A.43)} \end{aligned}$$

The spacetime metric can be expressed in terms of α, βi, and γ_{ij}. Eq.(A.41) gives the (t,t) component of the metric. Furthermore, (t,i) component and (i,j) component are given from the following equations:

$$(\partial_t)^\mu g_{\mu\nu} \gamma^\nu{}_\alpha (\partial_i)^\alpha = \beta_i, \tag{A.44}$$

$$(\partial_i)^\mu \gamma^\alpha{}_\mu g_{\alpha\beta} \gamma^\beta{}_\nu (\partial_j)^\nu = \gamma_{ij}. \tag{A.45}$$

Therefore, the metric is

$$g_{\alpha\beta} = \begin{pmatrix} -\alpha^2 + \beta_k \beta^k & \beta_j \\ \beta_i & \gamma_{ij} \end{pmatrix}, \tag{A.46}$$

and its inverse is

$$g^{\alpha\beta} = \begin{pmatrix} -\frac{1}{\alpha^2} & \frac{\beta^j}{\alpha^2} \\ \frac{\beta^i}{\alpha^2} & \gamma^{ij} - \frac{\beta^i \beta^j}{\alpha^2} \end{pmatrix}. \tag{A.47}$$

The Lie derivative of γ_{ij} and K_{ij} along to m can be expressed as follows:

$$\mathcal{L}_m \gamma_{ij} = \left(\frac{\partial}{\partial t} - \mathcal{L}_\beta \right) \gamma_{ij}, \tag{A.48}$$

$$\mathcal{L}_m K_{ij} = \left(\frac{\partial}{\partial t} - \mathcal{L}_\beta \right) K_{ij}. \tag{A.49}$$

By using these equations, rewriting the evolution equations of γ_{ij} and K_{ij}, we have

$$(\frac{\partial}{\partial t} - \mathcal{L}_\beta)\gamma_{ij} = -2\alpha K_{ij}, \tag{A.50}$$

$$(\frac{\partial}{\partial t} - \mathcal{L}_\beta)K_{ij} = -D_i D_j \alpha + \alpha\{R_{ij} + K K_{ij} - 2K_{ik}K^k{}_j + 4\pi((S-E)\gamma_{ij} - 2S_{ij})\}. \tag{A.51}$$

Since general relativity is a gauge theory, the time evolution cannot be determined by only the hamiltonian constraint Eq.(A.36), the momentum constraint Eq.(A.35), and evolution equations Eq.(A.50),Eq.(A.51). Hence, in addition to these equations, the gauge fix condition which determines the lapse function and shift vector, must be imposed.

A.2 spherically symmetric spacetime

So far, we have discussed the ADM decomposition of general spacetime. In this subsection, the metric which is given in above subsection is applied to the general spherically symmetric spacetime.

If the line element in an appropriate coordinate is given as

$$ds^2 = \gamma_{AB} dx^A dx^B + \gamma_{\theta\theta} d^2\Omega, \tag{A.52}$$

where γ_{AB} $(A, B = 0, 1)$ and $\gamma_{\theta\theta}$ are function of x, and $d^2\Omega$ is the line element of S^2, then the spacetime has a spherical symmetry. In particular, when the coordinates x^0 and x^1 are the time coordinate t and radial coordinate r, we have

$$ds^2 = \gamma_{tt} dt^2 + 2\gamma_{tr} dt dr + \gamma_{rr} dr^2 + \gamma_{\theta\theta} d^2\Omega. \tag{A.53}$$

Therefore, the 3-metric of general spherically symmetric spacetime is

$$\gamma_{ij} = \begin{pmatrix} \gamma_{rr} & 0 & 0 \\ 0 & \gamma_{\theta\theta} & 0 \\ 0 & 0 & \gamma_{\theta\theta}\sin^2\theta \end{pmatrix}, \tag{A.54}$$

and the shift vector β^i is

$$\beta^i = (\beta, 0, 0). \tag{A.55}$$

Furthermore, from the spherical symmetry, the extrinsic curvature form is

$$K_{ij} = \begin{pmatrix} K_{rr} & 0 & 0 \\ 0 & K_{\theta\theta} & 0 \\ 0 & 0 & K_{\theta\theta}\sin^2\theta \end{pmatrix}. \tag{A.56}$$

The lapse function α, shift vector β, γ_{rr}, $\gamma_{\theta\theta}$, K_{rr}, and $K_{\theta\theta}$ are functions of t and r.

Under the above anzats, we can write the Einstein equations. Firstly, the time evolution equations eqs.(A.50),(A.51), become

$$\dot{\gamma}_{rr} = 2\beta' - \gamma'_{rr}\beta - 2\alpha K_{rr}, \tag{A.57}$$

$$\dot{\gamma}_{\theta\theta} = \gamma'_{\theta\theta}\beta - 2\alpha K_{\theta\theta}, \tag{A.58}$$

$$\begin{aligned}\dot{K}_{rr} = {} & \beta K'_{rr} + 2\beta' K_{rr} - \left(\alpha'' - \frac{1}{2}\frac{\gamma'_{rr}}{\gamma_{rr}}\alpha'\right) + \alpha\left\{-\frac{\gamma''_{\theta\theta}}{\gamma_{\theta\theta}} + \frac{1}{2}\frac{\gamma'_{\theta\theta}(\gamma_{\theta\theta}\gamma_{rr})'}{\gamma^2_{\theta\theta}\gamma_{rr}} - \frac{K^2_{rr}}{\gamma_{rr}}\right. \\ & \left. + 2\frac{K_{\theta\theta}K_{rr}}{\gamma_{\theta\theta}} + 4\pi((S-E)\gamma_{rr} - 2S_{rr})\right\},\end{aligned} \tag{A.59}$$

$$\dot{K}_{\theta\theta} = \beta K'_{\theta\theta} - \frac{1}{2}\frac{\gamma'_{\theta\theta}}{\gamma_{rr}}\alpha' + \alpha\left\{\frac{1}{4}\frac{\gamma'_{rr}\gamma'_{\theta\theta}}{\gamma^2_{rr}} - \frac{1}{2}\frac{\gamma''_{\theta\theta}}{\gamma_{rr}} + \frac{K_{rr}K_{\theta\theta}}{\gamma_{rr}} + 4\pi((S-E)\gamma_{\theta\theta} - 2S_{\theta\theta})\right\}. \tag{A.60}$$

The constraint equations are

$$-2\frac{K'_{\theta\theta}}{\gamma_{rr}\gamma_{\theta\theta}} + \frac{\gamma'_{\theta\theta}}{\gamma_{\theta\theta}\gamma_{rr}}K_{rr} + \frac{\gamma'_{\theta\theta}}{\gamma^2_{\theta\theta}}K_{\theta\theta} - 8\pi p = 0, \tag{A.61}$$

$$-2\frac{\gamma''_{\theta\theta}}{\gamma_{rr}\gamma_{\theta\theta}} + \frac{1}{2}\frac{\gamma'_{\theta\theta}(\gamma_{\theta\theta}\gamma_{rr})'}{\gamma^2_{rr}\gamma^2_{\theta\theta}} + \frac{1}{2}\frac{\gamma'_{rr}\gamma'_{\theta\theta}}{\gamma_{\theta\theta}\gamma^2_{rr}} + 4\frac{K_{rr}K_{\theta\theta}}{\gamma_{rr}\gamma_{\theta\theta}} + 2\frac{K^2_{\theta\theta}}{\gamma^2_{\theta\theta}} - 16\pi E = 0. \tag{A.62}$$

A.2.1 boundary condition

In order to calculate the time evolution, we must impose the boundary conditions. The boundary condition of the far boundary in spherically symmetric spacetime is an asymptotically Minkowski, dS, or AdS spacetime. In this paper, we impose the asymptotically Minkowski spacetime, and to impose this boundary condition is not so difficult. On the other hand, it is necessary to pay attention to the boundary condition around the center, that is, we must impose two boundary conditions of each metric component at the center [39]. Around the center, since the areal radius is proportional to r^2, $\gamma_{\theta\theta}$ is expressed as:

$$\gamma_{\theta\theta}(t, r) \simeq \bar{\gamma}_{\theta\theta}(t, r)r^2, \tag{A.63}$$

where $\bar{\gamma}_{\theta\theta}$ is a function of t, r, and the value of $\bar{\gamma}_{\theta\theta}$ at the center is finite. We impose the two boundary conditions on γ_{rr}, $\bar{\gamma}_{\theta\theta}$, K_{rr} and $K_{\theta\theta}$. Firstly, in order that the spacetime is smooth around the center, we have

$$\begin{aligned}
\gamma_{rr}(t,r) &= \gamma_{rr}(t,0) + \mathcal{O}(r^2), && \text{(A.64)}\\
\bar{\gamma}_{\theta\theta}(t,r) &= \bar{\gamma}_{\theta\theta}(t,0) + \mathcal{O}(r^2), && \text{(A.65)}\\
K_{rr} &= K_{rr}(t,0) + \mathcal{O}(r^2), && \text{(A.66)}\\
K_{\theta\theta} &= K_{\theta\theta}(t,0) + \mathcal{O}(r^2). && \text{(A.67)}
\end{aligned}$$

In other word, the derivative of these variable must vanish at the center:

$$\gamma'_{rr}(t,0) = \bar{\gamma}'_{\theta\theta}(t,0) = K'_{rr}(t,0) = K'_{\theta\theta}(t,0) = 0. \qquad \text{(A.68)}$$

Second condition is a local flatness condition, that is

$$\begin{aligned}
\gamma_{rr}(t,0) &= \bar{\gamma}_{\theta\theta}(t,0), && \text{(A.69)}\\
K_{rr}(t,0) &= K_{\theta\theta}(t,0) = 0. && \text{(A.70)}
\end{aligned}$$

These boundary condition corresponds to the regularization of the singular term in equation of motion. To see this fact, let us focus on right hand side of Eq.(A.59). The singular terms in right hand side of the equation are regularized by boundary condition around the center as follows:

$$\begin{aligned}
(\text{RHS of eq.(A.59)})|_{\text{singular part}} &= -\frac{\gamma''_{\theta\theta}}{\gamma_{\theta\theta}} + \frac{1}{2}\frac{\gamma'_{\theta\theta}(\gamma_{\theta\theta}\gamma_{rr})'}{\gamma^2_{\theta\theta}\gamma_{rr}} - \frac{K^2_{rr}}{\gamma_{rr}} + 2\frac{K_{\theta\theta}K_{rr}}{\gamma_{\theta\theta}}\Big|_{\text{singular part}}\\
&< (\text{finite}). && \text{(A.71)}
\end{aligned}$$

Similarly, the constraint equations are also regularized by the boundary conditions:

$$\begin{aligned}
(\text{Ham})|_{\text{singular part}} &= -2\frac{\gamma''_{\theta\theta}}{\gamma_{rr}\gamma_{\theta\theta}} + \frac{1}{2}\frac{\gamma'_{\theta\theta}(\gamma_{\theta\theta}\gamma_{rr})'}{\gamma^2_{rr}\gamma^2_{\theta\theta}} + \frac{1}{2}\frac{\gamma'_{rr}\gamma'_{\theta\theta}}{\gamma_{\theta\theta}\gamma^2_{rr}} + 4\frac{K_{rr}K_{\theta\theta}}{\gamma_{rr}\gamma_{\theta\theta}} + 2\frac{K^2_{\theta\theta}}{\gamma^2_{\theta\theta}}\\
&< (\text{finite}). && \text{(A.72)}
\end{aligned}$$

Therefore, boundary conditions regularize the singular terms in evolution equations, and constraint equations.

Appendix B

Related topics of critical behavior

In this appendix, we introduce the two topics related to the critical collapse.

B.1 Primordial black hole

Primordial black hole (PBH) is a black hole which formed from the fluctuation in the early universe [23, 24]. Since the large fluctuation collapse to PBH, the distribution of PBH relates to the profile of the fluctuation. Therefore, the number density of PBH reflects the fluctuation in the early universe. In order to calculate the number density of PBH, we must know the relation between the strength of the fluctuation and the mass of the black hole. The critical behavior of the gravitational collapse gives us the relation around the threshold of the black hole formation [25]. Furthermore, in the fluid collapse with angular momentum, the spin parameter of Kerr black hole also obeys the scaling law. Gundlach et al. considered the non-spherical perturbation around the critical solution of the perfect fluid, which equation of state is given by $p = \kappa\rho$, and got the following formula;

$$\gamma_J(\kappa) = \frac{5(1+3\kappa)}{3(1+\kappa)}\gamma_M(\kappa), \quad \left(\frac{1}{9} < \kappa \lesssim 0.49\right) \tag{B.1}$$

where γ_M and γ_J are the exponents of the mass scaling and angular momentum scaling, respectively [34, 40]. By using this fact, we can estimate the spin distribution of the primordial black hole [41].

B.2 AdS instability

Since maximally symmetric spacetime is the most fundamental spacetime, a stability of the spacetime is an important topic of gravitation. Recently, the nonlinear instability of AdS spacetime of Einstein-massless scalar field theory with negative cosmological constant was reported in [42] The instability means that the initial arbitrarily small perturbation of the scalar field collapse to the black hole. The important point of this instability is that the outer boundary of an asymptotically AdS spacetime is the time-like boundary. In this spacetime, the massless scalar field can reach the far boundary in finite time.

In order to understand the process until the black hole formation, let us focus on the spherically symmetric and asymptotically AdS spacetime, and consider the time evolution of the initial data which has perturbation of the scalar field. Firstly, the in-going mode of the initial perturbation of the scalar field reaches the origin. If the energy of the in-going mode is large, the scalar field collapse to a black hole. On the other hand, if the energy is small, the scalar field does not collapse, dissipates, and reaches the outer boundary in finite time. Outer boundary reflects the scalar field, and the field reaches the center again. This process is repeated. During this process, the energy of the scalar field is transported to the short wavelength mode by the resonance. Thus, the weak turbulence occurs, and finally, a black hole appears.

In this behavior, it is reported that two critical behaviors appear. Now, we consider the initial data, which has initial parameter ϵ. ϵ characterizes the initial energy of the scalar field. In the case of the initial data which ϵ is large, the scalar field promptly collapses to a black hole. In the case that ϵ is small, a black hole appears after the reflection at the outer boundary. From the numerical simulation, there are the sequences in which the black hole appears after the n times reflections. The threshold of this sequence denotes as ϵ_n, that is, in the case that the initial data within the range $\epsilon_{n+1} < \epsilon < \epsilon_n$, the black hole appears after the n times reflections. Two critical behaviors appear around the threshold. First critical behavior is the original Choptuik's scaling, that is,

$$M(\epsilon) \propto |\epsilon - \epsilon_n|^{\gamma} \tag{B.2}$$

for $\epsilon = \epsilon_n + 0$. $M(\epsilon)$ is a black hole mass which corresponds to the initial parameter ϵ. γ is 0.37, and this value does not depend on n. The second critical behavior appears in $\epsilon = \epsilon_n - 0$ From the numerical simulation, there is a mass gap between $n-1$ sequence and n sequence, that is, $M_{\mathrm{gap},n} = M(\epsilon_n) \neq 0$, and second critical behavior is as follows:

$$M(\epsilon) - M_{\mathrm{gap},n} \propto |\epsilon_n - \epsilon|^{\xi}, \tag{B.3}$$

for $\epsilon = \epsilon_n - 0$. ξ is about 0.7, and this value is also universal with respect to the parametrization of the initial data and independent of n [43].

There are many the generalization of AdS instability [44]. Furthermore, these nonlinear instability can appear in not only AdS spacetime, but also confined spacetime [45–47].

Appendix C

Spacetime with a homothetic vector field

The critical solutions play an important role in the critical collapse. The critical solutions often have a symmetry. For example, the critical solution of the perfect fluid collapse has a continuous self-similarity, and the critical solution of the massless scalar collapse has a discrete self-similarity. Here, we summarize the properties of spacetime which has a continuous self-similarity.

Firstly, when the spacetime has conformal Killing vector ξ which satisfy the following equation, the spacetime has a conformal isometry;

$$\mathcal{L}_\xi g_{\mu\nu} = \alpha(x) g_{\mu\nu}, \tag{C.1}$$

where $\alpha(x)$ is a function of spacetime. In particular, when α is a constant, by normalizing ξ, we have

$$\mathcal{L}_\xi g_{\mu\nu} = -2 g_{\mu\nu}. \tag{C.2}$$

If the solution of this equation in given metric exists, the spacetime has a continuous self-similar symmetry. Then, the vector ξ^μ is a homothetic Killing vector.

Here, when the spacetime has a conformal isometry, we can prove the following equation;

$$\mathcal{L}_\xi R^\gamma{}_{\alpha\beta\delta} = \frac{1}{2}\left(\nabla_\delta\nabla^\gamma\alpha g_{\alpha\beta} - \nabla_\beta\nabla^\gamma\alpha g_{\alpha\delta} - \nabla_\delta\nabla_\alpha\alpha\delta^\gamma_\beta + \nabla_\beta\nabla_\alpha\alpha\delta^\gamma_\delta\right). \tag{C.3}$$

Let us derive this equation. Firstly, we use the following well-known equations:

$$\begin{aligned} \nabla_\beta\nabla_\gamma\xi_\alpha - \nabla_\gamma\nabla_\beta\xi_\alpha &= -R^\rho{}_{\alpha\beta\gamma}\xi_\rho, & \text{(C.4)}\\ R^\rho{}_{\alpha\beta\gamma} + R^\rho{}_{\beta\gamma\alpha} + R^\rho{}_{\gamma\alpha\beta} &= 0. & \text{(C.5)} \end{aligned}$$

By using these equations, we have

$$\nabla_\gamma(\nabla_\beta\xi_\alpha - \nabla_\alpha\xi_\beta) + \nabla_\beta(\nabla_\alpha\xi_\gamma - \nabla_\gamma\xi_\alpha) + \nabla_\alpha(\nabla_\gamma\xi_\beta - \nabla_\beta\xi_\gamma) = 0. \tag{C.6}$$

Furthermore, combing Eq.(C.1), we have

$$\nabla_\gamma\nabla_\beta\xi_\alpha + \nabla_\beta\nabla_\alpha\xi_\gamma + \nabla_\alpha\nabla_\gamma\xi_\beta = \frac{1}{2}\left(\nabla_\gamma\alpha g_{\alpha\beta} + \nabla_\beta\alpha g_{\alpha\gamma} + \nabla_\alpha\alpha g_{\beta\gamma}\right). \tag{C.7}$$

After some calculations, we get

$$\nabla_\beta \nabla_\alpha \xi_\gamma = -R^\mu{}_{\beta\gamma\alpha}\xi_\mu + \frac{1}{2}\left(-\nabla_\gamma \alpha g_{\alpha\beta} + \nabla_\beta \alpha g_{\alpha\gamma} + \nabla_\alpha \alpha g_{\beta\gamma}\right). \tag{C.8}$$

Acting the covariant derivative, we have

$$\nabla_\delta \nabla_\beta \nabla_\alpha \xi_\gamma = -\nabla_\delta R^\mu{}_{\beta\gamma\alpha}\xi_\mu - R^\mu{}_{\beta\gamma\alpha}\nabla_\delta \xi_\mu + \frac{1}{2}\left(-\nabla_\delta \nabla_\gamma \alpha g_{\alpha\beta} + \nabla_\delta \nabla_\beta \alpha g_{\alpha\gamma} + \nabla_\delta \nabla_\alpha \alpha g_{\beta\gamma}\right) \tag{C.9}$$

By using this equation, we get Eq.(C.3). In particular, when the spacetime has a homothetic Killing vector, Eq.(C.3) becomes

$$\mathcal{L}_\xi R^\gamma{}_{\alpha\beta\delta} = 0. \tag{C.10}$$

From this equation, the Lie derivative of Einstein tensor also vanish;

$$\mathcal{L}_\xi G_{\alpha\beta} = 0. \tag{C.11}$$

We can use the coordinate τ which is along ξ;

$$\xi = \frac{\partial}{\partial \tau}. \tag{C.12}$$

Then, the metric form is given as:

$$g_{\mu\nu}(\tau, x^i) = l^2 e^{-2\tau}\bar{g}_{\mu\nu}(x^i), \tag{C.13}$$

where l is a constant which has length scale. Let us introduce the coordinate (t, r^i), which is defined as $t \equiv -le^{-\tau}$ and $r^i \equiv (-t)x^i$. By using (t, r^i) coordinate, the line element is given as

$$\begin{aligned} ds^2 &= l^2 e^{-2\tau}(\bar{g}_{00}d\tau^2 + 2\bar{g}_{0i}d\tau dx^i + \bar{g}_{ij}dx^i dx^j) && \text{(C.14)} \\ &= \bar{g}_{00}dt^2 - 2t\bar{g}_{0i}dtdx^i + t^2\bar{g}_{ij}dx^i dx^j && \text{(C.15)} \\ &= (\bar{g}_{00} + 2\bar{g}_{0i}x^i + \bar{g}_{ij}x^i x^j)dt^2 + 2(\bar{g}_{0i} + \bar{g}_{ij}x^j)dr^i dt + \bar{g}_{ij}dr^i dr^j. && \text{(C.16)} \end{aligned}$$

From the definition of t, the region which is spanned by the coordinate (τ, x^i) corresponds to the region of $t < 0$. In the case of the spherically symmetric spacetime, the line element is written by using coordinate (τ, x, θ, ϕ) and coordinate (t, r, θ, ϕ) as follows;

$$\begin{aligned} ds^2 &= l^2 e^{-2\tau}(Ad\tau^2 + 2Bd\tau dx + Cdx^2 + F^2 d\Omega^2), && \text{(C.17)} \\ &= (A + 2xB + x^2 C)dt^2 + 2(B + C)dtdr + t^2 F^2 d\Omega^2, && \text{(C.18)} \end{aligned}$$

where $t \equiv -le^{-\tau}$, $r \equiv -tx$ and A, B, C, F are functions of x.

Now, we consider on the spacetime which has a homothetic Killing vector, and a perfect fluid as matter sector. From the Einstein equations, we have

$$\begin{aligned} \mathcal{L}_\xi G_{\mu\nu} &\propto \mathcal{L}_\xi T_{\mu\nu} \\ &= \mathcal{L}_\xi\left((\rho + p)u_\mu u_\nu + p g_{\mu\nu}\right) \end{aligned}$$

$$
\begin{aligned}
&= \mathcal{L}_\xi(\rho+p)u_\mu u_\nu + (\rho+p)(\mathcal{L}_\xi u_\mu)u_\nu + (\rho+p)u_\mu \mathcal{L}_\xi u_\nu + (\mathcal{L}_\xi p - 2p)g_{\mu\nu}, \\
&= 0. \qquad \text{(C.19)}
\end{aligned}
$$

where u^μ is a 4-velocity of fluid element. Therefore, we get following equations:

$$
\begin{aligned}
\mathcal{L}_\xi \rho &= 2\rho, \qquad \text{(C.20)} \\
\mathcal{L}_\xi p &= 2p, \qquad \text{(C.21)} \\
\mathcal{L}_\xi u^\mu &= 2u^\mu. \qquad \text{(C.22)}
\end{aligned}
$$

Eqs.(C.20-C.21) imply that only equation of state $p = k\rho$ allows for continuous self-similar solutions.

In the case of massless scalar field in continuous self-similar solution, the Lie derivative of the energy momentum tensor is

$$
\mathcal{L}_\xi T_{\mu\nu} = (\mathcal{L}_\xi \nabla_\mu \Phi)\nabla_\nu \Phi + \nabla_\mu \Phi(\mathcal{L}_\xi \nabla_\nu \Phi) - g_{\mu\nu}(\mathcal{L}_\xi \nabla_\rho \Phi)\nabla^\rho \Phi. \qquad \text{(C.23)}
$$

Since this value must vanish under the continuous self-similar solutions, we have

$$
\mathcal{L}_\xi((\xi^\mu \nabla_\mu \Phi)^2) = 0. \qquad \text{(C.24)}
$$

Therefore, the scalar field satisfy the following equation;

$$
\xi^\mu \nabla_\mu \Phi = \kappa, \qquad \text{(C.25)}
$$

where κ is a constant. Finally, we have

$$
\Phi(\tau, x) = f(x) + \kappa\tau, \qquad \text{(C.26)}
$$

where τ is a coordinate which is along ξ.

Appendix D

Type of the critical behavior

In this appendix, we summarize the type of the critical behavior, and discuss the relation between the critical solution and the scaling law.

D.1 Type I critical behavior

In this section, we focus on the type I critical behavior. As was mentioned in Sec.2.3.2, the critical solution of the type I critical behavior is a static solution or time periodic solution. We assume that the critical solution is a co-dimension one attractor. In other words, when the perturbation modes which is determined from the linear homogeneous differential equations under the appropriate boundary conditions is denoted as $\delta Z_{(i)} = e^{\kappa_{(i)}t} Z_{p(i)}(x)$, $\mathrm{Re}(\kappa_1) > 0$, and $\mathrm{Re}(\kappa_i) < 0$ for $i > 1$. $\mathrm{Re}(\kappa_1)$ is called "Lyapunov exponent". Here, we consider the case that the critical solution is a static solution. Since the static solution has a time like Killing vector ξ, we can introduce the natural coordinate time t, which is defined as:

$$\xi = \frac{\partial}{\partial t}. \tag{D.1}$$

The other coordinates are denoted as r. We express the variables of the system as $Z(r,t)$. Then, the profile of the critical solution can be written as $Z_{\mathrm{CS}}(r)$. When the initial parameter p is near the threshold of the black hole formation p_*, the intermediate state can be rewritten as

$$Z(t,r) \simeq Z_{\mathrm{CS}}(r) + \sum_i C_i(p) e^{\kappa_{(i)}t} Z_{p(i)}(r), \tag{D.2}$$

where the coefficients $C_i(p)$ is a function of the initial parameter. After the intermediate state, the growing mode dominates, and we have

$$Z(t,r) \simeq Z_{\mathrm{CS}}(r) + C_1(p) e^{\kappa_{(1)}t} Z_{p(1)}(r). \tag{D.3}$$

Since the initial parameter p exactly is equal to p_*, the spacetime becomes the critical solution. Therefore, we have

$$C_1(p) = \bar{C}_1(p - p_*) + \mathcal{O}((p - p_*)^2), \tag{D.4}$$

where $\bar{C}_1$ is a constant. Since the black hole formation means that the spacetime leaves the critical solution, the black hole formation time can be estimated by using τ which is defined as

$$\bar{C}_1(p - p_*)e^{\mathrm{Re}(\kappa_{(1)})\tau} = \epsilon, \tag{D.5}$$

where ϵ is a fixed constant. Therefore, we have

$$\tau = -\frac{1}{\mathrm{Re}(\kappa_{(1)})} \ln|p - p_*| + \text{const.} \tag{D.6}$$

From the expression, the relation between the Lyapunov exponent and the index of the scaling law becomes

$$\nu = -\frac{1}{\mathrm{Re}(\kappa_{(1)})}. \tag{D.7}$$

D.2 Type II critical behavior

The critical behavior of Type II associated with the continuous self-similar solution is discussed in Sec.2.2. In this section, we discussed the critical behavior of Type II associated with the discrete self-similar solution.

Firstly, let us introduce the discrete self-similarity of the spacetime. If the spacetime has the discrete self-similarity, the metric satisfy the following condition under the appropriate coordinate (σ, x^i);

$$g_{\mu\nu}(\sigma, x) = e^{2\sigma}\tilde{g}_{\mu\nu}(\sigma, x), \tag{D.8}$$

where $\tilde{g}_{\mu\nu}(\sigma, x)$ has a following property;

$$\tilde{g}_{\mu\nu}(\sigma, x) = \tilde{g}_{\mu\nu}(\sigma + \Delta, x), \tag{D.9}$$

where Δ is a real constant.

Here, we focus on the spherically symmetric spacetime. We use the coordinate $(\sigma, z, \theta, \phi)$ as the coordinate (σ, x). On the other hand, the line element under the polar- radius coordinate can be rewritten as

$$ds^2 = -\alpha^2(t, r)dt^2 + a^2(t, r)dr^2 + r^2 d^2\Omega, \tag{D.10}$$

where α is a lapse function, and a is a radial component of the metric. In order to see the relation between the coordinate $(\sigma, z, \theta, \phi)$ and (t, r, θ, ϕ), we consider the following coordinate transformation;

$$\begin{cases} t &= e^{\sigma}T(\sigma, z) \\ r &= e^{\sigma}R(\sigma, z) \end{cases} \tag{D.11}$$

where T and R are the periodic function in σ with period Δ. Under this coordinate transformation, we have

$$ds^2 = e^{2\sigma}\left\{-\alpha^2((T + \partial_\sigma T)d\sigma + \partial_z T dz)^2 + a^2((R + \partial_\sigma R)d\sigma + \partial_z R dz)^2 + R^2 d^2\Omega\right\}.$$

(D.12)

Therefore, if the spacetime has a discrete self-similarity, α and a satisfy the following periodic condition under the appropriate gauge condition of t;

$$\begin{cases} \alpha(t,r) &= \alpha(e^{n\Delta}t, e^{n\Delta}r) \\ a(t,r) &= a(e^{n\Delta}t, e^{n\Delta}r). \end{cases} \tag{D.13}$$

Here, we introduce the coordinate (τ, ζ), which is defined as

$$\begin{cases} \tau &= \ln\left(\frac{t}{r_0}\right) \\ \zeta &= \ln\left(\frac{r}{t}\right) - \xi_0(\tau), \end{cases} \tag{D.14}$$

where r_0 is a constant which fix the scale. This coordinate is include in the class of above (σ, x^i). In the coordinate (τ, ζ), the periodic condition Eq.(D.15) is expressed as

$$\begin{cases} a(\zeta, \tau + n\Delta) &= a(\zeta, \tau) \\ \alpha(\zeta, \tau + n\Delta) &= \alpha(\zeta, \tau). \end{cases} \tag{D.15}$$

We can construct the critical solution $Z_{\rm CS}(\tau, \zeta)$ of the critical collapse of the massless scalar field in this coordinate, which is a periodic with (see [10]).

Let us consider the 1-parameter family of the initial data, which is parameterized by p. We assume that p has a threshold p_* of the black hole formation, Furthermore, we assume that the critical solution is a co-dimension one attractor. Since the intermediate state which initial data has an initial parameter around p_* can be approximated as the critical solution, we have

$$Z(\zeta, \tau) \simeq Z_{\rm CS}(\zeta, \tau) + \sum_i C_i(p) e^{\kappa_{(i)}\tau} Z_{p(i)}(\zeta, \tau), \tag{D.16}$$

where the second term is a sum of the perturbation modes. Each perturbation mode is also periodic with respect to τ, its period is also Δ. Since the critical solution has one growing mode ($i = 1$), we can neglect the other decaying modes, and we have

$$Z(\zeta, \tau) \simeq Z_{\rm CS}(\zeta, \tau) + C_1(p) e^{\kappa_{(1)}\tau} Z_{p(1)}(\zeta, \tau). \tag{D.17}$$

If p is equal to p_*, exactly, the spacetime approach to the critical solution. Therefore, C_1 must vanish for $p = p_*$, and we get the following expressions;

$$C_1(p) = \bar{C}_1(p - p_*) + \mathcal{O}((p - p_*)^2), \tag{D.18}$$

where $\bar{C}_1$ is a constant. Let us define τ_p as a typical time in which the second term becomes comparable to the first term, that is;

$$|\bar{C}_1(p - p_*)| e^{{\rm Re}(\kappa_{(1)})\tau_{\rm p}} = \epsilon, \tag{D.19}$$

where ϵ is a fixed small value. From this equation, we have

$$\tau_{\rm p} = -{\rm Re}(\kappa_{(1)})^{-1} \ln|p - p_*| + {\rm const}, \tag{D.20}$$

and

$$Z(t(\tau_p), r) \simeq Z_{\rm CS}(\ln \frac{r}{L_p}, \tau_p) \pm \epsilon Z_{p(1)}(\ln \frac{r}{L_p}, \tau_p), \tag{D.21}$$

where

$$L_p \equiv r_0 e^{\tau_p + \xi_0(\tau_p)}. \tag{D.22}$$

Since the black hole mass has a dimension length, it is proportional to L_p, we have

$$M \propto L_p e^{\mu(\tau_p)}, \tag{D.23}$$

where $\mu(\tau)$ is a periodic function of τ. Therefore, we get the following formula;

$$M \propto r_0 (p - p_*)^\gamma e^{\bar{\mu}(\gamma \ln |p - p_*|)}, \tag{D.24}$$

where $\bar{\mu}(\tau)$ is a periodic function of τ. The index γ is defined as

$$\gamma = -\frac{1}{\lambda_1}. \tag{D.25}$$

Since the scalar field oscillates with period Δ, the physical quantities which has no length scale, like M/r oscillates with period $\Delta/2$.

Appendix E

G-BSSN formulation

E.1 G-BSSN formulation

In this appendix, G-BSSN formulation in general curvilinear coordinate is summarized.

G-BSSN formulation is generalization of the BSSN formulation [35, 36], and based on the ADM formulation. From the ADM formulation, we have following metric ansatz :

$$ds^2 = -\alpha^2 dt^2 + \gamma_{ij}(dx^i + \beta^i dt)(dx^j + \beta^j dt), \tag{E.1}$$

where α, β^i and γ_{ij} are a lapse function, a shift vector and 3-metric, respectively. Substituting above metric ansatz for Einstein equations, we have evolution equations :

$$\left(\frac{\partial}{\partial t} - \mathcal{L}_\beta\right)\gamma_{ij} = -2\alpha K_{ij}, \tag{E.2}$$

$$\left(\frac{\partial}{\partial t} - \mathcal{L}_\beta\right)K_{ij} = -D_i D_j \alpha + \alpha\{R_{ij} + KK_{ij} - 2K_{ik}K^k{}_j + 4\pi((S-E)\gamma_{ij} - 2S_{ij})\}, \tag{E.3}$$

and constraint equations :

$$R + K^2 - K_{ij}K^{ij} = 16\pi E, \tag{E.4}$$

$$D_j K^j{}_i - D_i K = 8\pi p_i. \tag{E.5}$$

K_{ij} is the extrinsic curvature, R_{ij} is the Ricci tensor associated with γ_{ij}, D_i is a covariant derivative associated with γ_{ij}, and $\mathcal{L}_\beta$ is a Lie derivative of β^i. Furthermore, E, ρ_i and S_{ij} are energy density, momentum density and a stress tensor of the matter sector, which are defined as follows: $E \equiv T_{\mu\nu}n^\mu n^\nu$, $p_i \equiv T_{\nu\mu}\gamma_i^\nu n^\mu$, and $S_{ij} \equiv T_{\mu\nu}\gamma_i^\mu \gamma_j^\nu$, respectively. S is a trace part of S_{ij}.

In BSSN formulation, we do not use γ_{ij} and K_{ij} as numerical variables, but use the following decomposed variables $(\phi, \tilde{\gamma}_{ij}, K, \tilde{A}_{ij})$:

$$\gamma_{ij} = e^{4\phi}\tilde{\gamma}_{ij}, \tag{E.6}$$

$$K_{ij} = e^{4\phi}\tilde{A}_{ij} + \frac{1}{3}\gamma_{ij}K, \tag{E.7}$$

where $\det(\tilde{\gamma}_{ij}) = 1$ and $K = \gamma^{ij}K_{ij}$. Furthermore, the following auxiliary field:

$$\tilde{\Gamma}^k = \tilde{\gamma}^{ij}\tilde{\Gamma}^k_{ij}, \tag{E.8}$$

In BSSN formulation, $(\phi, \tilde{\gamma}_{ij}, K, \tilde{A}_{ij}, \tilde{\Gamma}^i, \alpha, \beta^i)$ and dynamical variables of matter sector are used. Although it is known that BSSN formulation is powerful method, $\tilde{\Gamma}^i$ is not a vector under the coordinate transformation, and $\tilde{\gamma}_{ij}$ is not a tensor under the transformation. In order to apply the BSSN formulation to the general curvilinear coordinate, Brown generalize this formulation to G-BSSN formulation. There are two main differences between BSSN formulation and G-BSSN formulation. First point is a definition of $\tilde{\gamma}_{ij}$. Although $\tilde{\gamma}_{ij}$ is defined such that the determinant $\tilde{\gamma}$ is unity in BSSN formulation, $\tilde{\gamma}$ is determined from condition about the evolution of $\tilde{\gamma}$ and initial data in G-BSSN formulation. There are two natural condition which determines the evolution of $\tilde{\gamma}$, that is, $\partial_t\tilde{\gamma} = 0$ (Lagrangian type), and $\partial_\perp\tilde{\gamma} = 0$ (Eulerian type), where $\partial_\perp \equiv \partial_t - \mathcal{L}_\beta$. Furthermore, instead of $\tilde{\Gamma}^i$, the reference metric $\bar{\gamma}_{ij}$ is introduced and the following auxiliary field $\tilde{\Lambda}^k$ is defined such that

$$\tilde{\Lambda}^k = \tilde{\gamma}^{ij}(\tilde{\Gamma}^k_{ij} - \bar{\Gamma}^k_{ij}) = \tilde{\gamma}^{ij}\Delta\tilde{\Gamma}^k_{ij}, \tag{E.9}$$

where $\bar{\Gamma}^k_{ij}$ is the Christoffel symbols associated with $\bar{\gamma}_{ij}$. $(\phi, \tilde{\gamma}_{ij}, K, \tilde{A}_{ij}, \tilde{\Lambda}^i, \alpha, \beta^i)$ and the variables of the matter sector are the variables of the G-BSSN formulation. The evolution equations of this formalism are as follows:

$$\left(\frac{\partial}{\partial t} - \mathcal{L}_\beta\right)\phi = -\frac{1}{6}\alpha K + \sigma\frac{1}{6}\tilde{D}_k\beta^k, \tag{E.10}$$

$$\left(\frac{\partial}{\partial t} - \mathcal{L}_\beta\right)\tilde{\gamma}_{ij} = -2\alpha\tilde{A}_{ij} - \sigma\frac{2}{3}\tilde{\gamma}_{ij}\tilde{D}_k\beta^k, \tag{E.11}$$

$$\left(\frac{\partial}{\partial t} - \mathcal{L}_\beta\right)K = -\gamma^{ij}D_iD_j\alpha + \alpha(\tilde{A}_{ij}\tilde{A}^{ij} + \frac{1}{3}K^2) + 4\pi\alpha(E+S), \tag{E.12}$$

$$\left(\frac{\partial}{\partial t} - \mathcal{L}_\beta\right)\tilde{A}_{ij} = e^{-4\phi}\{-D_iD_j\alpha + \alpha(R_{ij} - 8\pi S_{ij})\}^{TF} + \alpha(K\tilde{A}_{ij} - 2\tilde{A}_{il}\tilde{A}^l_j) - \sigma\frac{2}{3}\tilde{A}_{ij}\tilde{D}_k\beta^k, \tag{E.13}$$

$$\left(\frac{\partial}{\partial t} - \mathcal{L}_\beta\right)\tilde{\Lambda}^i = \tilde{\gamma}^{mn}\bar{D}_m\bar{D}_n\beta^i - 2\tilde{A}^{im}\partial_m\alpha + 2\alpha(\Delta\tilde{\Gamma}^i{}_{jk}\tilde{A}^{jk} + 6\tilde{A}^{ij}\partial_j\phi - \frac{2}{3}\tilde{\gamma}^{ij}\partial_j K - 8\pi\tilde{\gamma}^{ij}S_j) + \frac{\sigma}{3}\{2\tilde{\Lambda}^i\tilde{D}_k\beta^k + \tilde{D}^i(\tilde{D}_k\beta^k)\}, \tag{E.14}$$

where $\mathcal{L}_\beta$ is the Lie derivative respect with β^i, a superscript TF means the traceless part with respect to γ_{ij}. The Ricci tensor in the equations can be expressed as:

$$R_{ij} = R^\phi_{ij} + \tilde{R}_{ij}, \tag{E.15}$$

$$\tilde{R}_{ij} = -\frac{1}{2}\tilde{\gamma}^{lm}\bar{D}_m\bar{D}_l\tilde{\gamma}_{ij} + \frac{1}{2}(\tilde{\gamma}_{ki}\bar{D}_j\tilde{\Lambda}^k + \tilde{\gamma}_{kj}\bar{D}_i\tilde{\Lambda}^k) + \frac{1}{2}(\tilde{\Lambda}^k\Delta\tilde{\Gamma}_{ijk} + \tilde{\Lambda}^k\Delta\tilde{\Gamma}_{jik}) + \tilde{\gamma}^{lm}(\Delta\tilde{\Gamma}^k{}_{li}\Delta\tilde{\Gamma}_{jkm} + \Delta\tilde{\Gamma}^k{}_{lj}\Delta\tilde{\Gamma}_{ikm} + \Delta\tilde{\Gamma}^k{}_{im}\Delta\tilde{\Gamma}_{klj}), \tag{E.16}$$

$$R^{\phi}_{ij} = -2\tilde{D}_i\tilde{D}_j\phi - 2\tilde{\gamma}_{ij}\tilde{D}^k\tilde{D}_k\phi + 4\tilde{D}_i\phi\tilde{D}_j\phi - 4\tilde{\gamma}_{ij}\tilde{D}^k\phi\tilde{D}_k\phi. \quad \text{(E.17)}$$

The parameter σ depends on the evolution of $\tilde{\gamma}$. Lagragian option corresponds to that $\sigma = 1$, and the Lorentzian choice corresponds to that $\sigma = 0$. Hamiltonian constraint and the momentum constraint can be written as:

$$\tilde{\gamma}^{ij}\tilde{D}_i\tilde{D}_j e^{\phi} - \frac{e^{\phi}}{8}\tilde{R} + \frac{e^{5\phi}}{8}\tilde{A}_{ij}\tilde{A}^{ij} - \frac{e^{5\phi}}{12}K^2 + 2\pi e^{5\phi}E = 0, \quad \text{(E.18)}$$

$$\tilde{D}_j(e^{6\phi}\tilde{A}^j{}_i) - \frac{2}{3}e^{6\phi}\tilde{D}_i K - 8\pi e^{6\phi}p_i = 0. \quad \text{(E.19)}$$

In addition to these constraint equations, Eq.(E.9) is also constraint equation.

E.2 Spatial coordinate transformation of the variables in G-BSSN formulation in spherically symmetric spacetime

In our study, we use the inhomogeneous grid method in spherically symmetric spacetime. the inhomogeneous grid method in spherically symmetric spacetime is a coordinate transformation for the radial coordinate. Here, we summarize the coordinate transformation from r_O to r_N in each variables;

$$\alpha_N = \alpha_O, \quad \text{(E.20)}$$

$$\beta_N = \frac{\partial r_N}{\partial r_O}\beta_O, \quad \text{(E.21)}$$

$$\phi_N = \phi_O, \quad \text{(E.22)}$$

$$a_N = (\frac{\partial r_O}{\partial r_N})^2 a_O, \quad \text{(E.23)}$$

$$b_N = (\frac{r_O}{r_N})^2 b_O, \quad \text{(E.24)}$$

$$A_N = (\frac{\partial r_O}{\partial r_N})^2 A_O, \quad \text{(E.25)}$$

$$B_N = (\frac{r_O}{r_N})^2 B_O, \quad \text{(E.26)}$$

$$\tilde{\Lambda}_N = \frac{\partial r_N}{\partial r_O}\tilde{\Lambda_O}, \quad \text{(E.27)}$$

$$\Pi_N = \frac{\partial r_O}{\partial r_N}\Pi_O, \quad \text{(E.28)}$$

$$E_N = E_O, \quad \text{(E.29)}$$

$$p_{rN} = \frac{\partial r_O}{\partial r_N}p_{rO}. \quad \text{(E.30)}$$

Appendix F

Iterative Crank Nicolson scheme

In this appendix, we explain the iterative Crank Nicolson scheme.

F.1 Iterative Crank Nicolson scheme

Let us consider the following model equations for $\{u(t,\vec{x})_\alpha\}$:

$$\frac{\partial}{\partial t}u(t,\vec{x})_\alpha = \mathcal{M}^{l\beta}{}_\alpha(u(t,\vec{x}))\frac{\partial}{\partial x^l}u(t,\vec{x})_\beta + \mathcal{N}_\alpha(u(t,\vec{x})), \tag{F.1}$$

where $\mathcal{M}^\beta{}_\alpha(u(t,\vec{x}))$ and $\mathcal{N}_\alpha(u(t,\vec{x}))$ are functions of $\{u(t,\vec{x})_\alpha\}$. This equation can be solved with Crank Nicolson (CN) scheme. CN discretization is given as

$$(u_\alpha)^{n+1}_{\vec{m}} = (u_\alpha)^n_{\vec{m}} + \frac{\Delta t}{2}\left(\mathcal{M}(u^{n+1}_{\vec{m}})^{\vec{e}_l\beta}_\alpha \delta_{\vec{e}_l}(u_\beta)^{n+1}_{\vec{m}} + \mathcal{N}(u^{n+1}_{\vec{m}})_\alpha + \mathcal{M}(u^n_{\vec{m}})^{\vec{e}_l\beta}_\alpha \delta_{\vec{e}_l}(u_\beta)^n_{\vec{m}} + \mathcal{N}(u^n_{\vec{m}})_\alpha\right), \tag{F.2}$$

where $(u_\alpha)^n_{\vec{m}} := u_\alpha(t = n\Delta t, \vec{x} = \vec{m}\Delta x)$, and $\delta_{\vec{e}_l}(u_\alpha)^n_{\vec{m}} = \dfrac{1}{2\Delta x}((u_\alpha)^n_{\vec{m}+\vec{e}_l} - (u_\alpha)^n_{\vec{m}-\vec{e}_l})$. Since $\{(u_\alpha)^{n+1}_{\vec{m}}\}_{\vec{m}}$ is expressed by using $\{(u_\alpha)^{n+1}_{\vec{m}}\}_{\vec{m}}$ and $\{(u_\alpha)^n_{\vec{m}}\}_{\vec{m}}$ in CN discretization, the profile of $\{(u_\alpha)^{n+1}_{\vec{m}}\}_{\vec{m}}$ is obtained as a solution of simultaneous equations.

Iterative Crank-Nicolson scheme is a one of the scheme to solve the above simultaneous equations. First, $\{(u^{(1)}_\alpha)_{\vec{m}}\}_{\vec{m}}$ is calculated by following equations:

$$(u^{(1)}_\alpha)_{\vec{m}} = (u_\alpha)^n_{\vec{m}} + \Delta t(\mathcal{M}(u^n_{\vec{m}})^{\vec{e}_l\beta}_\alpha \delta_{\vec{e}_l}(u_\beta)^n_{\vec{m}} + \mathcal{N}(u^n_{\vec{m}})_\alpha), \tag{F.3}$$

Next, by using the following recurrence formula interatively, u^i is obtained until u^i is converged;

$$(u^{(i+1)}_\alpha)_{\vec{m}} = (u_\alpha)^n_{\vec{m}} + \frac{\Delta t}{2}\left(\mathcal{M}(u^{(i)}_{\vec{m}})^{\vec{e}_l\beta}_\alpha \delta_{\vec{e}_l}(u_\beta)^{(i)}_{\vec{m}} + \mathcal{N}(u^{(i)}_{\vec{m}})_\alpha + \mathcal{M}(u^n_{\vec{m}})^{\vec{e}_l\beta}_\alpha \delta_{\vec{e}_l}(u_\beta)^n_{\vec{m}} + \mathcal{N}(u^n_{\vec{m}})_\alpha\right). \tag{F.4}$$

The maximal step of the iteration denote i_{max}. $(u_\alpha)^{n+1}_{\vec{m}}$ is given as $(u_\alpha)^{(i_{\max})}_{\vec{m}}$;

$$(u_\alpha)^{n+1}_{\vec{m}} = (u_\alpha)^{(i_{\max})}_{\vec{m}} \tag{F.5}$$

The numerical stability of ICN is discussed in [60].

References

[1] C. Gundlach, Phys. Rept. **376**, 339 (2003) doi:10.1016/S0370-1573(02)00560-4 [gr-qc/0210101].

[2] C. Gundlach and J. M. Martin-Garcia, Living Rev. Rel. **10**, 5 (2007) [arXiv:0711.4620 [gr-qc]].

[3] M. W. Choptuik, Phys. Rev. Lett. **70**, 9 (1993). doi:10.1103/PhysRevLett.70.9

[4] A. M. Abrahams and C. R. Evans, Phys. Rev. Lett. **70**, 2980 (1993).

[5] E. Sorkin, Class. Quant. Grav. **28**, 025011 (2011) [arXiv:1008.3319 [gr-qc]].

[6] C. R. Evans and J. S. Coleman, Phys. Rev. Lett. **72**, 1782 (1994) [gr-qc/9402041].

[7] D. Maison, Phys. Lett. B **366**, 82 (1996) [gr-qc/9504008].

[8] D. Garfinkle, C. Cutler and G. C. Duncan, Phys. Rev. D **60**, 104007 (1999) doi:10.1103/PhysRevD.60.104007 [gr-qc/9908044].

[9] E. Sorkin and Y. Oren, Phys. Rev. D **71**, 124005 (2005) doi:10.1103/PhysRevD.71.124005 [hep-th/0502034].

[10] C. Gundlach, Phys. Rev. D **55**, 695 (1997) [gr-qc/9604019].

[11] S. Hod and T. Piran, Phys. Rev. D **55**, 440 (1997) [gr-qc/9606087].

[12] T. Koike, T. Hara and S. Adachi, Phys. Rev. Lett. **74**, 5170 (1995) [gr-qc/9503007].

[13] D. Garfinkle and G. C. Duncan, Phys. Rev. D **58**, 064024 (1998) [gr-qc/9802061].

[14] I. Olabarrieta and M. W. Choptuik, Phys. Rev. D **65**, 024007 (2002) [gr-qc/0107076].

[15] P. R. Brady, C. M. Chambers and S. M. C. V. Goncalves, Phys. Rev. D **56**, R6057 (1997) [gr-qc/9709014].

[16] H. Okawa, V. Cardoso and P. Pani, Phys. Rev. D **89**, no. 4, 041502 (2014) doi:10.1103/PhysRevD.89.041502 [arXiv:1311.1235 [gr-qc]].

[17] E. Seidel and W. M. Suen, Phys. Rev. Lett. **66**, 1659 (1991). doi:10.1103/PhysRevLett.66.1659

[18] M. W. Choptuik, E. W. Hirschmann and R. L. Marsa, Phys. Rev. D **60**, 124011 (1999) doi:10.1103/PhysRevD.60.124011 [gr-qc/9903081].

[19] J. M. Martin-Garcia and C. Gundlach, Phys. Rev. D **59**, 064031 (1999) doi:10.1103/PhysRevD.59.064031 [gr-qc/9809059].

[20] M. W. Choptuik, E. W. Hirschmann, S. L. Liebling and F. Pretorius, Phys. Rev. D **68**, 044007 (2003) doi:10.1103/PhysRevD.68.044007 [gr-qc/0305003].

[21] I. Olabarrieta, J. F. Ventrella, M. W. Choptuik and W. G. Unruh, Phys. Rev. D **76**, 124014 (2007) doi:10.1103/PhysRevD.76.124014 [arXiv:0708.0513 [gr-qc]].

[22] J. Healy and P. Laguna, Gen. Rel. Grav. **46**, 1722 (2014) doi:10.1007/s10714-014-1722-2 [arXiv:1310.1955 [gr-qc]].

[23] S. Hawking, Mon. Not. Roy. Astron. Soc. **152**, 75 (1971).

[24] B. J. Carr, Astrophys. J. **201**, 1 (1975). doi:10.1086/153853

[25] J. C. Niemeyer and K. Jedamzik, Phys. Rev. Lett. **80**, 5481 (1998) [astro-ph/9709072].

[26] M. W. Choptuik, NATO Sci. Ser. B **332**, 155 (1994).

[27] L. M. Widrow, Phys. Rev. D **40**, 1002 (1989).

[28] D. Garfinkle and R. Zbikowski, Class. Quant. Grav. **29**, 095015 (2012) [arXiv:1201.1491 [gr-qc]].

[29] S. G. Rubin, M. Y. Khlopov and A. S. Sakharov, Grav. Cosmol. S **6**, 51 (2000) [hep-ph/0005271].

[30] K. Clough and E. A. Lim, arXiv:1602.02568 [gr-qc].

[31] Z. Cao, R. G. Cai and R. Q. Yang, arXiv:1604.03363 [gr-qc].

[32] A. Akbarian and M. W. Choptuik, Phys. Rev. D **92**, no. 8, 084037 (2015) doi:10.1103/PhysRevD.92.084037 [arXiv:1508.01614 [gr-qc]].

[33] T. W. Baumgarte and P. J. Montero, Phys. Rev. D **92**, no. 12, 124065 (2015) doi:10.1103/PhysRevD.92.124065 [arXiv:1509.08730 [gr-qc]].

[34] T. W. Baumgarte and C. Gundlach, Phys. Rev. Lett. **116**, no. 22, 221103 (2016) doi:10.1103/PhysRevLett.116.221103 [arXiv:1603.04373 [gr-qc]].

[35] M. Shibata and T. Nakamura, Phys. Rev. D **52**, 5428 (1995).

[36] T. W. Baumgarte and S. L. Shapiro, Phys. Rev. D **59**, 024007 (1999) [gr-qc/9810065].

[37] S. A. Teukolsky, Phys. Rev. D **61**, 087501 (2000) [gr-qc/9909026].

[38] M. Alcubierre, S. Brandt, B. Bruegmann, D. Holz, E. Seidel, R. Takahashi and J. Thornburg, Int. J. Mod. Phys. D **10**, 273 (2001) [gr-qc/9908012].

[39] M. Alcubierre and J. A. Gonzalez, Comput. Phys. Commun. **167**, 76 (2005) [gr-qc/0401113].

[40] C. Gundlach and T. W. Baumgarte, Phys. Rev. D **94**, no. 8, 084012 (2016) doi:10.1103/PhysRevD.94.084012 [arXiv:1608.00491 [gr-qc]].

[41] T. Chiba and S. Yokoyama, PTEP **2017**, no. 8, 083E01 (2017) doi:10.1093/ptep/ptx087 [arXiv:1704.06573 [gr-qc]].

[42] P. Bizon and A. Rostworowski, Phys. Rev. Lett. **107**, 031102 (2011) doi:10.1103/PhysRevLett.107.031102 [arXiv:1104.3702 [gr-qc]].

[43] D. Santos-Olivan and C. F. Sopuerta, Phys. Rev. Lett. **116**, no. 4, 041101 (2016) doi:10.1103/PhysRevLett.116.041101 [arXiv:1511.04344 [gr-qc]].

[44] P. Bizon and A. Rostworowski, Acta Phys. Polon. B **48**, 1375 (2017) doi:10.5506/APhysPolB.48.1375 [arXiv:1710.03438 [gr-qc]].

[45] R. G. Cai, L. W. Ji and R. Q. Yang, Commun. Theor. Phys. **68**, no. 1, 67 (2017) doi:10.1088/0253-6102/68/1/67 [arXiv:1609.02804 [gr-qc]].

[46] R. G. Cai, L. W. Ji and R. Q. Yang, Commun. Theor. Phys. **65**, no. 3, 329 (2016) doi:10.1088/0253-6102/65/3/329 [arXiv:1511.00868 [gr-qc]].

[47] M. Maliborski, Phys. Rev. Lett. **109**, 221101 (2012) doi:10.1103/PhysRevLett.109.221101 [arXiv:1208.2934 [gr-qc]].

[48] I. L. Bogolyubsky and V. G. Makhankov, JETP Lett. **24**, 12 (1976).

[49] E. J. Copeland, M. Gleiser and H.-R. Muller, Phys. Rev. D **52**, 1920 (1995) doi:10.1103/PhysRevD.52.1920 [hep-ph/9503217].

[50] E. P. Honda and M. W. Choptuik, Phys. Rev. D **65**, 084037 (2002) doi:10.1103/PhysRevD.65.084037 [hep-ph/0110065].

[51] G. Fodor, P. Forgacs, P. Grandclement and I. Racz, Phys. Rev. D **74**, 124003 (2006) doi:10.1103/PhysRevD.74.124003 [hep-th/0609023].

[52] H. Kodama, Prog. Theor. Phys. **63**, 1217 (1980). doi:10.1143/PTP.63.1217

[53] T. Harada, C. M. Yoo, T. Nakama and Y. Koga, Phys. Rev. D **91**, no. 8, 084057 (2015) doi:10.1103/PhysRevD.91.084057 [arXiv:1503.03934 [gr-qc]].

[54] J. D. Brown, Phys. Rev. D **79**, 104029 (2009) doi:10.1103/PhysRevD.79.104029 [arXiv:0902.3652 [gr-qc]].

[55] M. Alcubierre and M. D. Mendez, Gen. Rel. Grav. **43**, 2769 (2011) doi:10.1007/s10714-011-1202-x [arXiv:1010.4013 [gr-qc]].

[56] D. Christodoulou and S. Klainerman, *The global nonlinear stability of the Minkowski space* (Princeton University Press, Princeton, 1993).

[57] P. G. LeFloch and Y. Ma, arXiv:1511.03324 [gr-qc].

[58] M. Gleiser, Phys. Lett. B **600**, 126 (2004) doi:10.1016/j.physletb.2004.08.064 [hep-th/0408221].

[59] J. M. Martin-Garcia and C. Gundlach, Phys. Rev. D **68**, 024011 (2003) doi:10.1103/PhysRevD.68.024011 [gr-qc/0304070].

[60] S. A. Teukolsky, Phys. Rev. D **61**, 087501 (2000) doi:10.1103/PhysRevD.61.087501 [gr-qc/9909026].